

Identifying and characterizing novel invasion-related genes in Glioblastoma



Carina Fabian

Thesis for the degree of Philosophiae Doctor (PhD)
University of Bergen, Norway
2022

UNIVERSITY OF BERGEN



Identifying and characterizing novel invasion-related genes in Glioblastoma

Carina Fabian



Thesis for the degree of Philosophiae Doctor (PhD)
at the University of Bergen

Date of defense: 25.03.2022

© Copyright Carina Fabian

The material in this publication is covered by the provisions of the Copyright Act.

Year: 2022

Title: Identifying and characterizing novel invasion-related genes in Glioblastoma

Name: Carina Fabian

Print: Skipnes Kommunikasjon / University of Bergen

Scientific environment

This study was performed in the NORLUX Neuro-Oncology Laboratory in the Department of Oncology at the Luxembourg Institute of Health from the 15.11.2017 until the 14.12.2021 with an affiliation to the Department of Biomedicine, University of Bergen.

The work was supervised by Rolf Bjerkvig as main supervisor and Simone P. Niclou as co-supervisor.

The grant for this study was funded by the CANBIO DTU (PRIDE15/10675146) of the National Research Fund (FNR) of Luxembourg, by the Fondation Cancer of Luxembourg (INVGBM Project).



Acknowledgements

To be honest, I never believed that I would be once doing a PhD, especially after the many rejections I got, but here I am now finally defending my PhD thesis.

Back in school, my interest in cancer biology started growing. I was fascinated by a disease that is resisting basically every treatment. I wanted to learn more about the disease that is killing many people and which also did not stop in front of my grandfather. That was the moment when I was convinced that one day I will find something to cure cancer. By that time, I was not aware of how difficult that may be, but I was motivated to become a researcher with the goal to improve people's lives.

Therefore, you can imagine how happy I was when I got the position in the NORLUX neuro-oncology laboratory of the Luxembourg Institute of Health (LIH). Here I would like to thank all the people that made this happen and supported me over the years:

First of all, Rolf Bjerkgvig, my main supervisor, and Simone P. Niclou, my co-supervisor, who believed in me and allowed me to work on this project. They kept me motivated over the years no matter which problems occurred and many occurred. Thanks for the criticism, that pushed me to improve myself, start critical thinking and grow with upcoming challenges. Thanks for making this possible, I could not have wished for better supervisors with such a remarkable knowledge in neuro-oncology.

Anne Schuster, my first informal co-supervisor, who introduced me to experiments to study glioblastoma invasion. Thereby she straightened the way into my own project.

Virginie Neirinckx, my second informal co-supervisor and best supervisor I could have wished for, who was so nice to take over after Anne left. She took time for meetings, honest discussions and kept me motivated after failures, scientifically and privately.

Clement Thomas, member of my CET committee. Thanks for the fruitful discussions, good advices and constructive criticism during my CET meetings. It was great to have someone in my committee that was thinking in an objective manner.

The Fonds National de la Recherche (FNR) that provided the funding for my project and thereby enabled the work presented here.

Thanks to Margarethe Bittins, PhD coordinator of the Department of Biomedicine. She was so nice to answer all my questions and a great support with the required paperwork.

I want to thank Martha Enger and Nils Halberg for being part of my Midway Evaluation committee and that you took time for discussions, advices and constructive criticism.

Thank you Katharina Sarnow, PhD student in the Department of Biomedicine, who showed me rat brain organoids and spent time in the lab to run experiments for me.

Thanks to Michel Mittelbronn for providing me a tissue section of a human GBM.

Many thanks to Petr Nazarov. As bioinformatics expert he helped me to understand the performed analyses and always took time for meetings whenever I had questions.

Thanks to all NORLUX members: Monika Dieterle, Sabrina Fritah, Fred Fack, Anna Golebiewska, Ann-Christin Hau, Eliane Klein, Virginie Baus, Anais Oudin, May Wantz, Hugo Dosquet, Yabo Yahaya Abubakar, Andres Cano Galiano, Vanessa Barthelemy, Magretta Adiamah and Siu-Thinh Ho. Thanks for the nice teamwork, discussions, advices and for accepting the Austrian newcomer so nicely in your group.

Vanessa, thanks for helping wherever possible and for being there, especially in difficult times. She always knew how I am feeling. Thanks for becoming a good friend.

Thank you Sabrina for the nice theoretical and practical advices on the ZFAND3 project, you made the whole project a little easier with your expertise.

Big thanks to lovely Maggie, who is always friendly and helpful, professionally as well as privately. I enjoyed talking to her as she supported me in every kind of way.

Special thanks to one of my favourite people: Monika Dieterle, who always took time to discuss about my project. She was a great help and had the best ideas for the project. Besides having a lot of knowledge, she thought critically about experiments and honestly shared her opinion. This and the fact that she is humble are the reasons why I like her so much and highly appreciated her advices. So please never change and stay the person you are now. And thanks for taking me to Trier many Fridays after work.

Many thanks to Kim Eiden, a Master (now PhD) student, that helped me where she could during six months. Thanks for the hard work and nice time in and outside the lab,

because with you I gained a friend. All the best for your PhD, you will do great. Thanks for teaching me the very useful words Deckelsmouk and Nuesschnappech ;)

Thanks to some PhD students that became close friends over the years: Lia Pinto, Yolanda Pires Afonso, Mohamad Sarmini, Catherine Delbrouck, Lara Haase, Andrea Scafidi, Hugo Dosquet and Rédouane Slimani. As we were sitting in the same boat, you were the ones that understood me most and were the greatest support. You were there for me and cheered me up when my family was not able to, so you became my small family. You guys made the last 4 years more enjoyable and gave me the feeling that I am never alone. I will miss every single one of you, so I hope we stay in touch.

Lia, my little Stellina, from the first moment we met I liked you, maybe because you are as crazy as I am. I never thought I would gain an as amazing friend as you became over the years. You were my cornerstone throughout the years and I am glad that I got to know you. You always felt when I was feeling bad and had an open ear for my problems, scientifically and privately. It is crazy what we experienced, seeing Maroon5 and Ed Sheeran live, throwing flip-flops at random snoring guys in a hostel in Rotterdam and doing and finishing our PhD together. I love you so much and wish you all the best for your future as Post-Doc in Leeds and wife of the one and only Matthew.

Yolanda, because you are one of the nicest people I have ever met. I could not have wished for a better office neighbour. Thanks for always cheering me up and keeping me motivated even after you left LIH. Seeing your remarkable positivity was a huge motivation for me to keep strong. So please always stay as positive and great as you are. I wish you and Nathan all the best for whatever is coming next.

Moha, I will miss getting teased when you are bored. For me you were the big brother I never had but always wished for. So thanks for caring for me and protecting Lia and me from annoying guys when we were going out. Still, I cannot believe you are married now and did not tell me about it, so lucky you that you invited me for the big wedding in Sardinia. All the best for you and Giulia and I keep my fingers crossed for Harvard.

Catherine, your positivity, organization talent and patience are remarkable and cutting brain slices with you was lots of fun. I am sure you will finish your PhD as great as you worked throughout the years. So all the best and also for your private life with Jim.

Lara, I never thought that we are almost equally crazy, although I have to say you are a little crazier. Thanks for our weird discussion topics and our song discussions (“I sing a liad fir di”). Whenever I hear this song, I will think about you and laugh a lot.

Andrea, the little Bertuccia, it is evy to say goodbye. I want to thank you for being there when needed and trying to teach me Roman, so I say Ci vediamo eccetera, eccetera! I anyways have to call you once a month to remind you how many months you have left.

Hugo, you are weird and slightly stupid (your own words), but I knew from the first moment I met you that you are unique and this is significatif. I wish you all the best.

And Rédouane, thanks for always being there. Best of luck for your medical studies.

Many thanks to my parents, who supported me from Austria over the years. I think it was hard for them, especially for my mum, to see their little girl leaving Austria and starting a new life in a new country. Still they accepted my decision and their visits in Luxembourg, especially with my dog, gave me energy and motivation to continue. My dad became the proudest dad when I started a research career as it was his dream to become a researcher himself. Every week we had discussions on my work. Thanks to Whatsapp we could see each other daily, which helped me a lot in times when I missed home and especially my dog. So thanks mum and dad for always being at my side.

The most special thanks go to my grandparents Frieda and Konrad Zeitlhofer to whom I dedicate this thesis and the last years of hard work. Even though they are unfortunately not among us anymore, they have always been my greatest inspiration and motivation. They taught me to never give up and live my dream, even though that meant to move away from home and leave everything behind me, including family and friends. No matter what I did and no matter where I moved, they kept on supporting me and believing in me. I cannot be more thankful to have had them on my side throughout my life. And this is the reason why I am even more proud today to look up to them and tell them that I finally got my doctoral degree. I love and miss you so much!

So thanks to everyone that supported me during this intense time!

Carina Fabian

Luxembourg, December 2022

Contents

SCIENTIFIC ENVIRONMENT	2
ACKNOWLEDGEMENTS.....	3
CONTENTS.....	7
LIST OF PUBLICATIONS.....	10
LIST OF ABBREVIATIONS.....	12
ABSTRACT	17
GENERAL INTRODUCTION	19
1. TUMORS OF THE CENTRAL NERVOUS SYSTEM (CNS)	19
2. CLASSIFICATION OF BRAIN TUMORS	20
2.1. <i>Diffuse gliomas</i>	22
2.2. <i>Molecular characteristics of diffuse gliomas</i>	23
2.3. <i>Glioblastoma (GBM)</i>	26
2.4. <i>Glioblastoma subtyping based on gene expression</i>	28
2.5. <i>Standard of care and challenges of Glioblastoma treatment</i>	28
2.6. <i>Past and ongoing therapeutic approaches for Glioblastoma</i>	29
3. THE INVASIVE BEHAVIOUR OF GLIOBLASTOMA	32
3.1. <i>Routes of Glioblastoma cell invasion</i>	32
3.1.1. Invasion within the perivascular space	33
3.1.2. Invasion along white matter tracts	33
3.1.3. Invasion within the subarachnoid space.....	33
3.1.4. Invasion into the brain parenchyma	34
3.2. <i>Modes of Glioblastoma cell invasion</i>	34
3.2.1. Single cell invasion	34
3.2.2. Collective cell invasion	35
3.3. <i>Molecular mechanisms underlying the invasive behaviour</i>	36
3.3.1. The extracellular matrix (ECM) in Glioblastoma	36

3.3.2. The role of proteases and the tumor microenvironment during the invasive process in Glioblastoma	38
3.4. <i>The influence of metabolism on Glioblastoma cell invasion</i>	40
3.5. <i>Therapies aimed at targeting Glioblastoma cell invasion</i>	41
4. EXPERIMENTAL ASSAYS AND MODELS TO STUDY GLIOBLASTOMA CELL INVASION	44
5. PROTEIN DEGRADATION AND STRESS RESPONSE IN CANCER.....	46
5.1. <i>Protein degradation via autophagy</i>	46
5.2. <i>Protein degradation via the ubiquitin-proteasome system</i>	47
5.2.1. The process of ubiquitination	47
5.2.2. The process of protein degradation.....	49
6. CELLULAR STRESS RESPONSE	50
6.1. <i>Cytoplasmic stress granules</i>	51
6.1.1. Stress granule formation	51
6.1.2. Composition of stress granules	52
6.1.3. Stress granule clearance	53
6.1.3.1. Chaperones in stress granules	54
6.1.3.2. Valosin containing protein (VCP) in stress granules.....	54
6.1.3.3. Ubiquitin-proteasome system in stress granules.....	55
AIM OF THE THESIS	56
RESULTS	58
I. PAPER I: AN1-TYPE ZINC FINGER PROTEIN 3 (ZFAND3) IS A TRANSCRIPTIONAL REGULATOR THAT DRIVES GLIOBLASTOMA INVASION	58
II. PAPER II: THE ROLE OF ZFAND3 IN THE UBIQUITIN-PROTEASOME SYSTEM AND STRESS GRANULE CLEARANCE.....	59
III. PAPER III: LARGE-SCALE SHRNA INTERFERENCE SCREEN TO UNRAVEL GLIOBLASTOMA CELL INVASION	60
DISCUSSION	61
1. METHODS TO IDENTIFY INVASION-RELATED GENES.....	61
2. SHRNA INTERFERENCE VERSUS CRISPR/Cas9 SCREENS	62

2.1. <i>Biological read-outs for genetic screens investigating invasion</i>	63
3. DIVERSE FUNCTIONS OF ZFAND3	65
3.1. <i>Relevance of proteasomal degradation in Glioblastoma</i>	66
3.2. <i>Cytoplasmic stress granules and their influence on Glioblastoma</i>	66
4. THE ROLE OF GPX7 IN CANCER CELL INVASION	67
CONCLUSIONS	70
I. PAPER I: AN1-TYPE ZINC FINGER PROTEIN 3 (ZFAND3) IS A TRANSCRIPTIONAL REGULATOR THAT DRIVES GLIOBLASTOMA INVASION	70
II. PAPER II: THE ROLE OF ZFAND3 IN THE UPS AND STRESS GRANULE CLEARANCE	70
III. PAPER III: LARGE-SCALE SHRNA INTERFERENCE SCREEN TO UNRAVEL GLIOBLASTOMA INVASION	70
FUTURE PERSPECTIVES	71
REFERENCES	73

List of publications

The following thesis will be based on the below mentioned publications and manuscripts:

I. AN1-type zinc finger protein 3 (ZFAND3) is a transcriptional regulator that drives Glioblastoma invasion.

Schuster A, Klein E, Neirinckx V, Knudsen AM, Fabian C, Hau A-C, Dieterle M, Oudin A, Nazarov PV, Golebiewska A, Muller A, Perez-Hernandez D, Rodius S, Dittmar G, Bjerkvig R, Herold-Mende C, Klink B, Kristensen BW, Niclou SP. Nat Commun. 2020 Dec 11; 11(1): 6366. doi: 10.1038/s41467-020-20029-y.

II. The role of ZFAND3 in proteasomal degradation.

Fabian C, Eiden K, Dieterle M, Klein E, Fritah S, Perez Hernandez D, Niclou SP. Manuscript.

III. Large scale shRNA interference screen to unravel Glioblastoma invasion.

Fabian C, Nazarov PV, Schuster A, Sarnow K, Kanli G, Golebiewska A, Bjerkvig R, Niclou SP. Manuscript.

IV. Novel facets of glioma invasion. ¹

Fabian C, Han M, Bjerkvig R, Niclou SP. Int Rev Cell Mol Biol. 2021; 360: 33-64. doi: 10.1016/bs.ircmb.2020.08.001. Epub 2020 Oct 17. Review.

¹ Parts of this review were used for the general introduction, but will not be further mentioned within the thesis. Therefore, this review is also not attached in the thesis.

Additional publications that are not further discussed in this thesis:

V. Protocol for the derivation of organoids and patient-derived orthotopic xenografts from glioma patient tumors.

Oudin A, Baus V, Barthelemy V, Fabian C, Klein E, Dieterle M, Wantz M, Hau A-C, Dording C, Bernard A, Michelucci A, Yabo YA, Kanli G, Keunen O, Bjerkgvig R, Niclou SP, Golebiewska A.

STAR Protoc. 2021 May 12; 2(2): 100534. doi: 10.1016/j.xpro.2021.100534. eCollection 2021 Jun 18.

VI. Compound screening of primary and paired recurrent high-grade glioma patient tissues identifies stage selective vulnerabilities for epigenetic inhibitors.

Hau A-C, Klein E, Nazarov P, Fabian C, Fritah S, Oudin A, Wantz M, Kink B, Stieber D, Kwon YJ, Golebiewska A, Niclou SP. Manuscript in preparation.

List of abbreviations

ACTR1A	Actin-Related Protein 1A
ADAMs	A disintegrin and metalloproteinases
ADAMTSs	A disintegrin and metalloproteinases with thrombospondin motifs
AMPA	Alpha-amino-3-hydroxy-5-methyl-4-isoxazolepropionate
ATP	Adenosine triphosphate
ATRX	alpha thalassemia/mental retardation syndrome X-linked
Ca ²⁺	Calcium ion
Cas9	CRISPR associated protein 9
CDKN2A/B	Cyclin dependent kinase inhibitor 2A and 2B
CIC	Capicua Transcriptional Repressor
CK2	Casein kinase 2
Cl ⁻	chlorine
CNS	Central nervous system
Co-IP	Co-immunoprecipitation
COL6A2	Alpha-2 subunit of type IV collagen
CRISPRa	CRISPR activation
CRISPRi	CRISPR interference
CTLA-4	Cytotoxic T-lymphocyte associated protein 4
Cx43	Connexin 43
CX4945	Silmitasertib
Depatux-M	Depatuxizumab mafodotin
DRiPs	Defective ribosomal products
DUBs	Deubiquitinases
E1	Ubiquitin-activating enzyme

E2	Ubiquitin-conjugating enzyme
E3	Ubiquitin ligases
ECM	Extracellular matrix
EGFR	Epidermal growth factor receptor
EGFRvIII	Epidermal growth factor receptor variant III
eIF2 α	Eukaryotic translation initiation factor 2 subunit alpha
EphA3	Ephrin type-A receptor 3
FAK	Focal adhesion kinase
FDA	Food and drug administration
FLNA	Filamin A
FN1	Fibronectin 1
FUBP1	Far Upstream Element Binding Protein 1
G3BP1	Ras-GTPase-activating protein SH3-domain binding protein 1
GADD34	Growth arrest and DNA damage-inducible protein 34
GBM	Glioblastoma Multiforme
G-CIMP	CpG island methylator phenotype
GCN2	General control nonderepressible 2
GK	Glycerol Kinase
GluR1	Glutamate ionotropic receptor AMPA type subunit 1
GPX	Glutathione Peroxidase
GPX7	Glutathione Peroxidase 7
GRP78	78 kDa glucose-regulated protein
GTF2H1	General Transcription Factor IIH subunit 1
H ₂ O ₂	Hydrogen peroxide
HCFC1	Host cell factor C1

HRI	Hemeregulated eukaryotic translation initiation factor 2 alpha kinase
IDH	Isocitrate dehydrogenase
IL-1 β	Interleukin beta 1
IL-6	Interleukin 6
iPSCs	Induced pluripotent stem cells
IRE1	Inositol-requiring enzyme 1
IvyGAP	Ivy Glioblastoma Atlas Project
IRF3	Interferon regulatory factor 3
K ⁺	Potassium
KHSRP	KH-type splicing regulatory protein
LAG3	Lymphocyte activation gene 3
MAP4K4	Mitogen-activated protein kinase 4
MAPK	Mitogen-activated protein kinase
MGMT	O-6-methylguanine-DNA methyltransferase
MHC	Major histocompatibility complex
MMAF	Monomethyl auristatin F
MMP	Matrix metalloproteinase
MRI	Magnetic resonance imaging
mRNA	Messenger RNA
mRNPs	Messenger ribonucleoproteins
MT1-MMP	Membrane type-1 matrix metalloproteinase
mTOR	Mammalian target of rapamycin
MVP	Microvascular proliferation
Na	sodium
NF1	Neurofibromatosis type 1

Nrf2	Nuclear factor erythroid 2-related factor 2
NKCC1	sodium-potassium-chlorine cotransporter 1
NLS	Nuclear localization sequence
NRCAM	Neuronal cell adhesion molecule
PD-1	Programmed cell death 1
PDGFRA	Platelet derived growth factor receptor alpha
PD-L1	Programmed cell death ligand 1
PDOX	Patient-derived orthotopic xenograft
PERK	PKR-like endoplasmic reticulum kinase
PI3K	Phosphatidylinositol 3-kinase
PKR	Protein kinase R
PTEN	Phosphatase and tension homolog
Rac1	Rac family small GTPase 1
ROS	Reactive oxygen species
sEPSCs	Spontaneous excitatory postsynaptic currents
SGs	Stress granules
sgRNA	Single guide RNA
shRNA	Short hairpin RNA
siRNA	Small interfering RNA
SPARC	Secreted protein acidic and rich in cysteine
suPAR	Soluble urokinase-type plasminogen receptor
TCA	Tricarboxylic acid cycle
TERT	Telomerase reverse transcriptase
TGFBR1	Transforming growth factor beta receptor 1
TGF- β	Transforming growth factor- β

THBS1	Thrombospondin-1
TIA-1	T-cell intracellular antigen 1
TIM3	T cell immunoglobulin and mucin domain- containing protein 3
TMs	Tumor microtubes
TMZ	Temozolomide
TNF- α	Tumor necrosis alpha
TP53	Tumor protein 53
TTFs	Tumor treating fields
ULK1/2	Unc-51 like autophagy activating kinase 1 and 2
uPA	Urokinase-type plasminogen
UPR	Unfolded protein response
UPS	Ubiquitin-proteasome system
VCP	Valosin containing protein
VEGFR	Vascular endothelial growth factor receptor
WHO	World Health Organization
ZFAND3	AN1-type Zinc Finger Protein 3

Abstract

Glioblastoma (GBM) represents the most devastating brain tumor in adults. Its characteristic ability to extensively invade into healthy brain structures forms a major challenge in regard to treatment as these diffusely invading cells evade local and systemic therapy. GBM invasion therefore represents a leading cause for therapy resistance and tumour recurrence, resulting in a dismal prognosis of around 15 months. This highlights the need to better understand the mechanisms underlying the invasive phenotype of GBM cells.

The following thesis is based on a previously performed short hairpin RNA (shRNA) interference screen that was utilized for the identification of novel invasion-promoting and invasion-inhibiting genes in GBM. This genome-wide shRNA interference screen was done in a highly invasive patient-derived GBM cell line using an *in vitro* Boyden chamber invasion assay and led to the identification of candidate genes potentially involved in GBM invasion.

Following bioinformatic analyses, various candidate genes of interest were identified, from which some were selected for further investigation. One of the top hits from the invasion-promoting gene list was the AN1-type zinc finger protein 3 (*ZFAND3*), which we were able to identify as a novel driver of GBM cell invasion through the transcriptional regulation of invasion-related genes. We showed that a knockdown of *ZFAND3* reduced *in vitro*, *ex vivo* and *in vivo* invasion of invasive GBM cells, whereas its overexpression enhanced the invasion capacity of initially non-invasive GBM cells. We further determined that this activity required *ZFAND3* nuclear localization and its two integral zinc finger domains.

Proteomic analyses revealed a range of proteasomal subunits and ubiquitin-associated proteins as potential interaction partners of *ZFAND3*, suggesting an involvement in proteasomal protein degradation. This hypothesis was strengthened by the cytoplasmic localization of *ZFAND3* and by the fact that several other *ZFAND* proteins (*ZFAND1*, *ZFAND2A*, *ZFAND2B*, *ZFAND5* and *ZFAND6*) were already shown to be implicated in the ubiquitin/proteasome system (UPS) and stress response signalling. Indeed, we found that *ZFAND3* directly interacts with ubiquitin and with the ATP-selective

ATPase valosin containing protein (VCP, also known as p97). Furthermore we found that ZFAND3 is involved in the clearance of sodium arsenite-induced stress granules.

Additional candidate genes that were selected for further investigation included glutathione peroxidase 7 (*GPX7*) as potential invasion-promoting candidate gene, and glycerol kinase (*GK*), the general transcription factor IIIH subunit 1 (*GTF2H1*) and the actin-related protein 1A (*ACTR1A*) as putative invasion-inhibiting candidate genes. We show that the knockdown of *GPX7* reduced the *in vitro* and *ex vivo* invasion potential of invasive GBM cells, while its overexpression enhances the invasive capacity of initially non-invasive GBM cells. Overexpression of *GK*, *GTF2H1* or *ACTR1A* led to decreased invasion *in vitro* and partially *ex vivo*.

In conclusion, these results highlight the relevance of the shRNA interference screen as a powerful tool to identify novel drivers and inhibitors involved in the invasive process of GBM cells. In addition, we also started to unravel the cytoplasmic function of ZFAND3, which includes its potential involvement in the UPS and in the clearance of stress granules.

General introduction

1. Tumors of the central nervous system (CNS)

Brain and spinal tumors represent a heterogeneous group of neoplasms located in the central nervous system (CNS), which can develop as primary or secondary tumors. The more frequently occurring secondary brain tumors represent tumors that are not originating within the CNS, but metastasize from their tissue of origin into the brain. In contrast, primary brain tumors have their origin within the brain [1] and usually do not metastasize out of the brain.

The group of primary brain tumors can be separated into non-malignant and malignant tumors. The majority of primary brain tumors (almost 70%) is non-malignant, with meningiomas being the largest group. The remaining 30% represent the malignant primary brain tumors, where the greatest proportion (81%) corresponds to diffuse gliomas. Among diffuse gliomas, Glioblastoma (GBM) is the most abundant and most aggressive tumor type (**Figure 1**). Interestingly, non-malignant brain tumors occur more frequently in females (64%) compared to males (36%), whereas for malignant brain tumors males (55.4%) are slightly more often affected than females (44.6%). In general, the incidence for primary brain tumors rises with increasing age with an average age of 60 years at diagnosis [2]. Gliomas represent a rather rare tumor type with an annual incidence of 23.41 per 100.000 persons in the United States. Glioma patients with a younger age at diagnosis have a better outcome, indicating that age is prognostic factor [2]. Yet, primary brain tumors form the most frequently occurring solid tumors in infants and children aged 0-14 years and are also the most common reason for a cancer-related death in this age group [3].

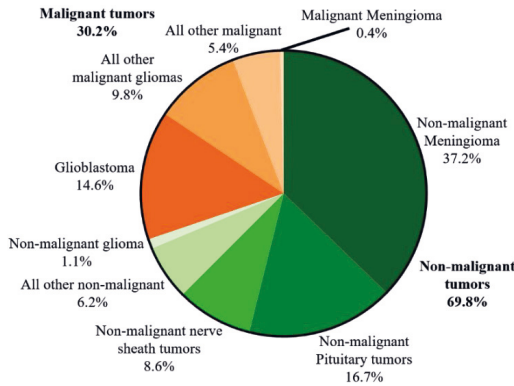


Figure 1: The distribution of non-malignant (shades of green) and malignant (shades of orange) primary brain tumors and other CNS tumors. Data from the US Cancer Statistics between 2012 and 2016. Adapted from [2] and created with Microsoft Powerpoint.

The only known risk factor for glioma development in children as well as adults is ionizing radiation of the head and neck during childhood. In addition, it was shown that a history of allergies may have a protective value with regard to gliomas as this reduces the risk for glioma development by around 30% [4, 5]. Interestingly, only 5% of gliomas have a familial component [6], while the remaining 95% occur sporadically without any known genetic predisposition. Up to now, no preventive measure for glioma development is known [7].

2. Classification of brain tumors

Among primary brain tumors, gliomas represent the most abundant type of malignant tumors, which used to be classified and graded based on their histological characteristics. As the World Health Organization (WHO) classifications on CNS tumors are regularly updated, the latest 2021 WHO classification also incorporates molecular features [8]. In general, tumors are grouped into different tumor families, where some tumors are identified based on shared genetic alterations (e.g. specific genetic mutations). Other tumors, as for instance glioneuronal and neuronal tumors that show varying molecular markers, are also grouped based on histological similarities.

Gliomas, glioneuronal tumors and neuronal tumors form the largest family that is subdivided into six subgroups: adult-type diffuse gliomas, pediatric-type diffuse low-grade gliomas, pediatric-type diffuse high-grade gliomas, circumscribed astrocytic gliomas, glioneuronal and neuronal tumors as well as ependymomas [8] (**Figure 2**).

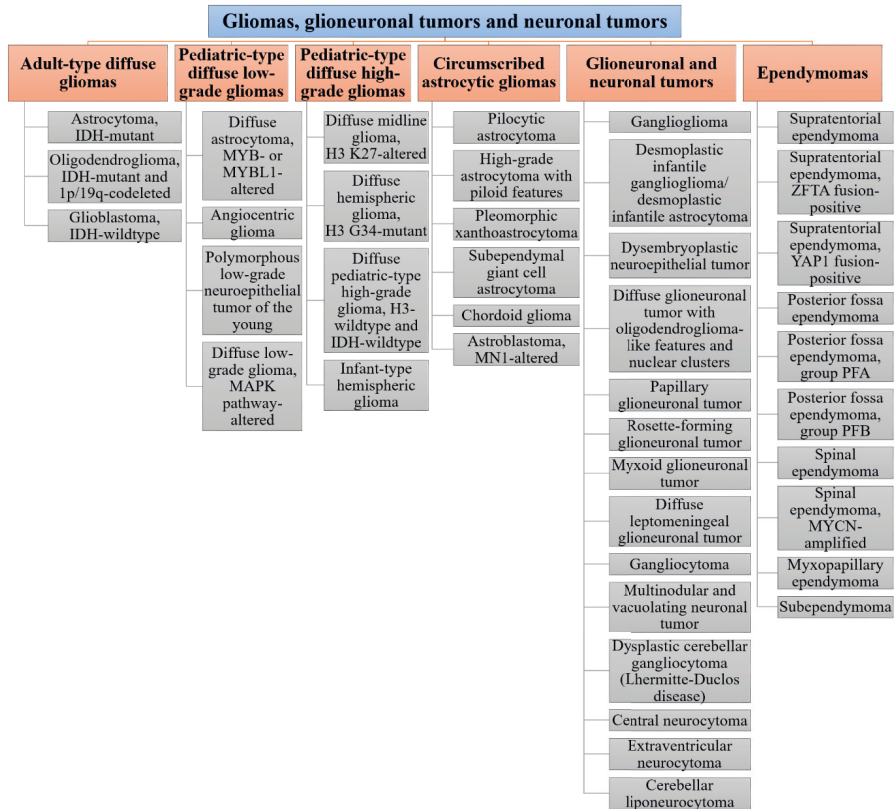


Figure 2: The current WHO classification of gliomas, glioneuronal and neuronal tumors. Adapted from [8] and created with Microsoft Powerpoint.

The individual tumor types are further assigned to one of four WHO grades, with grade 4 representing the most aggressive tumors with the worst prognosis. While this grading was based only on histological characteristics during the last decades, the current WHO classification also adds molecular markers as some specific molecular alterations have a prognostic value. This means that in certain cases molecular factors can add

information to the histological assessment and help in the assignment of a WHO grade [8]. Based on this, low-grade gliomas (grade 1 and 2) can be distinguished from high-grade gliomas (grade 3 and 4), which is reflected in the significant differences in patient survival. While the prognosis for low-grade glioma patients after maximal treatment lies between 10 to 15 years [9], high-grade gliomas, in particular GBM, have an estimated survival rate of only 12-14 months following standard of care therapy [10].

2.1. Diffuse gliomas

As the name indicates diffuse gliomas are defined by their ability to extensively invade into healthy surrounding brain structures. In contrast, non-diffuse gliomas like pilocytic astrocytomas and ependymomas display a slower and more circumscribed tumor growth [11, 12]. With increasing grade, diffuse gliomas display a faster and more aggressive disease progression and a higher degree of phenotypic heterogeneity. Lower-grade diffuse gliomas display a slower progression, but still represent deadly diseases as they also display a diffuse tumor cell infiltration into surrounding healthy brain structures and frequently transform to high-grade gliomas [13].

Diffuse gliomas can be divided into glioneuronal tumors and neuronal tumors. Among those, diffuse gliomas in children (pediatric-type) are distinguished from adult-type diffuse gliomas based on their molecular and prognostic differences (**Figure 2**). Pediatric-type diffuse gliomas are subdivided into low-grade gliomas, which have a predictable good prognosis, and high-grade gliomas, that display an aggressive phenotype [8].

Adult-type diffuse gliomas form the most abundant group of primary brain tumors in adults and are categorized into three distinct tumor types: (1) astrocytoma IDH-mutant, (2) oligodendroglioma IDH-mutant and 1p/19q-codeleted, and (3) Glioblastoma (GBM) IDH-wild-type [8]. These tumor types are further assigned to specific WHO grades based on a histological assessment and aggressive growth behaviour. An astrocytoma IDH-mutant can be assigned a WHO grade 2, 3 or 4, whereas an oligodendroglioma IDH-mutant and 1p/19q-codeleted can be WHO grade 2 or 3. In contrast, GBM IDH-wild-type tumors always corresponds to a WHO grade 4 [7].

2.2. Molecular characteristics of diffuse gliomas

The latest WHO classification (2021) incorporates several molecular features of diffuse gliomas as additive information to the histological assessment for tumor classification as described in **Figure 3** and discussed below:

- Mutations of the isocitrate dehydrogenase gene (*IDH*): The metabolic enzymes IDH1 (cytosolic) and IDH2 (mitochondrial) are responsible for the catalysis of isocitrate to α -ketoglutarate through a reversible oxidative decarboxylation [14]. The mutation of IDH1 at amino acid 132 confers a novel activity to the enzyme, converting α -ketoglutarate into the onco-metabolite D-2-hydroxyglutarate. IDH2 can be mutated at amino acid 172, although such mutations occur less frequently [15, 16]. Pathways that rely on α -ketoglutarate as substrate or co-factor are impaired by IDH1 mutations. Consequently, IDH1 mutations cause alterations of histone marks and aberrant DNA methylation. IDH mutant gliomas are characterized by DNA hypermethylation on specific CpG islands, leading to a CpG island methylator phenotype (G-CIMP) [17].
- Nuclear expression of the alpha thalassemia/mental retardation syndrome X-linked (*ATRX*): The transcriptional regulator ATRX is involved in chromatin remodelling, specifically at the chromosome ends (telomeres). Mutations of ATRX, which result in a loss of nuclear ATRX protein expression have been shown to be associated with an alternative lengthening of telomeres [18], promoting cellular longevity.
- Co-deletion of the two chromosome arms 1p and 19q: The 1p/19q co-deletion results in the loss of potential tumor suppressor genes like Far Upstream Element Binding Protein 1 (*FUBP1*) (on 1p) and Capicua Transcriptional Repressor (*CIC*) (on 19q) [7]. Chromosomal deletion of 1p and 19q is characteristic for oligodendroglioma [19] and is associated with a favourable patient outcome [20].
- Homozygous loss of the cyclin dependent kinase inhibitor 2A and B (*CDKN2A/B*): The tumor suppressors CDKN2A/B form important components of cell cycle regulation machinery, where its loss is associated with increased proliferation [21].

- Mutations of the telomerase reverse transcriptase (TERT) promoter: Mutations in the TERT promoter have been shown to activate telomerase activation, resulting in a lengthening of telomeres and consequently in cellular longevity [22].
- Genetic amplification of the epidermal growth factor receptor (EGFR): As a classical proto-oncogene, an amplification of the receptor tyrosine kinase EGFR leads to an activation of signalling pathways associated with cell proliferation, invasion as well as apoptosis resistance [7].
- Gain of chromosome 7 and loss chromosome 10: The gain of chromosome 7 involves genes like EGFR or the platelet derived growth factor alpha (PDGFA), which positively affect glioma progression. The loss of chromosome 10 leads to the loss of tumor suppressor genes like MGMT and phosphatase and tensin homolog (PTEN) [7].
- Mutations of the histone variant 3.3 G34R/V and histone 3 K27M: As structural components of nucleosomes that organize DNA, histones are critically involved in all DNA-related processes like gene expression, DNA repair or DNA replication [23]. Missense mutations in histones, and specifically in histone tails, can cause a deregulation of chromatin remodelling and epigenetic regulation of gene expression subsequently influencing genomic stability. Such mutations are often observed in pediatric gliomas, including amino acid substitutions in the tails of histone 3.3 at position 34 and histone 3 a position 27 [24].
- Promoter methylation of the O-6-methylguanine-DNA methyltransferase (MGMT): The promoter methylation of the DNA repair gene MGMT represents so far the only predictive factor for the response to therapy with the DNA-alkylating agent temozolomide (TMZ). GBM patients with a methylated MGMT promoter have an increased survival when treated with a combination of radio-and chemotherapy with TMZ, whereas patients without this methylation barely benefit from a TMZ-based chemotherapy [25]. The predictive power of MGMT methylation for DNA-alkylating-based therapy is restricted to wild-type IDH tumors [26].

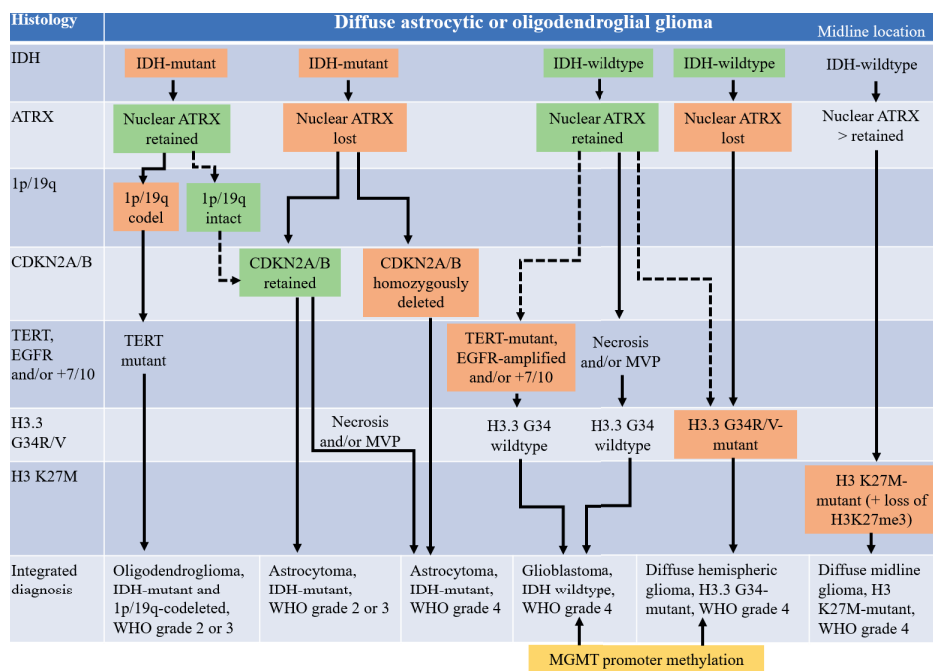


Figure 3: Classification of diffuse gliomas based on molecular markers. Green shapes represent markers that are wild-type, intact or present, while orange shapes correspond to markers that are mutated, deleted, amplified or lost. In yellow the MGMT promoter methylation is shown. Adapted from [7] and created with Microsoft Powerpoint.

According to the 2021 WHO classification diffuse gliomas are defined as follows:

An IDH mutation, a retained nuclear ATRX expression and a co-deletion of the two chromosome arms 1p and 19q are the molecular determinants for the diagnosis of an oligodendroglioma, IDH-mutant and 1p/19q-codeleted, WHO grade 2 or 3, which may also carry TERT mutations [7, 11]. An IDH mutation, lost ATRX expression and intact 1p/19q chromosome arms defines an astrocytoma, IDH-mutant. Additional loss of CDKN2A/B or the presence of necrosis and/or microvascular proliferation (MVP) assigns these tumors a WHO grade 4. The deletion of CDKN2A/B was found to have a prognostic impact and is associated with a reduced patient survival [7, 21, 27].

The diffuse hemispheric glioma, H3.3 G34-mutant, WHO grade 4 is defined by a wild-type IDH, a mutation in the position G34 of histone 3.3 and ATRX expression loss [7,

28]. Another histone mutation, in histone 3 at position K27, classifies together with a retained nuclear ATRX expression and a wild-type IDH the predominantly pediatric-type diffuse midline glioma, H3 K27M-mutant, WHO grade 4, which occurs in midline structures like the pons, the spinal cord, the thalamus and the brainstem [7, 11].

A Glioblastoma, IDH wild-type, WHO grade 4 is classified based on the presence of wild-type IDH and nuclear ATRX expression. GBMs do not show a deletion of the two chromosome arms 1p and 19q or the genetic loci for CDKN2A/B [7, 8, 29, 30]. The presence of necrosis and/or MVP displays an optional criterion for the classification of GBM as in their absence three additional molecular events are assessed. This includes EGFR amplification, TERT promoter mutation and the combination of chromosome 7 gain and chromosome 10 loss. Even if such tumors would be assigned a WHO grade 2 or 3 after histological assessment, the presence of one or more of these molecular events classifies them as WHO grade 4 [7, 29].

2.3. Glioblastoma (GBM)

Among adult-type diffuse gliomas GBM represents the most common primary brain tumor in adults [8] with an age-adjusted overall incidence of 3.22 out of 100.000 persons in the United States [2] (**Figure 4**). The incidence of GBM rises with age with a median age of 65 years and a peak between 75-84 years. In addition, the age at diagnosis plays a prognostic role and males are slightly more affected than females [2].

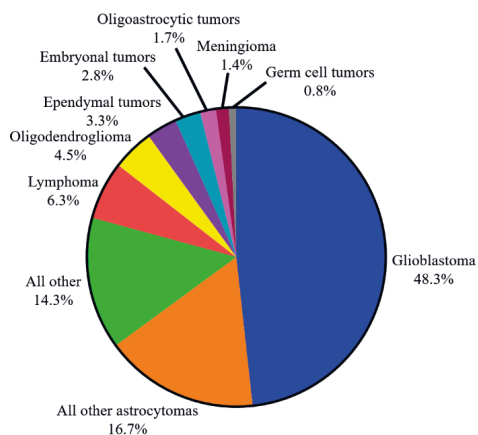


Figure 4: The distribution of malignant primary brain tumors and other CNS tumors based on histology. Data from the US Cancer Statistics between 2012 and 2016. Adapted from [2] and created with Microsoft Powerpoint.

Even though the cellular origin of GBM has not been elucidated, it is thought that GBMs develop from neuroglial progenitor cells [31]. Typical characteristics of GBM include nuclear atypia, high mitotic activity, diffuse infiltration, pseudo-palisading necrosis, MVP [11] as well as a prominent molecular and cellular heterogeneity [32]. Based on these features GBM forms the most aggressive tumor type among the adult-type diffuse gliomas. This is reflected by a low 5-year overall survival rate of only 6.8% [2], with a median patient survival of around 12-14 months [10] and a median survival of 24-44 weeks following tumor recurrence [33].

The majority of GBMs are diagnosed upon onset of neurological symptoms, which include focal neurologic deficits like impaired neuro-cognitive processes, epileptic seizures, vomiting, continuous headaches, vision problem, loss of appetite and an alteration of consciousness that are augmented to a large extent by an increased intracranial pressure [34, 35]. GBMs are usually detected by magnetic resonance imaging (MRI) showing a contrast-enhancing tumor surrounded by non-enhancing regions including edema and tumor infiltration (**Figure 5A and 5B**). Frequently, a multi-centric enhancement, haemorrhage and cystic abnormalities are also visible by MRI [36]. The infiltrative growth of GBM cannot be visualized to full extent by MRI. The final diagnosis of a GBM requires besides the histological assessment of the tumor (**Figure 5C**) also the presence or absence of specific molecular markers.

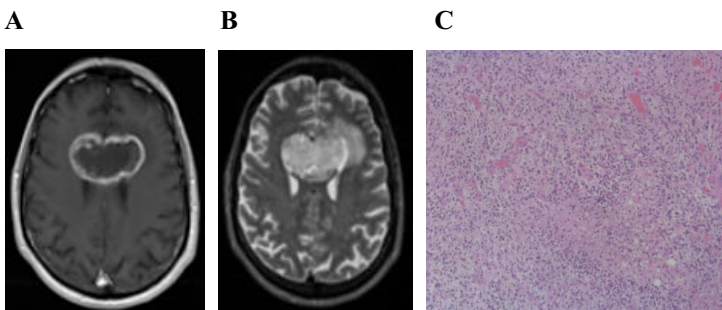


Figure 5: MRI images of a GBM patient taken from the cancer imaging archive [37]. **(A)** A T1-weighted MRI picture including contrast enhancement with gadolinium. **(B)** A T2-weighted MRI image. **(C)** Histological tissue section of a human GBM stained with haematoxylin-eosin. Kindly provided by Dr. Michel Mittelbronn.

2.4. Glioblastoma subtyping based on gene expression

Based on transcriptional profiling, three GBM subtypes have been proposed: proneural, classical and mesenchymal [38]. To some extent these subtypes correlate with specific genetic alterations. The proneural subtype is often linked to PDGFRA amplification as well as IDH1 and tumor protein 53 (TP53) mutations. The classical subtype is often associated with a combination of chromosome 7 gain and chromosome 10 loss as well as a CDKN2A/B deletion. In the mesenchymal subtype many tumors display abnormalities of the tumor suppressor genes neurofibromatosis type 1 (NF1) and PTEN [38, 39] (these studies were performed before the 2021 WHO classification). The clinical relevance of these subtypes is currently unclear as none has a predictive value in regard to therapy response [31]. More advanced technologies, like single-cell RNA sequencing point out that GBMs do not contain cells from just one subtype, but rather represent a mixed cell population of multiple subtypes [32]. Recent evidence indicates that GBM cells are highly plastic. It is, for instance, frequently noted that GBMs switch their transcriptional subtype upon recurrence [40]. It remains to be seen to what extent transcriptional subtyping may become useful for clinical decision making.

2.5. Standard of care and challenges of Glioblastoma treatment

The standard treatment of GBM includes a maximal safe resection, which is followed by concomitant radio- and chemotherapy with TMZ [10]. The extent of tumor resection correlates with a prolonged patient survival [41], especially in recurrent GBM [42]. Still, tumor recurrence is inevitable. The invasive behaviour of GBM constitute a clinical challenge as these cells are not targeted by local therapies like surgery and radiotherapy and form a reservoir of GBM cells that facilitate recurrence. When the tumor recurs, no standard of care exists. Repeated surgery or radio- and chemotherapy

can be considered, although the overall survival after recurrence is around 30 weeks [43]. Other factors that make GBM treatment difficult include the high proliferative rate, inter- and intratumoral heterogeneity and the presence of a largely intact blood-brain barrier. An additional difficulty can arise from the frailty of the often elderly patients, which may have comorbidities, tolerate therapy-related toxicities less, need longer to recover and have a worse prognosis compared to younger patients [44, 45].

A therapy option that impacts GBM cell proliferation and invasion are tumor treating fields (TTFs) [46], which are thought to affect the mitotic spindle apparatus during cell division through low intensity, intermediate frequency alternating electric fields [47]. TTFs were shown to increase the median overall survival of newly diagnosed GBM patients to around 21 months when combined with TMZ [48]. Still, this therapy is controversially debated within the field of neuro-oncology. Reasons why TTFs are not used as a standard therapy include the high device costs [49], major practical implications for the patient and the notion that it is not clear which patients will benefit from this treatment [50]. In patients with recurrent GBM the survival benefit of TTFs is comparable to that obtained with chemotherapy as shown in a phase III trial [51].

2.6. Past and ongoing therapeutic approaches for Glioblastoma

A wide range of drugs has been tested for GBM treatment from which only a few made it into phase III trials. Unfortunately none has shown a therapeutic benefit. Efforts have been made for the establishment of new treatments involving the development of potentially better drugs for the same target, trying new drug combinations, developing drugs for novel targets or initiating innovative drug delivery systems. Below is a list of the most important drug targets that have been under investigation during recent years:

- **EGFR:** EGFR affects proliferation, angiogenesis and invasion [52]. Over 50% of GBMs harbour EGFR alterations [53], with EGFR variant III (EGFRvIII) being the most abundant. It is defined by a truncated extracellular domain, inducing constitutive and ligand-independent receptor activation [54]. EGFR and EGFRvIII are attractive therapy targets, yet monoclonal antibodies or small molecule tyrosine kinase inhibitors did not show efficacy in GBM patients [55]. This includes the antibody cetuximab, which did

not reach phase III trials due to lack of efficacy in earlier studies [56, 57]. The antibody nimotuzumab made it into a phase III trial, but did not cause a survival benefit in newly diagnosed GBM patients [58]. Sym-004, a combination of the antibodies futuximab and modotuximab against distinct epitopes on EGFR, was tested on recurrent GBM patients in a phase II trial (NCT02540161), but no results are published yet. The antibody GC1118, which had an anti-tumoral effect in mouse models [59], is currently tested in a phase II trial for recurrent GBM patients with EGFR amplification (NCT03618667). None of the tyrosine kinase inhibitors against EGFR reached phase III trials, including erlotinib [60, 61], gefitinib [62, 63], afatinib [64] and dacomitinib [65].

- **PI3K/AKT/mTOR:** This pathway is often upregulated in GBM and includes the kinases phosphatidylinositol 3-kinase (PI3K), AKT and the mammalian target of rapamycin (mTOR). PI3K inhibitors, like buparlisib [66] and sonolisib [67], were not effective in recurrent GBM in a phase II clinical trial. The AKT inhibitor enzastaurin did not show a survival benefit in a phase III clinical trial in recurrent GBM [68]. The mTOR inhibitors temsirolimus [69] and everolimus [70] were unsuccessful in newly diagnosed GBM patients in a phase II clinical trial. Anti-AKT agents in preclinical studies include perifosine [71] and MK2206 [72]. In an ongoing phase II clinical trial the mTOR inhibitor ABI-009 is tested in newly diagnosed GBM patients (NCT03463265).
- **Anti-angiogenic therapy:** GBM is a highly vascularized tumor, suggesting angiogenesis as effective target, especially the vascular endothelial growth factor receptor (VEGFR) and its ligand VEGF [73]. Unfortunately, agents against VEGFR, like tyrosine kinase inhibitors and monoclonal antibodies, did not show clinical efficacy. This includes cediranib, an inhibitor blocking all three VEGFRs, which did not prolong the survival of patients with recurrent GBM in a phase III trial [74]. Also, the anti-VEGFR antibody bevacizumab did not result in an improvement of overall survival of newly diagnosed GBM patients in two large phase III clinical trials [75, 76]. The failure of anti-VEGFR therapies may be explained by other factors influencing angiogenesis and compensating for a VEGFR inhibition, like c-MET [77]. A phase I clinical trial in newly diagnosed GBM patients using crizotinib, which blocks the receptor tyrosine kinases c-MET and ALK, is in progress (NCT02270034). Also, the anti-VEGFR-2 antibody tanibirumab is

assessed in an ongoing phase II clinical study on recurrent GBM (NCT03856099). The multi-kinase inhibitor regorafenib, which also targets VEGFR-2, was tested on recurrent GBM patients in a phase II trial and showed a survival benefit [78].

- **Immune checkpoint inhibitors:** Immune checkpoints regulate immune responses by modulating T-cell activation [79]. The effector cell activation is influenced by the balanced signalling of stimulatory and inhibitory receptors. Inhibitory receptors include cytotoxic T-lymphocyte associated protein 4 (CTLA-4), programmed cell death 1 (PD-1), lymphocyte activation gene 3 (LAG3) and T cell immunoglobulin and mucin domain-containing protein 3 (TIM3). An upregulation of inhibitory checkpoint pathways is linked to GBM progression [80]. Almost 90% of GBM cells express the programmed cell death ligand 1 (PD-L1) [81]. The anti-PD-1 antibody nivolumab was unsuccessful in newly diagnosed GBM patients in a phase III trial (NCT02617589). Recent phase I trials use the alternative immune checkpoints LAG3 and TIM3 either as single agents or combined with anti-PD-1 therapy (NCT02658981 and NCT02817633). A combination of nivolumab and the anti-CTLA4 antibody ipilimumab is currently tested in a phase III clinical trial in recurrent GBM patients (NCT02017717).
- **Proteasome inhibitors:** The proteasome regulates protein degradation [82]. In GBM the proteasome degrades several essential proteins triggering the activation or deactivation of cancer-associated pathways [83]. Various proteasome inhibitors have been tested in clinical trials. Among those, bortezomib showed promising effects in combination with standard of care in a phase II study, especially in patients with MGMT promoter methylation [84]. A more recently developed proteasome inhibitor is marizomib, which crosses the blood-brain-barrier. After a successful assessment in phase I and II studies, a phase III trial in newly diagnosed GBM patients is ongoing (NCT03345095) [85].
- **Oncolytic viruses:** Therapy with oncolytic viruses can be based on viruses that are used as vectors for therapeutic gene delivery or viruses designed to infect tumor cells without affecting surrounding healthy cells [86]. Oncolytic viruses have gained attention in GBM therapy and are currently tested in clinical studies for their efficacy. This includes among others, engineered adeno, parvo and herpes simplex viruses (reviewed in [80]).

- **Vaccines:** Among vaccines, peptide-based are distinguished from cell-based vaccines. Peptide-based vaccines focus on antigen epitopes from upregulated or mutated GBM-specific proteins. For cell-based vaccines, antigen-presenting cells are isolated from patients, expanded and stimulated *ex vivo* and injected back into the patients. Currently such vaccines are tested in clinical trials for their efficacy in GBM (reviewed in [87]).

A problem for most therapies is the invasion of GBM cells that may evade local and systemic therapies and form a source for tumor recurrence. This highlights the need to better understand the mechanisms underlying GBM cell invasion. As we published a review on GBM invasion (paper IV), the most important aspects are described below.

3. The invasive behaviour of Glioblastoma

Although cells have an inherent ability to move, cell movement is tightly regulated in the healthy organism and limited to defined processes like embryonic development or immune surveillance. In cancer cells this physiological cell movement is deregulated leading to uncontrolled motility and tissue disruption. With regard to cell motility two mechanisms can be distinguished, namely migration and invasion. While cell migration refers to an active cell movement on a surface, invasion is defined as cell movement, which requires prior disruption of the tissue-specific matrix the cell is invading into. Cell invasion plays an important role in diffuse gliomas and in particular GBM, which is characterized by an extensive invasion potential into surrounding brain structures. In contrast to other solid tumors, which use the blood and lymphatic system as route for metastasis, intravasation of GBM cells into blood vessels rarely occurs [88]. Instead to facilitate their invasion GBM cells use pre-existing routes in the brain.

3.1. Routes of Glioblastoma cell invasion

As early as in 1938, the German neuropathologist Hans-Joachim Scherer carried out a comprehensive study where he serially sectioned the brains of 100 GBM patients and examined the tumor and the surrounding brain. He found that the tumors preferentially

migrate along pre-existing brain structures such as blood vessels, white matter tracts and the leptomeningeal space, which are today known as the Scherer's structures [89].

3.1.1. Invasion within the perivascular space

GBM cells show extensive invasion along vascular structures, in particular the cerebrospinal fluid-filled perivascular space (Virchow Robin Space). Here, the tumor cells have access to extracellular matrix (ECM) components of the basal lamina of endothelial cells, as well as the glia limitans, the physical barrier of the blood brain barrier formed by astrocytic end feet. The implantation of GBM cells into the rodent brain has shown that most cells outside the tumor bulk locate in proximity to blood vessels, suggesting perivascular invasion as frequent GBM invasion route (**Figure 6A**) [90]. Preclinical studies showed that this is at least partially due to the bradykinin release from endothelial cells, resulting in activation of the bradykinin receptor and intracellular calcium (Ca^{2+}) changes in GBM cells, suggesting bradykinin 2 receptor antagonists like Icatibant as potential targets to interfere with GBM invasion [91, 92].

3.1.2. Invasion along white matter tracts

In 1928, the neurosurgeon Walter Dandy performed brain hemispherectomies to cure GBM patients. These efforts failed since contralateral tumor recurrences were observed in the opposite hemispheres. By this, it was realized that GBM cells migrate over long distances along white matter tracts from the primary tumor mass to the contralateral hemisphere [93]. The white matter is composed of myelinated axons connecting various brain compartments, such as the corpus callosum between the two hemispheres. These structures represent ideal 'highways' for cell movement along parallel fiber spaces, a phenomenon also observed in pre-clinical models (**Figure 6B**) [90].

3.1.3. Invasion within the subarachnoid space

The subarachnoid space represents the cerebrospinal fluid-filled area between the arachnoid layer and the pia mater. It is part of the meninges that separates the brain

from the skull. Since the subarachnoid space is continuous with the perivascular space, it also represents an, albeit less common, route for GBM cell invasion. GBM cells that invade the perivascular space may reach the surface of the brain and continue to invade the subarachnoid space. This route most likely involves a dissemination of single cells mediated by the shear flow of the cerebrospinal fluid and active cell movement [94].

3.1.4. Invasion into the brain parenchyma

Gliomas further diffusely infiltrate the neuropil of the gray matter composed of neuronal cell bodies and glial cells (**Figure 6C**). Compared to the nerve fibers and blood vessels, the parenchyma is of a softer matrix but with a high cellular density providing more physical hindrance for cell movement [90]. The patterns of invasion in this context may be subdivided into single cell and collective cell invasion.

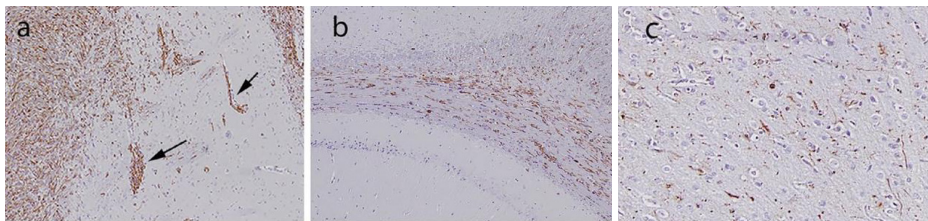


Figure 6: Routes of GBM cell invasion shown in a patient-derived xenograft model after implanting a human GBM orthotopically into immunodeficient rats [95, 96]. **(A)** GBM cell invasion within perivascular spaces. **(B)** GBM cells invading along white matter tracts. **(C)** Single GBM cells invading the gray matter [90].

3.2. Modes of Glioblastoma cell invasion

3.2.1. Single cell invasion

Single cell invasion can occur in the form of amoeboid or mesenchymal invasion. Amoeboid invasion is a rather fast process that involves a weak adhesion with limited proteolytic ECM degradation. It is characterized by rapid changes in cell shape and the development of filopodia allowing cells to scan their environment and move through small gaps in the matrix [97]. It was shown that this process is accompanied by a

reduction in cell volume (30–35%) which relies on potassium (K^+) and chlorine (Cl^-) channels expelling unbound water from the cytoplasm. Inhibitors of these K^+ and Cl^- channels were found to reduce cell migration *in vitro* [98], pointing at a potential therapy option. This includes the food and drug administration (FDA)-approved drug bumetanide blocking the sodium-potassium-chlorine (Na-K-Cl) cotransporter NKCC1, which was shown to influence GBM cell migration. Yet it should be emphasized that bumetanide shows limited blood brain barrier penetration [99].

Mesenchymal invasion, in contrast, is characterized by cells adopting an elongated, spindle-like shape. It represents a slow and complex process, which is associated with integrin-mediated adhesion and proteolytic ECM degradation [100]. GBM cells were shown to preferentially invade as single cells or small groups in a mesenchymal mode irrespective of the used invasion path [13].

It has become evident that tumor cells can switch between amoeboid and mesenchymal invasion, indicating that these processes are highly dynamic involving a migratory plasticity in response to changes in the brain microenvironment. It appears that changes in ECM stiffness can influence the transition between these two invasion modes [101].

3.2.2. Collective cell invasion

In contrast to single cell invasion, collective cell invasion is characterized by the coherent movement of groups of cells maintaining contact with each other [102]. The presence of cell-cell junctional processes between tumor cells is accompanied by a reorganization of the actin cytoskeleton. A number of leading cells, which sense and process potential guidance signals mediate invasive traction (Haeger et al., 2015).

The concept of collective invasion has gained renewed momentum following the discovery of tumor microtubes (TMs) in GBMs, which may increase in number during tumor progression [103]. Generally larger than nanotubes, these TMs represent long (>500 μ m) and thin (1-2 μ m) filamentous membrane protrusions. It is postulated that TMs represent tracks for invasion by establishing large networks of glioma cells. The TM network may vary according to the tumor type, the ECM microenvironment and its anatomical location. For instance, TMs were described in astrocytomas of various

grades, including GBM, but not in oligodendrogliomas. TM networks functionally connect and coordinate communication between astrocytoma cells. This connection is facilitated by gap junctions, which form channels allowing molecular exchange between cells like Ca^{2+} . Inhibition of intracellular Ca^{2+} waves through the cellular networks reduced their invasion capacity. As a component of gap junctions connexin 43 (Cx43) plays a role in TM-linked connections between astrocytoma cells [103]. In addition, GBM cell invasion is promoted by a Cx43-mediated communication between GBM cells and astrocytes at the tumor border. *In vitro* and *ex vivo* GBM cell invasion was reduced, when surrounding astrocytes were deficient for Cx43 [104].

Besides Cx43, also the armadillo repeat-containing protein p120-catenin is required for TM-mediated cell-cell interactions as it induces adherens junctions during collective migration [105]. Knockdown of either Cx43 or p120-catenin impaired TM formation and glioma cell invasion [103, 105]. Interestingly, such multicellular connections may also render GBM cells resistant to chemo- and radiotherapy while single tumor cells could be eradicated more effectively by these treatments [103, 106].

A recent study showed that the transforming growth factor- β (TGF- β) can increase TM formation and calcium-mediated communication between GBM cells. Blocking the TGF- β cascade resulted in a decrease of TMs and in a reduced *in vitro* and *in vivo* GBM cell invasion [107].

3.3. Molecular mechanisms underlying the invasive behaviour

3.3.1. The extracellular matrix (ECM) in Glioblastoma

The ECM represents an important substrate for glioma cell invasion, comprising around 20% of the adult brain volume [108]. The ECM composition varies depending on the invasion location (**Figure 7**). In the perivascular space the ECM is rather rigid based on the presence of laminins, collagens, fibronectin, heparan sulfate, entactin and vitronectin [108-110]. In contrast, the normal brain parenchyma contains a softer ECM with tenascin-C, thrombospondin (THBS1), hyaluronan, glycosaminoglycans and various proteoglycans as main components [108]. Glioma cells have the ability to adapt to these different ECMs at the transcriptional and metabolic level [111]. An

upregulation of THBS1, tenascin-C and secreted protein acidic and rich in cysteine (SPARC) has been observed in the perivascular space, whereas in the brain parenchyma, a downregulation of versican and THBS1 has been reported, accompanied by an upregulation of hyaluronan, vitronectin, osteopontin, collagens and tenascin-C [108, 112]. THBS1 is known to be involved in angiogenesis, yet recently it has been shown that TGF β 1 can induce THBS1 expression thereby contributing to the invasive behaviour of GBM cells [113]. Tenascin-C, which besides resident glia is also produced by glioma cells, was found to be overexpressed in the GBM infiltrative areas where it supports invasion while reducing proliferation [114]. In addition, integrin transmembrane receptors are important for cell-cell and cell-matrix interactions and can influence GBM cell invasion. For instance, integrin β 1, involved in tenascin-C signalling, is upregulated at the mRNA level in GBM compared to normal brain tissue (GlioVis portal: <http://gliovis.bioinfo.cnio.es/> [115]). GBM cell invasion is further promoted by an enhanced integrin β 1-mediated adhesion to ECM factors and by the phosphorylation of the focal adhesion kinase (FAK) as well as activation of the Rac Family Small GTPase 1 (Rac1) [116]. The expression of FAK was found to be upregulated in glioma cells, particularly in infiltrating areas [117].

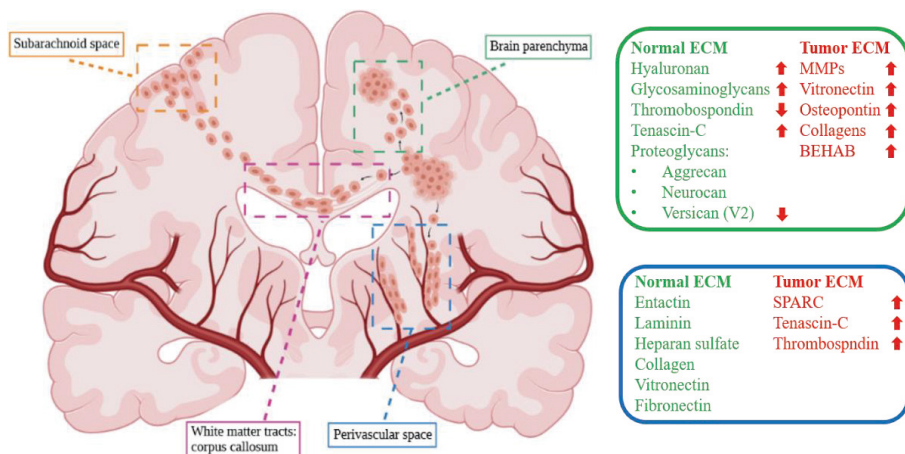


Figure 7: Paths used by GBM cells to invade the brain tissue. The corresponding ECM composition in these brain areas and the modulations of the ECM structure during the invasion process are indicated. Adapted from [108] and created with BioRender.com.

3.3.2. The role of proteases and the tumor microenvironment during the invasive process in Glioblastoma

Glioma cell invasion involves the degradation of the brain ECM, which can be mediated by several proteases, like matrix metalloproteinases (MMPs), urokinase-type plasminogen activator (uPA), cathepsins, a Disintegrin and Metalloproteinases (ADAMs) and ADAMs with Thrombospondin motifs (ADAMTSs) (**Figure 8**) [88].

One important group of proteases are MMPs, which are endopeptidases involved in tissue remodeling through the proteolytic degradation of various ECM proteins. Although non-malignant cells like endothelial cells, microglia and macrophages can also secrete MMPs, glioma cells are the main source of these proteases. Especially the secreted MMP-2 and MMP-9 as well as MT1-MMP (membrane type 1-matrix metalloproteinase, also known as MMP-14) play important roles in GBM invasion and their expression is correlated with tumor grade (Hagemann et al., 2012; Hatoum et al., 2019). This is confirmed by public databases showing an upregulation of these MMPs at the mRNA level compared to normal brain. All three MMPs also show the highest expression in GBM compared to astrocytoma and oligodendroglioma (<http://gliovis.bioinfo.cnio.es/> [115]). GBM cell expression of MT1-MMP can be induced, at least *in vitro*, by interleukin-6 (IL-6) released by astrocytes [118]. In this context, it has also been shown that tumor-associated microglia and macrophages express MT1-MMP. MT1-MMP supports glioma cell invasion by the proteolytic cleavage of glioma cell-derived pro-MMP-2 into its active form [119].

uPA is a serine protease involved in ECM degradation. The secretion of uPA occurs as soluble pro-uPA and requires activation via plasmin-mediated cleavage. Another important ECM-degrading molecule in GBM is the lysosomal cysteine protease cathepsin B, which is involved in direct and indirect pro-uPA and pro-MMP activation, including MMP-2 and MMP-9 [88]. According to the Gliovis data portal, cathepsin B and uPA mRNA are highly upregulated in GBM compared to normal brain and lower grade gliomas [115]. Moreover, uPA has been reported to be preferentially expressed at the invasive front of GBM (Colin et al., 2009). GBM cell invasion is also promoted through the cross-talk between GBM cells and reactive tumor-associated astrocytes.

This crosstalk can induce the interaction between uPA and its corresponding receptor uPAR on the astrocyte surface resulting in the activation of plasmin, which can in turn activate MMP-2 and thereby promote GBM cell invasion [120].

Furthermore, GBM cells harbouring EGFRvIII have been shown to upregulate the expression of uPAR and the release of soluble uPAR (suPAR), resulting in enhanced suPAR plasma levels. By this, suPAR can activate cell signalling in a paracrine fashion to stimulate GBM cell migration and invasion independent of uPA. An increase of uPAR expression was observed upon addition of exogenous EGF, which was diminished by the EGFR tyrosine kinase inhibitor AG1478. The reduced uPAR expression upon EGFR blockade is compensated by an uPA upregulation, which could explain the resistance to anti-EGFR therapies frequently seen in GBM patients [121].

Also, the metalloproteinases ADAMs and ADAMTSs affect cell adhesion through integrin interactions via their disintegrin domain [122]. They can also act as 'sheddas' by cleaving the extracellular fragment of transmembrane proteins to release soluble ectodomains. Particularly ADAMTS-4/5 are upregulated in GBM surgical samples and show confined expression in astroglial and GBM cells. *In vitro* expression can be increased by cytokines like interleukin-1 β (IL-1 β) and TGF- β , resulting in enhanced GBM cell invasion [88, 123]. ADAMTS-5 may also promote invasion through cleavage of the brain-specific ECM proteoglycan brevican. ADAM-17 may affect GBM invasion through its function as sheddase for activation of EGFR ligands such as tumor necrosis factor α (TNF- α) and TGF- β [122].

Endothelial cells, as components of the perivascular niche, have been shown to play a role in GBM invasion. Upon recruitment, they release large amounts of proangiogenic factors, like VEGF. The interaction between glioma cells and endothelial cells is controlled by an axis consisting of the growth factor angiopoetin 1 and the tyrosine kinase receptor Tie2, which further promotes GBM cell invasion [124]. Still, targeting angiopoetin 1 and 2 with the peptibody trebananib, a peptide fused to an antibody, did not prolong the survival of patients with recurrent GBM in a phase II study [125].

Interestingly, it was also found that the number of regulatory T cells is enhanced in glioma patients. In addition, invading glioma cells display a reduced expression of

major histocompatibility complex (MHC) class I and II molecules, suggesting that these infiltrative cells escape an immune response and can thereby invade the brain parenchyma without being sensed and attacked by the immune system [126].

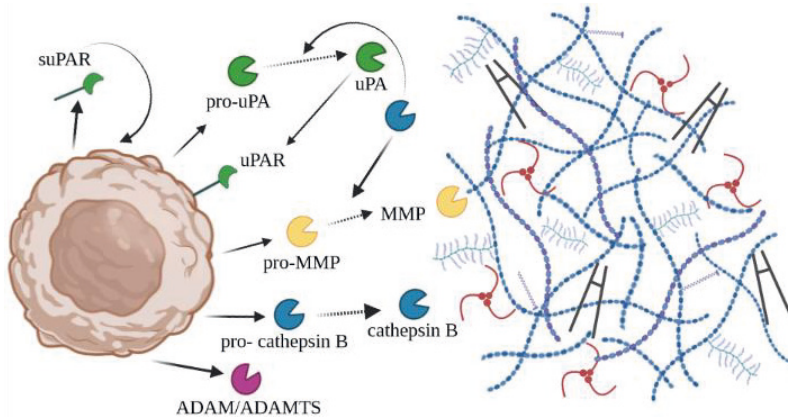


Figure 8: Proteases involved in the ECM degradation during GBM cell invasion. Adapted from [88] and created with BioRender.com.

3.4. The influence of metabolism on Glioblastoma cell invasion

The energy required for invasion and for the adaptation to different oxygen and nutrient concentrations can be facilitated by a reprogramming of the cellular metabolism [127]. This includes an upregulation of glucose transporters, which facilitates the enhanced uptake of glucose observed in GBM, which besides affecting signalling pathways also influence GBM cell invasion [128], as shown for the glucose transporter 3 [129].

As early as in 1999 it was recognized that GBM cells release considerable amounts of glutamate [130], which results in elevated glutamate levels in the tumor as well as in the surrounding environment [131]. It was shown that glutamate levels are reduced in clinical samples of lower grade IDH mutant gliomas compared to GBM [132]. This might be explained by the fact that in IDH mutant gliomas, glutamate is needed to fulfil metabolic demands, such as tricarboxylic acid (TCA) cycle replenishment in the absence of α -ketoglutarate. It may be that xCT transporters that export glutamate are less active in IDH mutant gliomas and instead glutamate may be taken up from the

surroundings [133]. The secretion of high glutamate levels confers a growth advantage to glioma cells transplanted into the rat brain [134]. This may be explained by the fact that high glutamate levels are excitotoxic [130], thereby killing nearby neurons and offering space for the tumor to expand and invade the surrounding brain tissue.

In addition, GBM cell-released glutamate acts in an autocrine fashion through Ca^{2+} -permeable α -amino-3-hydroxy-5-methyl-4-isoxazolepropionate (AMPA) receptors to stimulate cell motility via intracellular Ca^{2+} signalling [135]. In line with this, recent work suggests that TM networks underlie electrochemical communication through synapses between presynaptic neurons and postsynaptic GBM cells [136, 137]. Such neuro-gliomal synapses were found to elicit spontaneous excitatory postsynaptic currents (sEPSCs), including Ca^{2+} -permeable AMPA receptor associated currents. The AMPA receptors, specifically its most common subunit the glutamate ionotropic receptor AMPA type subunit 1 (GluR1), were shown to support perivascular GBM invasion. Pharmacological inhibition of AMPA receptors may lead to decreased glioma growth and to reduced Ca^{2+} -mediated invasion of TM-connected GBM cells [136].

3.5. Therapies aimed at targeting Glioblastoma cell invasion

Extensive glioma cell invasion into healthy brain structures represents a major clinical challenge. A problem is that GBM cells have invaded the brain far beyond the tumor core when clinical disease manifestations occur, which explains the high recurrence rates seen in patients. To target the diffuse infiltration of gliomas including GBM poses challenges. One of them is that the invasive cells are situated within CNS areas where the blood brain barrier represents a pharmacokinetic barrier for drug delivery. The notion of a pure anti-invasive strategy may therefore be futile. Still, reducing invasion would ideally complement current strategies of targeting the tumor core with surgery and radio-chemotherapy. Benefits of such combination treatments may lead to a more compact tumor that is potentially more drug-penetrable with a switch to a proliferative state rendering tumor cells more sensitive to anti-proliferative treatment [138].

Interestingly, it has been hypothesized that cell proliferation and invasion are mutually exclusive, indicating that GBM cells may either proliferate or invade but not both

simultaneously. This is supported by the notion that cells from the tumor core upregulate signalling of the mitogen-activated protein kinase (MAPK) pathway, favouring cell proliferation. In contrast, infiltrative GBM cells showed a reduced MAPK signalling, but an increased signalling through the AKT, corresponding to the activation of cell survival pathways [139]. Still, this phenomenon is highly debated as there are also studies reporting contrary observations [140, 141].

Nevertheless, it would be beneficial to reduce GBM cell invasion. Even though considerable advances have been made over the past decades, there is still no possibility to interfere with GBM invasion. To target GBM cell invasion, several agents were or are currently tested in clinical trials for their efficacy, which includes:

- MMPs: The use of broad-spectrum MMP inhibitors like marimastat failed to improve GBM patient survival in a phase II study [142]. These broad-spectrum MMP inhibitors result in musculoskeletal pain as major adverse effect and inhibit various MMPs, some of which may also have anti-tumoural functions [122]. To overcome these aspects the more specific inhibitor prinomastat was developed, which specifically targets MMP-2 and MMP-9. Unfortunately, also prinomastat failed to increase patient survival in a phase II study in combination with TMZ [143].
- TGF- β receptor 1 (TGFBR1): TGFBR1 is involved in the regulation of various cellular processes, including differentiation, proliferation, invasion and apoptosis. Therapeutic approaches have been unsuccessful so far, including galunisertib, a small molecule inhibitor, which did not show beneficial effects in a phase I/II trial [144].
- Ephrin type-A receptor 3 (EphA3): Among receptor tyrosine kinases, ephrin receptors together with their ligands are essential for the development of the nervous system as they control axon guidance, cell adhesion and migration in the brain [145]. The pathway of ephrins and their receptors is upregulated in invasive GBM cells compared to cells from the tumor core [146]. A recent phase I trial tested the monoclonal antibody KB004 against the ephrin receptor EphA3 to target GBM cell invasion (NCT03374943), but no results are published so far.
- Integrins: Integrins have been studied in GBM as they influence invasion through their function in cell adhesion. Latest efforts to target integrins in GBM were based on the

α v β 5 integrin antagonist cilengitide. The promising effect on GBM patient survival shown in a phase I/II study [147] was not confirmed in a phase III trial [148].

- **Fibulin-3**: Fibulin-3 is an ECM glycoprotein enriched in GBM. Its functional motif can be blocked by the antibody mAb428.2. In preclinical studies this inhibition resulted in an increase of apoptosis and in a reduction of invasion and vascularization [149].
- **Casein kinase 2 (CK2)**: The serine/threonine kinase CK2 negatively regulates interferon regulatory factor 3 (IRF3), a transcription factor repressing ECM genes, which support GBM invasion. Preclinical studies show that a CK2 blockade by the small-molecule inhibitor silmitasertib (CX4945) activates IRF3 and reduces GBM cell invasion [150].
- **Metabolic targets**: Attempts have been made to inhibit glutamate release and/or target glutamate receptors, which have been shown to be involved in neuro-gliomal synapse regulation [135, 151]. Furthermore, ion channels such as K⁺ and Cl⁻ channels as well as the ion transporter NKCC, for which the inhibitor bumetanide is available, are promising targets [99]. In addition, targeting calcium channels may be considered as a treatment option based on the important role of calcium signalling in GBM invasion. Mibefradil, a selective T-type calcium channel blocker was tested in a phase I study in recurrent GBM and reported that the combination with TMZ was well tolerated and showed response in some patients, highlighting the need for further studies [152].
- **Targeting cytoskeletal elements**: In general, cancer cell invasion can be impaired by targeting cytoskeletal elements directed towards actin (e.g. latrunculin A, cytochalasin D and jasplakinolide) and microtubules (e.g. vincristine, taxol and taxotere). With regard to GBM, a tubulin-binding peptide was found to be specifically taken up by GBM cell lines causing a reduction in GBM cell proliferation and motility *in vitro*, accompanied by a disruption of the microtubule network [153]. This drug appears to be still in pre-clinical development [154]. Another drug that interferes with microtubules is depatuxizumab mafodotin (Depatux-M), an antibody-drug conjugate linking the anti-microtubule agent monomethyl auristatin F (MMAF) to an antibody against EGFR. Depatux-M binds to EGFR and as soon as the complex is internalized MMAF is released, resulting in apoptosis [155]. A phase II study in recurrent GBM patients suggests a potential clinical benefit of Depatux-M in combination with TMZ [156].

4. Experimental assays and models to study Glioblastoma cell invasion

To study cell invasion, various experimental models are available with different degrees of physiological relevance. This ranges from basic *in vitro* assays to very laborious *in vivo* experiments. As cell invasion is a characteristic feature of GBM, it is of high importance to utilize appropriate experiments to capture GBM cell invasion in a reliable and reproducible way. Some assays to investigate GBM cell invasion (**Figure 9**) are summarized and briefly explained with their advantages and disadvantages. Except for the scratch assay, all mentioned models were also used in the present thesis.

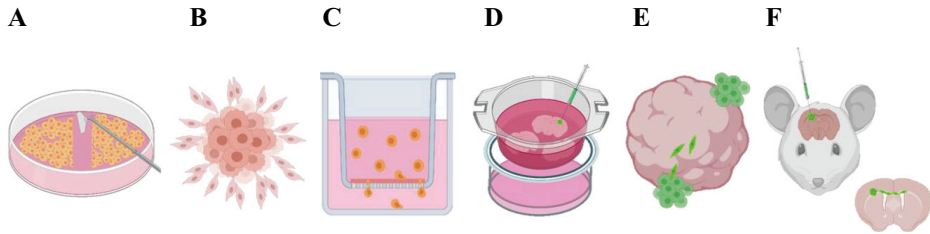


Figure 9: Representation of available models to study GBM cell invasion experimentally. Created with Microsoft Powerpoint and BioRender.com.

A: Scratch assay: A scratch is made into a confluent adherent cell monolayer, which can be covered with ECM. To close the «wound» the cells need to invade through the ECM, which can be measured and quantified. This assay is easy, cheap and fast to perform and can be used to study migration (without coating) and invasion (by covering the scratch with ECM). The low physiological relevance and the impact of proliferation form disadvantages.

B: Sprouting assay: Three-dimensional tumor spheroids are placed into a well coated with ECM and collagen and covered with ECM. The distance of cells moving away from the core can be quantified and corresponds to the invasive potential of the cells. This model is easy, cheap and fast to perform, but has a limited physiological relevance.

C: Boyden chamber assay: The membrane (0.8 μm pore size) of a 24-well insert is coated with an ECM-collagen layer. The cells are seeded on top of this matrix and

invade through it to reach the chemoattractant in the lower chamber. Invaded cells can be fixed and stained for quantification. This assay is easy, cheap and fast to perform and can be used to study migration (without coating) as well as invasion (with coating of the membrane). A major advantage here is that both invading cells (on the bottom of the membrane) and non-invading cells (remaining on the top of the membrane) can be separately collected and analysed. Disadvantages include the limited physiological relevance, the variability between assays and the impact of cell proliferation.

D: Murine brain slice cultures: A mouse brain is cut into 400 μm thin sections, which are cultured for a few days on 6-well inserts with 1 μm pore size before fluorescently labeled tumor cells are implanted directly above the corpus callosum. This model maintains the brain tissue architecture and allows the analysis of real-time single cell invasion in a mature brain tissue. As an *ex vivo* system, this is probably the closest system to recapitulate invasion in the adult brain. It requires animals, special equipment and sufficient technical expertise.

E: Brain organoid model: Brain organoids can be produced from human induced pluripotent stem cells (iPSCs) or from fetal rat brains, which can be co-cultured with fluorescently labeled tumor spheroids. Organoids reestablish to some extent the brain tissue architecture and allow high-throughput assessment. This model is time-consuming due to prior organoid differentiation and may be challenging to quantify depending on brain organoid size (up to 3mm) and image resolution.

F: Patient-derived orthotopic xenograft (PDOX): Patient-derived tumor cells are implanted orthotopically into the brain of an immunodeficient rodent. For invasion analysis, consecutive sections are microscopically imaged and tumor cells found away from the tumor core or in the contralateral hemisphere can be counted and quantified. This model shows the highest physiological relevance and allows studying invasion in a living organism. Still, the disadvantages include the requirement of special equipment and trained personnel. This model is based on animals, which does not allow for high-throughput. Additionally, imaging single cell invasion is difficult. Furthermore, this model is time-consuming because of the multiple handling steps (animal preparation, sectioning, immuno-histochemistry staining, data analysis).

5. Protein degradation and stress response in cancer

To ensure protein homeostasis, cells utilize protein quality control processes including protein folding and protein degradation processes like autophagy and the ubiquitin-proteasome system (UPS) [157]. By utilizing such processes cells remove misfolded and damaged proteins and thereby prevent an accumulation of defective and potentially harmful proteins, ensuring cellular integrity essential for normal cell physiology [158].

Compared to normal cells, cancer cells display a higher proliferation rate and consequently a higher demand for macromolecules, indicating the importance of functional protein synthesis. The enhanced proliferation and the genomic instability observed in cancer cells suggest that cancer cells compared to healthy cells rely more on efficient protein degradation systems to degrade misfolded, excessive and disrupted proteins [159]. This is supported by the fact that cancer cells show an increased proteasomal activity [160]. Still, before misfolded proteins are degraded, chaperones try to refold them. If this is not successful, the proteins are sent for degradation [158].

A deregulation of the main protein degradation mechanism, the UPS, can be associated with different malignancies like cancer [161, 162]. Such deregulations can be caused by a gain-of-function mutation in an ubiquitin-related enzyme leading to enhanced protein degradation or by a loss-of-function mutation stabilizing the substrates [163].

Autophagy plays a dual role in cancer cells. It can be tumor suppressive through the removal of damaged proteins and organelles, but can also serve as a survival mechanism for tumor cells through the regeneration of nutrients [164].

5.1. Protein degradation via autophagy

A major cellular degradation system forms autophagy, which is a process that stimulates the degradation of cytoplasmic components within specific organelles called lysosomes. Substrates targeted for autophagy can be of exogenous origin like bacteria or viruses as well as of endogenous origin including cytoplasmic protein aggregates, long-lived proteins and defective organelles like mitochondria [165, 166]. Autophagy can occur in three forms: (1) chaperone-mediated autophagy, which uses chaperones

for the lysosomal protein degradation, (2) microautophagy, which subjects substrates directly to the lysosome and (3) macroautophagy that depends on the formation of autophagosomes to sequester and subsequently degrade the substrate [166, 167].

The fact that autophagy requires lysosomal activity distinguishes it from proteasomal degradation, which functions independent of lysosomes [168]. The connection between autophagy and the proteasome is shown in cases of compromised proteasome activity, through proteasome inhibition or genetic alterations [169], which increases autophagic activity [170]. Reduced proteasomal activity causes an accumulation of ubiquitinated proteins, which can form protein aggregates that are too large to be degraded by the proteasome [171]. The link between autophagy and the proteasome is also shown by proteaphagy, a process in which defect proteasomes are degraded through autophagy, induced upon proteasome inhibition or mutations in proteasomal subunits [172].

5.2. Protein degradation via the ubiquitin-proteasome system

Besides autophagy, the UPS represents the main mechanism for the controlled degradation of unnecessary, disrupted or misfolded nuclear and cytoplasmic proteins in proliferating mammalian cells [82]. Its proper function is essential for the control of intracellular protein level and the maintenance of cellular processes [173]. The UPS, which is responsible for over 80% of intracellular protein degradation [174], is composed of the multi-catalytic 26S proteasome complex and the 76 amino acids long ubiquitin proteins. The 26S proteasome complex is built up by a 20S core particle, forming the catalytic component, and two 19S regulatory subunits (a base and a lid) (**Figure 10A**), which enable adenosine triphosphate (ATP) and ubiquitin-dependent protein degradation [82]. It is thought that the majority of the 26S proteasome complexes are inactive in cells and get rapidly activated upon stress induction [175].

5.2.1. The process of ubiquitination

The attachment of ubiquitin (ubiquitination) to a specific target protein requires three members of different enzyme families being an ubiquitin-activating enzyme 1 (E1), an ubiquitin-conjugating enzyme (E2) and an ubiquitin protein ligase (E3). E1 enzymes

utilize ATP for the C-terminal adenylation of ubiquitin, which is followed by a thioester bond between E1 and ubiquitin [176] and the transfer of ubiquitin to E2 enzymes. Besides activating E2 enzymes, E3 enzymes also catalyse the ubiquitin transfer from E2 enzymes to target proteins, which represents the last step of ubiquitination [177, 178] (**Figure 10B**).

Before transferring the ubiquitin from the E2 enzyme to the target protein, the substrate protein has to be recognized and bound by an E3 enzyme, which thereby plays a significant role in UPS specificity. Substrate proteins can be recognized either via primary signals that allow direct binding to E3 enzymes or require secondary signals for recognition. Primary signals represent specific structural motifs within the target protein, whereas post-translational modifications, like phosphorylation, form secondary signals for protein recognition. Additionally, ancillary proteins like chaperones can assist substrate recognition [163, 179].

An important determinant for the specificity of the UPS forms ubiquitination, which labels proteins for proteasomal degradation. Ubiquitination is reversible and can occur in different forms. This includes the attachment of a single ubiquitin (mono ubiquitin) as well as poly- or multi-ubiquitination at one of seven lysine residues (K6, K11, K27, K29, K33, K48 and K63) within the ubiquitin. The length and the linkage of the ubiquitin chains enhance specificity by determining distinct degradation processes [180]. The most abundant poly-ubiquitin chains are K48-linked (aggregated poly-ubiquitin) and subject proteins to 26S proteasome-mediated degradation [181], while mono ubiquitin or K63-linked linear poly-ubiquitin chains induce non-proteasomal mechanisms like autophagy or endocytosis [182].

Deubiquitinating proteins (deubiquitinases or DUBs) play an essential role during the process of protein degradation as they catalyse the removal of ubiquitin from target proteins (deubiquitination), which is required before a protein can be degraded [183]. With the removal of ubiquitin DUBs simultaneously remove the signal for proteasomal degradation and can thereby increase protein stability. Thus, DUBs can influence the cellular protein homeostasis [184]. Additionally, DUBs are involved in the restoration of the ubiquitin pool within a cell [185].

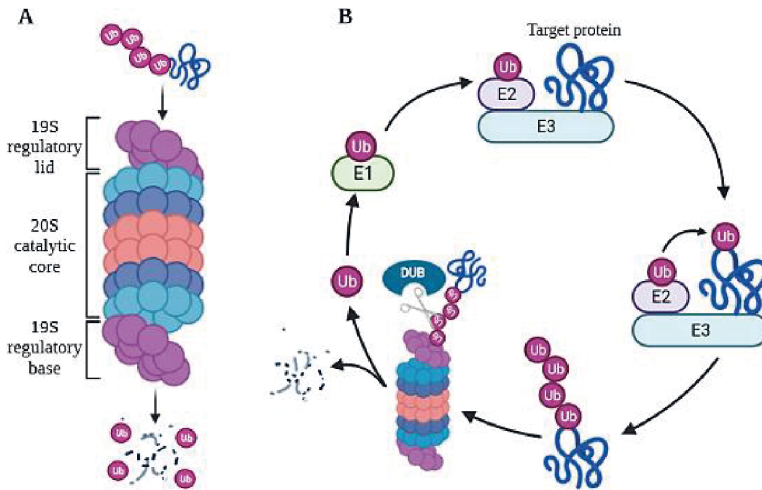


Figure 10: (A) The 26S proteasome complex involving the 20S catalytic core as well as the 19S regulatory lid and base. (B) Ubiquitin-dependent protein degradation by the 26S proteasome and the involved components facilitating ubiquitination. Ub: ubiquitin, E1: ubiquitin-activating enzyme, E2: ubiquitin-conjugating enzyme, E3: ubiquitin protein ligase and DUB: deubiquitinating protein. Created with BioRender.com.

5.2.2. The process of protein degradation

Ubiquitination of a protein does not represent the final determinant for its degradation. Also ubiquitinated proteins and even proteins that are already associated with the proteasome are not automatically degraded. In addition to recognizing ubiquitin, the proteasome also needs to recognize a region within the target protein that is loosely folded [186]. These two factors determine if a protein is degraded. Thus the proteasome is not an automated complex randomly degrading proteins, but makes a selective decision which proteins are degraded. The duration of proteasome-mediated substrate binding, referred to as dwell-time, determines if a protein is degraded. This occurs in a two-step process. Firstly, the ubiquitin chain attached to the target protein binds to receptors on the 26S proteasome. This binding is still reversible [183, 187]. The dwell-time can be affected by DUBs, which remove ubiquitin proteins and prevent degradation of the protein [188, 189]. However, once the loosely folded region of the target protein is tightly bound to the proteasome the activation of proteasome-

associated ATPases and subsequently the degradation of the protein is initiated [190]. Therefore, the 19S regulatory complex selects the ubiquitinated protein, unfolds it, removes the ubiquitin chains via 19S-associated DUBs and regulates its translocation to the 20S catalytic core, where hydrolysis of the protein into small peptides occurs, which are then available for *de novo* protein production [190] (**Figure 10A**).

6. Cellular stress response

Stressors are defined as stimuli, intrinsic or extrinsic, inducing a stress situation within the cell that requires adaptation. In response to stress, cells either activate survival pathways to adapt and survive the stress or undergo apoptosis if the stress is too severe and adaptation cannot be facilitated. This decision largely depends on the cell type and on the type and duration of the stress [191]. Rather than recognizing the stressor itself, cells usually sense the stress-induced insults like damaged DNA or a decrease in ATP synthesis. Upon stress detection, cells initiate signalling cascades, resulting in altered gene expression. Most stress factors trigger the induction of a network of integrated pathways to cope with the multiple damages a single stressor can cause. Stressors often target macromolecules like DNA, RNA, proteins or lipids, which negatively affects cellular integrity. Therefore, the first response to severe stress includes a cell cycle arrest to prevent the distribution of defective macromolecules, especially DNA [158].

Compared to normal cells, cancer cells are constantly exposed to a diverse range of intracellular and external stressors. Examples for intracellular stressors are mitotic, oxidative, metabolic and endoplasmic reticulum stress. External stressors include hypoxia, nutrient deprivation and DNA damage stress induced by chemotherapeutic agents [192-194]. In cancer cells the stress response can additionally be induced by an activated oncogene [195]. While normal cells would undergo apoptosis under such conditions, cancer cells are more plastic and able to adapt to such stressors. To do so, besides induction of genomic instability and mutations, cancer cells also trigger alterations in gene expression and metabolic signalling to circumvent growth arrest [196]. This is underlined by the finding that, compared to normal cells, cancer cells have a more pronounced basal level of stress response due to their high proliferative

rate, which requires an increased protein synthesis [195, 197]. Thus, the stress response can on the one hand promote cell survival and on the other hand favor apoptosis, thereby influencing tumor progression and therapy response [198].

6.1. Cytoplasmic stress granules

Upon cellular stress, cells induce adaptation mechanisms such as protection of macromolecules and conservation of energy [199]. Different stress situations like heat, oxidative stress or the exposure to chemicals (e.g. sodium arsenite) [200] can induce the formation of cytoplasmic stress granules (SGs) as an adaptive stress response. The most important function of SGs is to transiently store messenger RNAs (mRNAs) in stress conditions [201] and protect them from degradation [199]. Thus, SGs act as transient pro-survival structures assisting cells to overcome stressful situations [202]. SGs are transient and membrane-less aggregates with a diameter of 200-400 nm in mammalian cells [203], which form during liquid-liquid phase separation that induces liquid-like compartments of RNA and proteins in the cytoplasm. It is triggered by high local RNA and protein concentrations, which create a condensed compartment that behaves like a membrane-less organelle. This process can be supported by protein-protein and protein-RNA interactions driven by SG-mediated factors [204].

In cancer it was found that radio-or chemotherapy can promote SG formation, rendering tumor cells more resistant to treatment and consequently promoting tumor progression including metastasis. In this regard SGs represent an adaptive response to stress by protecting the cells from chemotherapy-induced apoptosis [193, 205].

6.1.1. Stress granule formation

Cellular stress may lead to a translation stop and a disassembly of polysomes, an aggregate of ribosomes on mRNA. The translation arrest is in most cases initiated by the phosphorylation of the eukaryotic translation initiation factor 2 subunit alpha (eIF2 α) [206], by one of four stress-sensing sentinel kinases: protein kinase R (PKR), PKR-like endoplasmic reticulum kinase (PERK), general control nonderepressible 2 (GCN2), or hemeregulated eukaryotic translation initiation factor 2 alpha kinase (HRI)

[207]. Stalled translation initiation complexes release ribosomal subunits, translation initiation factors and mRNAs, which upon recruitment of RNA-binding proteins form the substrate for the formation of SGs [199, 208]. Upon stress, SGs shelter mRNAs together with translation-related components, preventing stress-induced apoptosis and allowing a re-entry into translation once the stress is resolved [209].

The assembly of messenger ribonucleoprotein particles (mRNPs), which is mRNA bound to proteins, initiates SG formation that is stimulated by RNA-binding proteins like the Ras-GTPase-activating protein SH3-domain binding protein 1 (G3BP1) [210] and the T-cell intracellular antigen 1 (TIA-1) [211].

Upon stress G3BP1 is dephosphorylated at Ser-149, which induces its multimerization [210] that stimulates SG formation. Knockdown of G3BP1 leads to a reduction of SG formation [201]. G3BP1 plays also a role in liquid-liquid phase separation as G3BP1 can induce the RNA-dependent liquid-liquid phase separation upon increased intracellular concentrations of free RNA [212].

TIA-1 shuttles between the nucleus and the cytoplasm and shows a cytoplasmic accumulation upon stress [208]. TIA-1 contains three RNA-recognition motifs that facilitate RNA binding and a glutamine-rich prion-related domain, which allows self-association of the protein required for the formation of SGs [213].

6.1.2. Composition of stress granules

It was shown that depending on the type of cell, stress and disease condition, the composition of SGs can vary. Although hundreds of proteins were found as factors involved in the formation and clearance of SGs, the main components defining a SG include stalled pre-initiation complexes, translation initiation factors, nucleating RNA-binding proteins, like G3BP1 and TIA-1, mRNAs and core 40S ribosomal subunits [203, 214]. SGs are composed of a stable core and a more dynamic shell. While the core is defined as a region of high protein and mRNA concentration as well as a high level of protein-protein interactions, the surrounding shell is classified by a low protein and mRNA concentration. After the SG core is formed, additional proteins can be recruited to establish the more dynamic shell around the core [215, 216] (**Figure 11**).

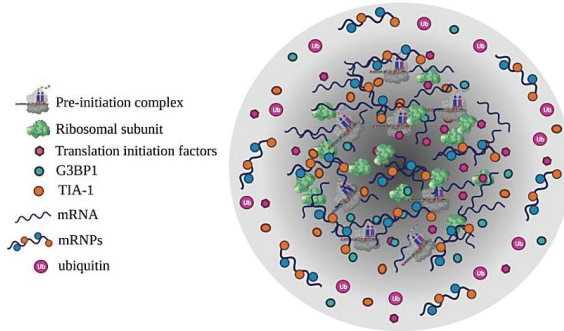


Figure 11: Main components of SGs. The darker area represents the core, while the lighter outer region displays the SG shell. G3BP1: Ras-GTPase-activating protein SH3-domain binding protein 1, TIA-1: T-cell intracellular antigen 1, mRNA: messenger RNA, mRNPs: messenger ribonucleoprotein particles. Created with BioRender.com.

6.1.3. Stress granule clearance

An essential characteristic of SGs is their dynamic nature. SGs form within minutes to hours upon stress and are cleared minutes (after cold shock [217]) to hours (after sodium arsenite [218]) after the stress is resolved. The clearance of SGs is important for normal cell physiology as a deregulated or non-efficient SG clearance results in an alteration of SG composition and dynamics. This may cause an accumulation of aberrant SGs, which persist longer than their normal counterparts. Aberrant SGs as well as mutations in SG-associated RNA-binding proteins are implicated in neurodegenerative diseases [203, 209]. While normal SGs form a response to stress, persistent SGs may suggest a pathological condition [219].

The clearance of SGs starts with the dissipation of the shell, which is followed by the clearance of the core [215]. An essential action for SG clearance is the dephosphorylation of eIF2 α , which is facilitated by the stress-stimulated phosphatase, growth arrest and DNA damage-inducible protein 34 (GADD34) or by the protein phosphatase CREP. This allows the re-initiation of translation [220]. The mode of SG clearance can be affected by several factors. One such factor is the duration of stress and hence the lifetime of SGs. Normal SGs are usually degraded via autophagy-independent mechanisms involving chaperones [213] or the 26S proteasome, while

persistent SGs are cleared by an autophagy-mediated process called granulophagy [221, 222]. Additional determinants for the mechanism of clearance represent the cell type and the type of stress [223].

6.1.3.1. Chaperones in stress granules

It is hypothesized that chaperones control the dynamic exchange of proteins between the SG core and the shell. A defective exchange negatively impacts SG kinetics and results in an accumulation of aberrant SGs [216]. The maintenance of SG composition and dynamics is called granulostasis, which defines the cellular SG homeostasis. Chaperones play an important role in granulostasis as they refold misfolded proteins within SGs. This includes the HSPB8-BAG3-HSP70 complex, which assures that defective ribosomal products (DRiPs) and misfolded proteins are sent for degradation. Like this, chaperones support the clearance of SGs before they become aberrant [224].

6.1.3.2. Valosin containing protein (VCP) in stress granules

VCP (valosin containing protein, also known as p97 or Cdc48) is a predominantly cytosolic ATPase that acts as an ubiquitin-selective and ATP-dependent segregase. VCP is important for maintaining protein homeostasis as it is involved in the UPS through the segregation of ubiquitinated proteins from protein aggregates, chromatin or membranes [225, 226]. Thus, VCP is required in various ubiquitin-mediated processes [227]. Additionally, VCP is essential for endolysosomal trafficking and autophagy of ubiquitinated substrates, defective lysosomes and SGs [221, 228, 229].

VCP is an essential component for the maintenance of granulostasis. It is involved in SG clearance through supporting the proteasomal degradation of ubiquitinated SG proteins [218], but also facilitates the clearance of aberrant SGs through autophagy (granulophagy) [221]. To initiate the autophagy-dependent clearance of SGs, the unc-51 like autophagy activating kinase 1 and 2 (ULK1/2) induces the phosphorylation and subsequent activation of VCP [230]. The importance of VCP in SG clearance is shown by the observation that mutations in VCP hinder an efficient SG clearance, resulting in an accumulation of aberrant SGs often linked to pathogenesis [221].

6.1.3.3. Ubiquitin-proteasome system in stress granules

It is becoming evident that the UPS is involved in SG granulostasis as VCP [221] and the 26S proteasome [218] have been shown to associate with SGs. Also ubiquitin associates with SGs. This was predominantly seen in the dynamic shell of SGs and the abundance of ubiquitin varied among SGs induced by different stressors. More specifically, ubiquitin associated with SGs in form of K48- or K63-linked conjugates. The K48-linked ubiquitin chains were shown to co-localize with VCP and the proteasome at the periphery of SG cores [231]. This is in line with the association of VCP and the 26S proteasome with SGs to facilitate their clearance [218, 221]. The SG clearance is negatively affected by blocking the ubiquitin system [231] or by inhibiting the 26S proteasome, which results in aberrant SGs, suggesting that the 26S proteasome supports SG clearance through the degradation of ubiquitinated proteins from SGs, which cannot be refolded by the HSPB8-BAG3-HSP70 chaperone complex. Additionally, it seems likely that VCP supports the 26S proteasome in that process as it was shown to be essential for an efficient SG clearance [218].

So, an efficient SG clearance requires the combined action of the HSPB8-BAG3-HSP70 chaperone complex [224], VCP and the 26S proteasome [218] (**Figure 12**).

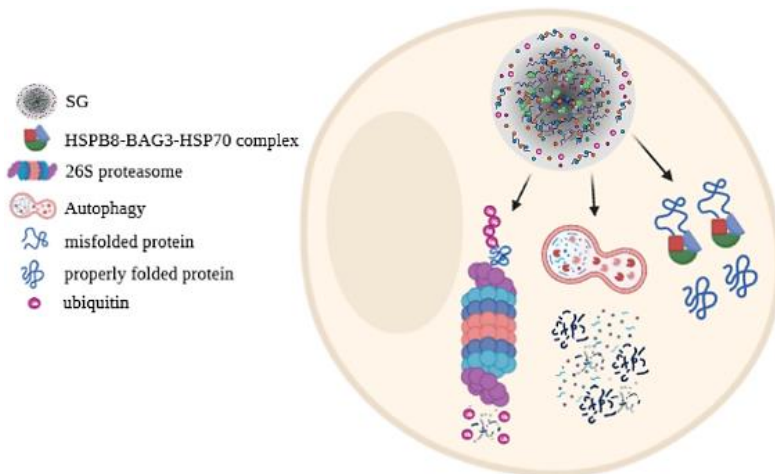


Figure 12: Mechanisms facilitating SG clearance, including proteasomal degradation, autophagy and the HSPB8-BAG3-HSP70 complex. Created with BioRender.com.

Aim of the thesis

The ability of GBM cells to extensively invade into normal brain structures forms a major challenge in the treatment of this aggressive brain tumour. Current therapy options are limited and, in particular, no treatment specifically targets the invasive GBM cells. Therefore, the aim of this PhD project was to identify novel genes involved in the invasive process of GBM cells and to propose new targets for treatment.

This work is based on a whole-genome shRNA interference screen previously performed in the lab to identify novel invasion-related genes in GBM (**Figure 13**).

The specific aims included:

- To characterize potential invasion-promoting and invasion-inhibiting genes in GBM selected from a large-scale shRNA interference screen and validate their involvement in GBM cell invasion by using *in vitro* and *ex vivo* invasion models.
- To unravel additional functions of identified proteins.

These specific aims were reached by:

- I.** The identification of ZFAND3 as novel driver of GBM cell invasion
- II.** The elucidation of the potential involvement of ZFAND3 in the UPS and SG clearance
- III.** The analysis of additional invasion-related genes (*GPX7*, *GK*, *GTF2H1* and *ACTR1A*) at the functional level

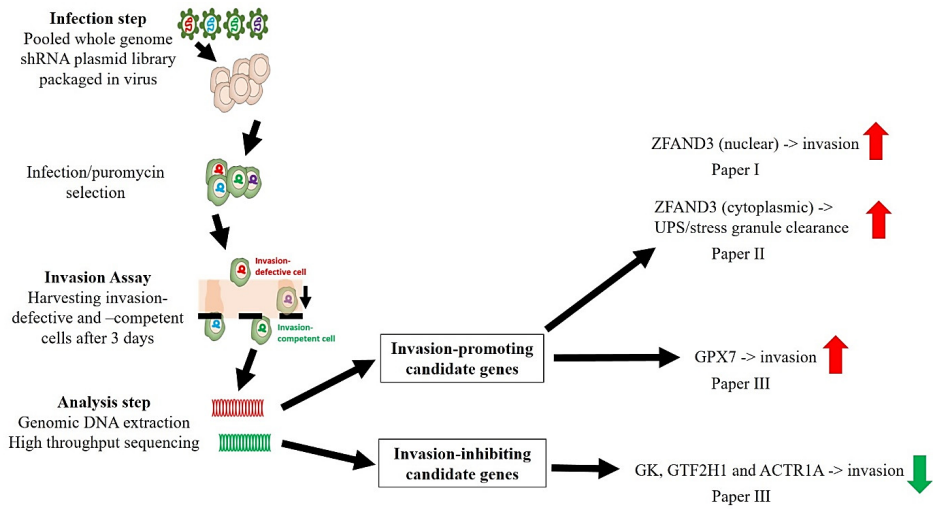


Figure 13: Schematic workflow of the performed shRNA interference screen, indicating the identified candidate genes that were used for further investigation.

Results

I. Paper I: AN1-type zinc finger protein 3 (ZFAND3) is a transcriptional regulator that drives Glioblastoma invasion

This paper focuses on GBM cell invasion and starts by introducing our patient-derived GBM cell lines and their invasive behaviours *in vitro*, *ex vivo* and *in vivo*. Based on several assay we could distinguish non-invasive, invasive and highly-invasive GBM cell lines. One of these highly-invasive GBM cell lines was used to perform a whole genome shRNA interference screen to identify novel invasion-promoting and -inhibiting genes in GBM. The analysis of the screen data, which focused on invasion-promoting genes, identified the zinc finger protein ZFAND3, one of the top hits among the invasion-promoting candidate genes. At first, we showed that ZFAND3 is more highly expressed in invasive GBM cell lines compared to non-invasive ones. Next, we confirmed a role of ZFAND3 in GBM cell invasion, since its downregulation reduced the invasion potential of invasive GBM cells, whereas its overexpression enhanced the invasive capacity of initially non-invasive GBM cells. In addition, we show the importance of the nuclear localization sequence (NLS) and the integral zinc finger domains (AN1 and A20). Indeed, the mutation of the NLS as well as the deletion of the zinc finger domains led to a loss of the invasive phenotype. To unravel ZFAND3's mechanism of action, we performed a RNA-sequencing on ZFAND3 knockdown cells, which revealed 58 downregulated genes. Gene ontology analyses linked these genes with migration- and invasion-related pathways. Among those genes we found the alpha-2 subunit of type VI collagen (*COL6A2*), the neuronal cell adhesion molecule (*NRCAM*) and fibronectin 1 (*FN1*), suggesting a transcriptional regulation of these genes by ZFAND3. Furthermore, we performed proteomic analyses to identify potential ZFAND3 interacting partners. Several of those proteins were involved in RNA regulation and transcriptional processes according to gene ontology analyses. We were able to show a direct interaction of ZFAND3 with the splicing factor PUF60 by co-immunoprecipitation (Co-IP). Mechanistically by using luciferase gene reporter assays and ChIP-qPCRs, we found that ZFAND3 associates with the promoter regions of *COL6A2*, *NRCAM* and *FN1* to regulate gene transcription, indicating that ZFAND3

acts as a transcriptional regulator of these invasion-related genes to promote the invasive behaviour of GBM cells (**Figure 15**).

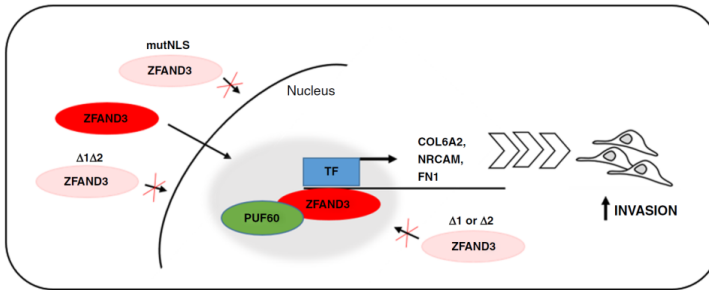


Figure 15: Schematic of the potential mechanism of action of ZFAND3 as nuclear transcriptional regulator of invasion-related genes to drive GBM cell invasion [232].

II. Paper II: The role of ZFAND3 in the ubiquitin-proteasome system and stress granule clearance

In the second paper we unravel the cytoplasmic functions of ZFAND3. As our protein-protein interaction studies pointed to an interaction of ZFAND3 with proteasomal subunits and several ZFAND members are known to be involved in the UPS system and stress response, we aimed here to investigate a similar role of ZFAND3. At first, we could validate that ZFAND3 is able to bind ubiquitin and that its N-terminal A20 domain is responsible for this binding. In addition, we were able to show in a Co-IP that ZFAND3 is directly interacting with VCP and that it co-localizes with transiently formed, cytoplasmic stress granules upon sodium arsenite-induced stress. Furthermore, we investigated the impact of ZFAND3 in the formation and clearance of sodium arsenite-induced stress granules. While the formation of stress granules was not affected by a modulation of ZFAND3 expression, we found that the clearance of stress granules is significantly less efficient upon knockdown of ZFAND3. In contrast, ZFAND3 overexpression improved the clearance of sodium arsenite-induced stress granules. This effect was lost upon deletion of the N-terminal A20, the C-terminal AN1 or both zinc finger domains, suggesting that both zinc finger domains are required for an efficient clearance of arsenite-induced SGs.

These data indicate that, in addition to its role as transcriptional regulator, ZFAND3 is involved in the UPS and especially in the clearance of cytoplasmic sodium arsenite-induced SGs.

III. Paper III: Large-scale shRNA interference screen to unravel Glioblastoma cell invasion

The third paper aims to analyse additional gene lists from our previously performed shRNA interference screen to identify novel invasion-related genes in GBM. We used the screen data described in paper I for the selection of additional invasion-promoting candidate genes and selected the glutathione peroxidase 7 (*GPX7*) for further investigation. We also re-analysed the screen data to identify potential invasion-inhibiting genes and focused on the glycerol kinase (*GK*), the general transcription factor IIIH subunit 1 (*GTF2H1*) and the actin-related protein 1A (*ACTR1A*) for additional analysis. At first, we show that *GPX7* is more highly expressed in invasive GBM cell lines compared to non-invasive ones, whereas *GK*, *GTF2H1* and *ACTR1A* reveal a higher expression in non-invasive GBM cell lines. Knockdown of *GPX7* in an invasive patient-derived GBM cell line led to a significant reduction of *in vitro* and *ex vivo* invasion potential, while *GPX7* overexpression enhanced the invasion capacity of initially non-invasive GBM cells *in vitro* and partially *ex vivo*. In conclusion, we find that *GPX7* may to some extent be involved in GBM cell invasion, but it remains to be determined whether this conclusion can be generalized to other cell lines and to the *in vivo* situation.

With regard to the potential invasion-inhibiting genes we overexpressed *GK*, *GTF2H1* and *ACTR1A* in an invasive GBM cell line. These overexpressions were able to reduce the invasion potential of invasive GBM cells *in vitro* and partially *ex vivo*.

This manuscript highlights the potential and challenges of the performed shRNA interference screen as a tool to identify novel invasion-related genes in GBM.

Discussion

This thesis focuses on the identification and characterization of novel invasion-related genes in GBM through a large-scale shRNA interference screen. The selection of genes for further investigation included *ZFAND3* and *GPX7* as invasion-promoting candidate genes and *GK*, *GTF2H1* and *ACTR1A* as invasion-inhibiting candidate genes. We functionally validated these genes in *in vitro* and *ex vivo* assays after shRNA-mediated knockdowns of *ZFAND3* and *GPX7* and overexpressions of *GK*, *GTF2H1* or *ACTR1A*, which led to a reduction of GBM cell invasion. To our knowledge, this is the first report showing the putative involvement of these genes in GBM cell invasion. Additionally, except *GPX7* none of these genes has been linked to GBM so far. These results underline the potential of shRNA interference screens to unravel novel invasion-related genes in GBM, which may also represent possible drug targets for GBM therapy.

1. Methods to identify invasion-related genes

For the identification of invasion-related genes in GBM, several options are available. The simplest approach, for instance, would be to perform an *in vitro* invasion assay, like a Boyden chamber invasion assay, where the invasive cells can be clearly separated from the non-invasive cells and be subjected to bulk or single cell RNA sequencing to interrogate transcriptional differences between these two cell populations.

A way to increase the physiological relevance may be the use of an *ex vivo* model based on brain organoids, which can be confronted with fluorescently labeled GBM spheroids. GBM cell invasion into the organoids can then be microscopically visualized and dissected, enabling a clear separation of invasive from non-invasive tumor cells. RNA sequencing of invasive versus non-invasive GBM cells then allows to identify transcriptional differences between these two cell populations. This differential gene expression analysis together with the invasion assay as functional read-out can indicate which genes may play a role in GBM cell invasion.

In addition, gene expression analyses of different cell lines, like in our case invasive and non-invasive patient-derived GBM cell lines, can be utilized to identify genes that

are differentially expressed between invasive and non-invasive cell lines and may therefore represent potential invasion-related genes. In this case publically available databases, like the GlioVis portal [115] or the Ivy Glioblastoma Atlas Project (IvyGAP), which focuses on transcriptional changes based on anatomic locations [233], can be used to support the identification of potential invasion-related genes. To confirm if these genes are involved in GBM cell invasion, genetic approaches like gene knockdown, knockout or overexpression may be applied. Subsequently, to validate the function of the gene, invasion assays can be performed.

2. shRNA interference versus CRISPR/Cas9 screens

When performing gene expression analyses, a limitation may be that gene expression is just be correlated with invasion, but not necessary for invasion. To circumvent this, genetic approaches can be applied in form of large-scale screens to study the function of genes. Among loss-of-function screens, RNA interference using shRNAs or small interfering RNAs (siRNAs) can be distinguished from CRISPR/Cas9 technologies, which utilize single guide (sg) RNAs [234]. While RNA interference screens are based on partial gene knockdowns, CRISPR/Cas9 knockout screens rely on full gene knockouts [234, 235]. In general, many genetic screens have been performed in GBM cells focusing on cell proliferation, survival or cell surface markers (reviewed in [236]), but only a low number, including ours, was performed to study GBM cell migration or invasion [232, 237, 238]. A large-scale CRISPR/Cas9 screen, for instance, revealed the mitogen-activated protein kinase 4 (MAP4K4) as an invasion-promoting gene in GBM [237]. Moreover, a genome-wide RNA interference screen identified the host cell factor C1 (HCFC1), KH-type splicing regulatory protein (KHSRP) and filamin A (FLNA) as genes inhibiting migration of GBM cells [238].

As we planned our screen in a three-dimensional stem-like GBM cell line, which are not easy to transfect, we decided to perform a pooled whole genome shRNA interference screen as such screens rely on the endogenous RNA interference machinery. Therefore, prior to infecting the cells with the shRNA library, the introduction of foreign sequences and proteins is not required [234]. In addition,

shRNA interference screens are also not influenced by the conformation of the chromatin, by the accessibility of the locus or by the ploidy of the cells as the RNA interference system works on RNA localized in the cytoplasm. These aspects are important in cancer cells, which are often aneuploid. Nevertheless, a difficulty of shRNA interference screens is to identify essential genes that show low to moderate expression levels. Moreover, variable knockdown efficiencies between shRNAs, different cell types and off-target effects are major reasons for the limited overlap between different studies and the limited gene validation [239].

Alternatively, CRISPR/Cas9-based knockout screens can be used, where the efficiency of the knockout relies on a one-time editing event. This explains the higher detection specificity and sensitivity for essential genes, especially those that show moderate expression [239]. Disadvantages of CRISPR/Cas9-based knockout screens include the poor cutting efficiency and off-target effects. This increases the potential of false positive and false negative hits, which makes a reliable analysis more difficult. Reducing these off-target effects can be achieved by using CRISPR interference (CRISPRi), which is based on a nuclease-deficient Cas9 that targets regulatory sequences like gene promoters close to transcriptional start sites [240]. In addition, CRISPRi screens show higher knockdown efficiencies compared to shRNA interference screens [241].

Depending on the biological question, loss-of function screens can be distinguished from gain-of-function screens, where genes are exogenously overexpressed [242]. In this case, an option represents the CRISPR activation (CRISPRa) system, which relies on the activation and increase of gene expression through a nuclease-deficient Cas9 combined with transcriptional activators [240].

2.1. Biological read-outs for genetic screens investigating invasion

A common challenge for genetic screens in the context of cell invasion is the biological read-out. A genetic screen ideally requires a straightforward and scalable assay where the invasive cells can be clearly distinguished and physically separated from the non-invasive cells.

In our case, we used an *in vitro* Boyden chamber invasion assay as biological read-out, which allows the clear separation of invasive and non-invasive cells. Although this assay is easy to perform and can be carried out with varying cell numbers, limitations include the limited physiological relevance and the fact that it does not allow to study invasion over time as it represents an end-point assay. Additionally, variability between replicates can occur depending on the cell line used and the experimenter, although normalization can account for that in most cases. High variability between biological replicates, as observed in our screen, made a reliable analysis more difficult and different analysis tools, which should give similar results, revealed different results.

Nevertheless, the Boyden chamber invasion assay is the most commonly used invasion assay in research and also the few genetic screens that are published on GBM cell migration or invasion, including ours, used this assay for biological read-out [232, 237, 238]. The difficulty of other models like the scratch assay is to clearly distinguish the invading from the non-invading cells. While this problem may be overcome with a sprouting assay, the number of cells obtained may be a limiting factor here.

In addition to *in vitro* models, the physiological relevance can be increased by moving such screens into *ex vivo* or *in vivo* systems. This is more time-consuming and makes a high-throughput setting difficult due to the workload and the requirement of animals for most models. Such approaches enable the maintenance of the tissue architecture as well as the interaction of tumor cells with the ECM and non-malignant stromal cells of the microenvironment. To a limited extent this also holds true for *ex vivo* models such as *ex vivo* brain slice cultures or brain organoids, as used here for validation purposes. To our knowledge, no genetic *in vivo* screen on GBM cell invasion has been performed so far. This may be due to the fact that major difficulties for an *in vivo* screen studying invasion remain shRNA representation and the fact that only low cell numbers can be obtained. An additional problem may be a clear separation of invasive from non-invasive cells *in vivo* as a proper visualization of cell invasion in the brain is challenging. That may be the reason why most large-scale screens performed on GBM cells do not focus on cell migration or invasion.

3. Diverse functions of ZFAND3

We characterized the nuclear activity of ZFAND3 within a proposed transcriptional protein complex regulating the transcription of invasion-related genes to drive GBM invasion [232]. We also unraveled cytoplasmic functions of ZFAND3, including ubiquitin binding, interaction with VCP and involvement in sodium arsenite-induced SG clearance, suggesting a dual role of ZFAND3 depending on its subcellular localization.

Although the nuclear expression of ZFAND3 dominates, it is also regularly found in the cytoplasm. When querying the Human Protein Atlas (<http://www.proteinatlas.org>) [243] it appears that the expression pattern of ZFAND3 and ZFAND5 are highly similar, with a predominant nuclear, but also cytoplasmic localization. This is striking as ZFAND3 is the only ZFAND protein containing a NLS. Proteins without a NLS can still be transported into the nucleus, but lack the interaction with transport receptors.

We found that both ZFAND3 zinc finger domains are crucial for its nuclear function as their deletion resulted in a loss of the invasion phenotype. This might be explained by the fact that the deletion of the zinc finger domains may impair a potential binding of ZFAND3 to the promoter regions of invasion-related genes or hinder the formation of a putative transcriptional complex involving ZFAND3. The zinc finger domains also seem to be important for cytoplasmic SG clearance, while only the N-terminal A20 domain was required for ubiquitin binding. Whether the AN1 domain is responsible for the interaction with the 26S proteasome or VCP, as shown for other ZFAND proteins (ZFAND1 [218], ZFAND2A [244], ZFAND2B [245] and ZFAND5 [246]), remains to be seen.

The deletion of one or both zinc finger domains may also affect the protein conformation of ZFAND3, which may lead to its dysfunction. This does not seem to be the case for the AN1 domain deletion as this still allowed ubiquitin binding, but it may be the case for the deletion of both domains. This hypothesis is strengthened by the finding that upon deletion of both zinc finger domains the translocation of ZFAND3 to the nucleus was impaired, which was not observed for the single domain deletions [232].

3.1. Relevance of proteasomal degradation in Glioblastoma

We showed the impact of ZFAND3 on SG clearance in HEK293T and LN229 GBM cells, indicating that this cytoplasmic function of ZFAND3 may also be of importance in cancer and specifically in GBM. This is supported by the notion that cancer cells often show increased proteasomal activity [160], suggesting that this may also be the case for GBM. Many signalling pathways in GBM show an increased activity, translating into increased proliferation and protein production [247]. This indicates the importance of the UPS in GBM as it regulates the activation or deactivation of several signalling cascades [83]. While there is no report linking mutations in E1 enzymes and GBM, all other three enzyme classes involved in ubiquitination (E2, E3 and DUBs) were shown to influence oncogenic features like proliferation, invasion, apoptosis and drug resistance in GBM [248]. E3 enzymes and DUBs can exert oncogenic or tumor suppressive activity depending on their target protein. For DUBs the oncogenic abilities dominate, like stabilizing oncoproteins and compromising tumor suppressors, thereby maintaining oncogenic signalling [83]. Overexpression of DUBs in GBM is often associated with increased cell proliferation and invasion (reviewed in [83, 184]). The vital role of these three enzyme classes following malignant transformation in GBM suggests them as potential therapeutic targets.

Additionally, several important signalling proteins, like EGFR, its mutant variant EGFRvIII or AKT, as well as ECM-degrading components, such as MMP-2 or uPA, associated with GBM cell invasion are regulated by proteasomal degradation (reviewed in [249]), suggesting a link between the UPS and GBM cell invasion. This raises the question if the nuclear and the cytoplasmic activity of ZFAND3 may be linked or are independent from each other.

3.2. Cytoplasmic stress granules and their influence on Glioblastoma

Even though the role of SGs in GBM has not been extensively studied so far, it has been shown that the mRNA expression level of G3BP1, PERK, GCN2 and GADD34 are increased in GBM tissue compared to lower-grade gliomas, suggesting a more active stress response in GBM [207]. Therefore, SG formation as well as SG clearance

may be important in GBM to maintain a high proliferation rate. It remains to be seen to what extent SGs are involved in GBM cell invasion.

This hypothesis is supported by the notion that G3BP1 promotes invasion of pancreatic cancer [250] and renal cell carcinoma cells [251]. An inactivation of G3BP1 in sarcoma cells reduced SG formation *in vivo* as well as the invasive capacity [205].

In GBM cells, a G3BP1 knockdown resulted in a reduction of SG formation upon proteasomal inhibition by bortezomib. Additionally, the level of apoptosis was rising in G3BP1 depleted cells treated with bortezomib [252]. Also G3BP2 has an impact on GBM as its knockdown or pharmacological inhibition blocks stress-stimulated PD-L1 expression, suggesting G3BP2 as novel drug target in GBM, whose inhibition might potentiate the efficacy of immune checkpoint inhibitors [253].

In a drug screen, Attwood et al identified 129 drugs that delay the clearance of hypoxia-stimulated SGs in GBM cells. One of them was raloxifene, a selective estrogen receptor modulator. Combining raloxifene with hypoxia caused an inhibition of autophagy and increasing numbers of apoptotic GBM cells [207].

As SGs contain multiple proteins and mRNAs, it might also be possible that SGs either harbor anti-invasive proteins or specifically store mRNAs that encode for anti-invasive proteins, allowing SG-containing cells to invade [205]. Still, it remains to be determined if SGs are directly linked to an invasive phenotype in cancer.

4. The role of GPX7 in cancer cell invasion

GPX7 is one of eight members of the glutathione peroxidase (GPX) family, which are antioxidant enzymes involved in the management of reactive oxygen species (ROS). In contrast to GPX1-4 and GPX6, which represent classical GPXs, GPX5, GPX7 and GPX8 form the group of non-selenocysteine-containing GPXs harboring a cysteine instead of the glutathione-binding selenocysteine in their catalytic center [254]. While classical GPXs use glutathione as major substrate, GPX5, GPX7 and GPX8 use different substrates like thioredoxin or protein disulfide isomerase [255].

The importance of GPX7 in physiology is shown by a GPX7 knockout mouse, which shows a shortened lifespan due to increased oxidative stress and higher risk of cancer development [255]. In this work we have shown that GPX7 has an impact on *in vitro* and *ex vivo* GBM cell invasion by manipulating expression levels.

Interestingly, also other GPXs were shown to be implicated in tumor cell invasion. GPX1 stimulates migration and invasion of esophageal cancer cells [256] and its knockdown reduces the invasion of triple-negative breast cancer cells [257]. In contrast, GPX2 has an inhibitory effect on colon cancer cell migration and invasion [258]. Moreover, an upregulation of GPX3 expression negatively affects the migration and invasion of esophageal squamous cell carcinoma cells [259]. GPX4 is involved in the invasion of pancreatic cancer cells as its knockdown reduces their invasive ability [260]. In addition, GPX4 is overexpressed in glioma tissues and its knockdown causes a reduction of glioma cell migration [261]. Furthermore, GPX8 is highly expressed in non-small cell lung cancer and promotes the invasive behavior of these cells [262], while also stimulating the migratory phenotype of breast cancer cells [263].

GPX7 functions as an oxidative stress sensor through the transmission of ROS signals to redox-sensitive proteins like chaperones. A GPX7 loss resulted in impaired function of the chaperone 78 kDa glucose-regulated protein (GRP78) leading to an accumulation of misfolded proteins and increased oxidative stress [255]. As GPX7 is situated in the ER [264], we thought that GPX7 might be involved in the ER-induced unfolded protein response (UPR), which can influence cell invasion (reviewed in [265, 266]). Assessing the expression of the main UPR marker inositol-requiring enzyme 1 (IRE1), PERK and GRP78 after GPX7 knockdown and overexpression did not reveal a significant difference at the gene expression level (data not shown). Also GRP78 protein level stayed unaffected (data not shown), suggesting that GPX7 exerts its function independent from the UPR.

To further study the impact of GPX7 on invasion, we generated a CRISPR/Cas9-mediated knockout of GPX7 in an invasive GBM cell line. Surprisingly, GPX7 knockout (34 single knockout clones analyzed) did not show a consistent impact on

GBM cell invasion *in vitro*. An ongoing study in immunodeficient rats aims to investigate the impact of a GPX7 knockout on *in vivo* GBM cell invasion.

As a systemic GPX7 knockout leads to increased oxidative stress [255], we thought to investigate the expression level of the nuclear factor erythroid 2-related factor 2 (Nrf2), a transcriptional regulator of ROS signalling, upon GPX7 knockdown, knockout or overexpression. While no change of Nrf2 mRNA and protein expression upon GPX7 knockdown or overexpression was observed, we saw a decreased Nrf2 protein expression in GPX7 knockout clones (data not shown). It has been shown that Nrf2, which is upregulated in GBM compared to normal brain (GlioVis portal [115]), promotes GPX7 expression via binding the antioxidant response elements in the GPX7 promoter. Under physiological conditions enhanced GPX7 expression serves as protection against oxidative stress and may extend lifespan as its loss leads to premature senescence [267]. So one could hypothesize that enhanced GPX7 expression induced by Nrf2 protects the tumor from increasing ROS level, while a GPX7 loss results in too high ROS level, which might lead to apoptosis or senescence. We were not able to confirm this hypothesis as we did not observe increased level of apoptosis upon GPX7 knockdown or knockout, also not when the cells were challenged with increasing concentrations of hydrogen peroxide (H₂O₂) (data not shown). It may be that GBM cells have developed alternative pathways to regulate oxidative stress response, thereby becoming largely independent of GPX7.

Conclusions

I. Paper I: AN1-type zinc finger protein 3 (ZFAND3) is a transcriptional regulator that drives Glioblastoma invasion

A whole genome shRNA interference screen on invasive GBM cells led to the identification of the zinc finger protein ZFAND3 as a putative invasion-promoting gene. Its loss reduced GBM cell invasion, while its overexpression induced the motility of initially non-invasive GBM cells *in vitro*, *ex vivo* and *in vivo*. ZFAND3 was proposed to act in a nuclear protein complex regulating the transcription of invasion-related genes to promote the invasive behaviour of GBM cells.

II. Paper II: The role of ZFAND3 in the UPS and stress granule clearance

Besides the nuclear function of ZFAND3 in promoting GBM cell invasion, it seems to have a cytoplasmic function in the regulation of the UPS as it directly binds ubiquitin via its N-terminal A20 domain and interacts with VCP. Additionally, ZFAND3 co-localizes with sodium arsenite-induced SGs and promotes their clearance as overexpression of ZFAND3 resulted in a more efficient SG clearance. More work is required to unravel if ZFAND3 acts in a direct mechanism on SGs or if additional factors are involved.

III. Paper III: Large-scale shRNA interference screen to unravel Glioblastoma invasion

This paper highlights the relevance of a large-scale shRNA interference screen as powerful tool for the identification of novel invasion-related genes in GBM. This is shown by the functional validation of the invasion-promoting gene *GPX7* and the invasion-inhibiting candidate genes *GK*, *GTF2H1* and *ACTR1A* as the knockdown of *GPX7* as well as the overexpression of *GK*, *GTF2H1* or *ACTR1A* reduced the *in vitro* and partially the *ex vivo* invasion potential of GBM cells. For a conclusion on the exact function of these genes in GBM cell invasion, more research is required.

Future perspectives

The extensive invasion potential of GBM cells into normal brain structures remains a major challenge for an effective treatment, as these cells often escape therapy and represent a leading cause for tumor recurrence. Until now there is no treatment specifically targeting GBM cell invasion. The present work aimed to identify novel drivers and inhibitors of GBM cell invasion in order to develop novel therapeutic options. A promising therapeutic strategy may be to combine drugs targeting the invasive nature of GBM cells as well as their high proliferative capacity. A prior anti-invasive treatment, leading to a more circumscribed tumor, may further improve the extent of surgical tumor removal.

shRNA interference as well as CRISPR/Cas9-based screens have gained considerable attention as they can be used to study the function of genes in a large-scale setting. To make the performed invasion screen more robust and account for the high variability between biological replicates, it would be useful to run multiple biological replicates. It may also be necessary to repeat this screen in additional invasive GBM cell lines and focus on the genes that are common among them in order to find the most relevant hits. Furthermore, to increase the physiological relevance of such screens it should be considered to perform them in an *ex vivo* or *in vivo* setting, which until now remains a challenge, especially *in vivo*.

ZFAND3 was shown to be important for GBM cell invasion as well as for the efficient clearance of sodium arsenite-induced SGs. Although we showed that ZFAND3 drives GBM cell invasion through the transcriptional regulation of invasion-related genes, it remains to be elucidated if ZFAND3 itself is binding to DNA to fulfil the transcriptional activation or if it associates with a transcriptional complex that activates the expression of invasion-related genes. ZFAND3 binding to a specific DNA sequence could be investigated by DNA electrophoretic mobility shift assays. Furthermore, it would be interesting to identify additional target genes of ZFAND3, besides *NRCAM*, *FNI* and *COL6A2*.

The exact mechanism by which ZFAND3 promotes the clearance of SGs remains elusive. As a mutation of its NLS leads to a cytoplasmic accumulation of ZFAND3 [232], it would be interesting to investigate if this could potentiate the effect on SG clearance. Additionally, studying the recruitment of ZFAND3 to SGs may be facilitated by live cell imaging using a fluorescently labelled ZFAND3 construct expressed in the cells.

In analogy to ZFAND1 [218], ZFAND3 may recruit VCP and the 26S proteasome to SGs to facilitate their clearance. This hypothesis could be tested through co-localization studies, which in case of a lost co-localization upon ZFAND3 knockdown, would indicate that ZFAND3 is required for the recruitment of VCP and the 26S proteasome. Moreover, this may also be assessed with the zinc finger domain deletion constructs to investigate which domain is responsible for the interaction and recruitment of VCP and the 26S proteasome.

A major question remains if there is a link between the nuclear and the cytoplasmic function of ZFAND3, pointing at a connection between cell invasion and SGs. It could be speculated that ZFAND3 contributes to SG formation and clearance as a survival mechanism under stress, which at the same time would activate a transcriptional invasion program, as part of an escape mechanism to reach better growth conditions. This hypothesis could be tested in the context of hypoxia, which is known to increase the invasion potential of GBM cells [268].

References

1. Patchell, R.A., *The management of brain metastases*. Cancer Treatment Reviews, 2003. **29**(6): p. 533-540.
2. Ostrom, Q.T., et al., *CBTRUS Statistical Report: Primary Brain and Other Central Nervous System Tumors Diagnosed in the United States in 2012-2016*. Neuro-oncology, 2019. **21**(Suppl 5): p. v1-v100.
3. Ostrom, Q.T., et al., *Alex's Lemonade Stand Foundation Infant and Childhood Primary Brain and Central Nervous System Tumors Diagnosed in the United States in 2007-2011*. Neuro Oncol, 2015. **16 Suppl 10**(Suppl 10): p. x1-x36.
4. Amirian, E.S., et al., *Approaching a Scientific Consensus on the Association between Allergies and Glioma Risk: A Report from the Glioma International Case-Control Study*. Cancer epidemiology, biomarkers & prevention : a publication of the American Association for Cancer Research, cosponsored by the American Society of Preventive Oncology, 2016. **25**(2): p. 282-290.
5. Ostrom, Q.T., et al., *Risk factors for childhood and adult primary brain tumors*. Neuro Oncol, 2019. **21**(11): p. 1357-1375.
6. Ranger, A.M., et al., *Familial syndromes associated with intracranial tumours: a review*. Childs Nerv Syst, 2014. **30**(1): p. 47-64.
7. Weller, M., et al., *EANO guidelines on the diagnosis and treatment of diffuse gliomas of adulthood*. Nature reviews. Clinical oncology, 2021. **18**(3): p. 170-186.
8. Louis, D.N., et al., *The 2021 WHO Classification of Tumors of the Central Nervous System: a summary*. Neuro Oncol, 2021.
9. Duffau, H., *Diffuse low-grade glioma, oncological outcome and quality of life: a surgical perspective*. Curr Opin Oncol, 2018. **30**(6): p. 383-389.
10. Stupp, R., et al., *Radiotherapy plus concomitant and adjuvant temozolomide for glioblastoma*. N Engl J Med, 2005. **352**(10): p. 987-96.
11. Louis, D.N., et al., *The 2016 World Health Organization Classification of Tumors of the Central Nervous System: a summary*. Acta Neuropathol, 2016. **131**(6): p. 803-20.
12. Perry, A. and P. Wesseling, *Histologic classification of gliomas*. Handb Clin Neurol, 2016. **134**: p. 71-95.
13. Claes, A., A.J. Idema, and P. Wesseling, *Diffuse glioma growth: a guerilla war*. Acta neuropathologica, 2007. **114**(5): p. 443-458.
14. Pirozzi, C.J. and H. Yan, *The implications of IDH mutations for cancer development and therapy*. Nat Rev Clin Oncol, 2021. **18**(10): p. 645-661.
15. Dang, L., et al., *Cancer-associated IDH1 mutations produce 2-hydroxyglutarate*. Nature, 2009. **462**(7274): p. 739-44.
16. Yan, H., et al., *IDH1 and IDH2 mutations in gliomas*. N Engl J Med, 2009. **360**(8): p. 765-73.
17. Turcan, S., et al., *IDH1 mutation is sufficient to establish the glioma hypermethylator phenotype*. Nature, 2012. **483**(7390): p. 479-483.
18. Heaphy Christopher, M., et al., *Altered Telomeres in Tumors with ATRX and DAXX Mutations*. Science, 2011. **333**(6041): p. 425-425.

19. Chan, A.K.-Y., et al., *Loss of CIC and FUBP1 expressions are potential markers of shorter time to recurrence in oligodendroglial tumors*. *Modern Pathology*, 2014. **27**(3): p. 332-342.
20. Mizoguchi, M., et al., *Clinical implications of molecular analysis in diffuse glioma stratification*. *Brain Tumor Pathol*, 2021. **38**(3): p. 210-217.
21. Shirahata, M., et al., *Novel, improved grading system(s) for IDH-mutant astrocytic gliomas*. *Acta Neuropathol*, 2018. **136**(1): p. 153-166.
22. Bell, R.J.A., et al., *Cancer. The transcription factor GABP selectively binds and activates the mutant TERT promoter in cancer*. *Science (New York, N.Y.)*, 2015. **348**(6238): p. 1036-1039.
23. Filipescu, D., S. Müller, and G. Almouzni, *Histone H3 variants and their chaperones during development and disease: contributing to epigenetic control*. *Annu Rev Cell Dev Biol*, 2014. **30**: p. 615-46.
24. Schwartzentruber, J., et al., *Driver mutations in histone H3.3 and chromatin remodelling genes in paediatric glioblastoma*. *Nature*, 2012. **482**(7384): p. 226-231.
25. Hegi, M.E., et al., *MGMT gene silencing and benefit from temozolomide in glioblastoma*. *N Engl J Med*, 2005. **352**(10): p. 997-1003.
26. Wick, W., et al., *Prognostic or predictive value of MGMT promoter methylation in gliomas depends on IDH1 mutation*. *Neurology*, 2013. **81**(17): p. 1515-22.
27. Brat, D.J., et al., *cIMPACT-NOW update 5: recommended grading criteria and terminologies for IDH-mutant astrocytomas*. *Acta Neuropathol*, 2020. **139**(3): p. 603-608.
28. Louis, D.N., et al., *cIMPACT-NOW update 6: new entity and diagnostic principle recommendations of the cIMPACT-Utrecht meeting on future CNS tumor classification and grading*. *Brain pathology (Zurich, Switzerland)*, 2020. **30**(4): p. 844-856.
29. Brat, D.J., et al., *cIMPACT-NOW update 3: recommended diagnostic criteria for "Diffuse astrocytic glioma, IDH-wildtype, with molecular features of glioblastoma, WHO grade IV"*. *Acta Neuropathol*, 2018. **136**(5): p. 805-810.
30. Tesileanu, C.M.S., et al., *Survival of diffuse astrocytic glioma, IDH1/2 wildtype, with molecular features of glioblastoma, WHO grade IV: a confirmation of the cIMPACT-NOW criteria*. *Neuro Oncol*, 2020. **22**(4): p. 515-523.
31. Wen, P.Y., et al., *Glioblastoma in adults: a Society for Neuro-Oncology (SNO) and European Society of Neuro-Oncology (EANO) consensus review on current management and future directions*. *Neuro Oncol*, 2020. **22**(8): p. 1073-1113.
32. Patel, A.P., et al., *Single-cell RNA-seq highlights intratumoral heterogeneity in primary glioblastoma*. *Science*, 2014. **344**(6190): p. 1396-401.
33. Clarke, J.L., et al., *Is surgery at progression a prognostic marker for improved 6-month progression-free survival or overall survival for patients with recurrent glioblastoma?* *Neuro Oncol*, 2011. **13**(10): p. 1118-24.

34. So, J.S., H. Kim, and K.S. Han, *Mechanisms of Invasion in Glioblastoma: Extracellular Matrix, Ca(2+) Signaling, and Glutamate*. *Front Cell Neurosci*, 2021. **15**: p. 663092.
35. Weller, M., et al., *European Association for Neuro-Oncology (EANO) guideline on the diagnosis and treatment of adult astrocytic and oligodendroglial gliomas*. *Lancet Oncol*, 2017. **18**(6): p. e315-e329.
36. Ly, K.I., P.Y. Wen, and R.Y. Huang, *Imaging of Central Nervous System Tumors Based on the 2016 World Health Organization Classification*. *Neurol Clin*, 2020. **38**(1): p. 95-113.
37. Kinahan, P.M., Mark; Bialecki, Brian; Coombs, Laura, *Data from ACRIN-FMISO-Brain*. *The Cancer Imaging Archive*. 2018.
38. Wang, Q., et al., *Tumor Evolution of Glioma-Intrinsic Gene Expression Subtypes Associates with Immunological Changes in the Microenvironment*. *Cancer Cell*, 2018. **33**(1): p. 152.
39. Verhaak, R.G., et al., *Integrated genomic analysis identifies clinically relevant subtypes of glioblastoma characterized by abnormalities in PDGFRA, IDH1, EGFR, and NF1*. *Cancer Cell*, 2010. **17**(1): p. 98-110.
40. Wang, J., et al., *Clonal evolution of glioblastoma under therapy*. *Nat Genet*, 2016. **48**(7): p. 768-76.
41. Lacroix, M., et al., *A multivariate analysis of 416 patients with glioblastoma multiforme: prognosis, extent of resection, and survival*. *J Neurosurg*, 2001. **95**(2): p. 190-8.
42. Bloch, O., et al., *Impact of extent of resection for recurrent glioblastoma on overall survival: clinical article*. *J Neurosurg*, 2012. **117**(6): p. 1032-8.
43. Gallego, O., *Nonsurgical treatment of recurrent glioblastoma*. *Current oncology (Toronto, Ont.)*, 2015. **22**(4): p. e273-e281.
44. Iwamoto, F.M., et al., *Patterns of care in elderly glioblastoma patients*. *Ann Neurol*, 2008. **64**(6): p. 628-34.
45. Wick, A., et al., *Glioblastoma in elderly patients: solid conclusions built on shifting sand?* *Neuro Oncol*, 2018. **20**(2): p. 174-183.
46. Kim, E.H., et al., *Tumor treating fields inhibit glioblastoma cell migration, invasion and angiogenesis*. *Oncotarget*, 2016. **7**(40): p. 65125-65136.
47. Kirson, E.D., et al., *Alternating electric fields arrest cell proliferation in animal tumor models and human brain tumors*. *Proceedings of the National Academy of Sciences*, 2007. **104**(24): p. 10152.
48. Stupp, R., et al., *Maintenance Therapy With Tumor-Treating Fields Plus Temozolomide vs Temozolomide Alone for Glioblastoma: A Randomized Clinical Trial*. *Jama*, 2015. **314**(23): p. 2535-43.
49. Bernard-Arnoux, F., et al., *The cost-effectiveness of tumor-treating fields therapy in patients with newly diagnosed glioblastoma*. *Neuro Oncol*, 2016. **18**(8): p. 1129-36.
50. Cloughesy, T.F. and A.B. Lassman, *NovoTTF: where to go from here?* *Neuro-Oncology*, 2017. **19**(5): p. 605-608.
51. Stupp, R., et al., *NovoTTF-100A versus physician's choice chemotherapy in recurrent glioblastoma: a randomised phase III trial of a novel treatment modality*. *Eur J Cancer*, 2012. **48**(14): p. 2192-202.

52. Normanno, N., et al., *Epidermal growth factor receptor (EGFR) signaling in cancer*. *Gene*, 2006. **366**(1): p. 2-16.
53. Ni, J., et al., *Targeting EGFR in glioblastoma with a novel brain-penetrant small molecule EGFR-TKI*. *bioRxiv*, 2021: p. 2021.01.09.426030.
54. Furnari, F.B., et al., *Heterogeneity of epidermal growth factor receptor signalling networks in glioblastoma*. *Nature reviews. Cancer*, 2015. **15**(5): p. 302-310.
55. Keller, S. and M.H.H. Schmidt, *EGFR and EGFRvIII Promote Angiogenesis and Cell Invasion in Glioblastoma: Combination Therapies for an Effective Treatment*. *Int J Mol Sci*, 2017. **18**(6).
56. Hasselbalch, B., et al., *Cetuximab, bevacizumab, and irinotecan for patients with primary glioblastoma and progression after radiation therapy and temozolomide: a phase II trial*. *Neuro Oncol*, 2010. **12**(5): p. 508-16.
57. Neyns, B., et al., *Stratified phase II trial of cetuximab in patients with recurrent high-grade glioma*. *Annals of Oncology*, 2009. **20**(9): p. 1596-1603.
58. Westphal, M., et al., *A randomised, open label phase III trial with nimotuzumab, an anti-epidermal growth factor receptor monoclonal antibody in the treatment of newly diagnosed adult glioblastoma*. *European Journal of Cancer*, 2015. **51**(4): p. 522-532.
59. Lee, K., et al., *Therapeutic Efficacy of GC1118, a Novel Anti-EGFR Antibody, against Glioblastoma with High EGFR Amplification in Patient-Derived Xenografts*. *Cancers (Basel)*, 2020. **12**(11).
60. Clarke, J.L., et al., *A single-institution phase II trial of radiation, temozolomide, erlotinib, and bevacizumab for initial treatment of glioblastoma*. *Neuro Oncol*, 2014. **16**(7): p. 984-90.
61. Raizer, J.J., et al., *A phase II study of bevacizumab and erlotinib after radiation and temozolomide in MGMT unmethylated GBM patients*. *J Neurooncol*, 2016. **126**(1): p. 185-192.
62. Chakravarti, A., et al., *RTOG 0211: a phase I/2 study of radiation therapy with concurrent gefitinib for newly diagnosed glioblastoma patients*. *Int J Radiat Oncol Biol Phys*, 2013. **85**(5): p. 1206-11.
63. Uhm, J.H., et al., *Phase II evaluation of gefitinib in patients with newly diagnosed Grade 4 astrocytoma: Mayo/North Central Cancer Treatment Group Study N0074*. *Int J Radiat Oncol Biol Phys*, 2011. **80**(2): p. 347-53.
64. Reardon, D.A., et al., *Phase I/randomized phase II study of afatinib, an irreversible ErbB family blocker, with or without protracted temozolomide in adults with recurrent glioblastoma*. *Neuro Oncol*, 2015. **17**(3): p. 430-9.
65. Sepúlveda-Sánchez, J.M., et al., *Phase II trial of dacomitinib, a pan-human EGFR tyrosine kinase inhibitor, in recurrent glioblastoma patients with EGFR amplification*. *Neuro-Oncology*, 2017. **19**(11): p. 1522-1531.
66. Wen, P.Y., et al., *Buparlisib in Patients With Recurrent Glioblastoma Harboring Phosphatidylinositol 3-Kinase Pathway Activation: An Open-Label, Multicenter, Multi-Arm, Phase II Trial*. *Journal of Clinical Oncology*, 2019. **37**(9): p. 741-750.
67. Pitz, M.W., et al., *Phase II study of PX-866 in recurrent glioblastoma*. *Neuro Oncol*, 2015. **17**(9): p. 1270-4.

68. Wick, W., et al., *Phase III study of enzastaurin compared with lomustine in the treatment of recurrent intracranial glioblastoma*. Journal of clinical oncology : official journal of the American Society of Clinical Oncology, 2010. **28**(7): p. 1168-1174.
69. Wick, W., et al., *Phase II Study of Radiotherapy and Temsirolimus versus Radiochemotherapy with Temozolomide in Patients with Newly Diagnosed Glioblastoma without MGMT Promoter Hypermethylation (EORTC 26082)*. Clin Cancer Res, 2016. **22**(19): p. 4797-4806.
70. Ma, D.J., et al., *A phase II trial of everolimus, temozolomide, and radiotherapy in patients with newly diagnosed glioblastoma: NCCTG N057K*. Neuro-Oncology, 2015. **17**(9): p. 1261-1269.
71. Ramezani, S., et al., *Perifosine enhances bevacizumab-induced apoptosis and therapeutic efficacy by targeting PI3K/AKT pathway in a glioblastoma heterotopic model*. Apoptosis, 2017. **22**(8): p. 1025-1034.
72. Narayan, R.S., et al., *The allosteric AKT inhibitor MK2206 shows a synergistic interaction with chemotherapy and radiotherapy in glioblastoma spheroid cultures*. BMC Cancer, 2017. **17**(1): p. 204.
73. Cruz Da Silva, E., et al., *A Systematic Review of Glioblastoma-Targeted Therapies in Phases II, III, IV Clinical Trials*. Cancers (Basel), 2021. **13**(8).
74. Batchelor, T.T., et al., *Phase III randomized trial comparing the efficacy of cediranib as monotherapy, and in combination with lomustine, versus lomustine alone in patients with recurrent glioblastoma*. Journal of clinical oncology : official journal of the American Society of Clinical Oncology, 2013. **31**(26): p. 3212-3218.
75. Chinot, O.L., et al., *Bevacizumab plus Radiotherapy–Temozolomide for Newly Diagnosed Glioblastoma*. New England Journal of Medicine, 2014. **370**(8): p. 709-722.
76. Gilbert, M.R., et al., *A randomized trial of bevacizumab for newly diagnosed glioblastoma*. N Engl J Med, 2014. **370**(8): p. 699-708.
77. Huang, M., et al., *c-Met-mediated endothelial plasticity drives aberrant vascularization and chemoresistance in glioblastoma*. J Clin Invest, 2016. **126**(5): p. 1801-14.
78. Lombardi, G., et al., *Regorafenib compared with lomustine in patients with relapsed glioblastoma (REGOMA): a multicentre, open-label, randomised, controlled, phase 2 trial*. Lancet Oncol, 2019. **20**(1): p. 110-119.
79. Preusser, M., et al., *Prospects of immune checkpoint modulators in the treatment of glioblastoma*. Nature reviews. Neurology, 2015. **11**(9): p. 504-514.
80. Janjua, T.I., et al., *Frontiers in the treatment of glioblastoma: Past, present and emerging*. Advanced Drug Delivery Reviews, 2021. **171**: p. 108-138.
81. Berghoff, A.S., et al., *Programmed death ligand 1 expression and tumor-infiltrating lymphocytes in glioblastoma*. Neuro-oncology, 2015. **17**(8): p. 1064-1075.
82. Wang, X., T. Meul, and S. Meiners, *Exploring the proteasome system: A novel concept of proteasome inhibition and regulation*. Pharmacol Ther, 2020. **211**: p. 107526.

83. Maksoud, S., *The Role of the Ubiquitin Proteasome System in Glioma: Analysis Emphasizing the Main Molecular Players and Therapeutic Strategies Identified in Glioblastoma Multiforme*. Mol Neurobiol, 2021. **58**(7): p. 3252-3269.
84. Kong, X.-T., et al., *Phase 2 Study of Bortezomib Combined With Temozolomide and Regional Radiation Therapy for Upfront Treatment of Patients With Newly Diagnosed Glioblastoma Multiforme: Safety and Efficacy Assessment*. International Journal of Radiation Oncology*Biophysics, 2018. **100**(5): p. 1195-1203.
85. Roth, P., et al., *Proteasome inhibition for the treatment of glioblastoma*. Expert Opin Investig Drugs, 2020. **29**(10): p. 1133-1141.
86. Kaufmann, J.K. and E.A. Chiocca, *Glioma virus therapies between bench and bedside*. Neuro-oncology, 2014. **16**(3): p. 334-351.
87. Srinivasan, V.M., et al., *Tumor Vaccines for Malignant Gliomas*. Neurotherapeutics, 2017. **14**(2): p. 345-357.
88. Hatoum, A., R. Mohammed, and O. Zakieh, *The unique invasiveness of glioblastoma and possible drug targets on extracellular matrix*. Cancer Manag Res, 2019. **11**: p. 1843-1855.
89. Scherer, H.J., *Structural Development in Gliomas*. The American Journal of Cancer, 1938. **34**(3): p. 333-351.
90. Fabian, C., et al., *Chapter Two - Novel facets of glioma invasion*, in *International Review of Cell and Molecular Biology*, C. Thomas and L. Galluzzi, Editors. 2021, Academic Press. p. 33-64.
91. Cuddapah, V.A., et al., *Bradykinin-induced chemotaxis of human gliomas requires the activation of KCa3.1 and CIC-3*. The Journal of neuroscience : the official journal of the Society for Neuroscience, 2013. **33**(4): p. 1427-1440.
92. Montana, V. and H. Sontheimer, *Bradykinin promotes the chemotactic invasion of primary brain tumors*. J Neurosci, 2011. **31**(13): p. 4858-67.
93. Dandy, W.E., *Removal of Right Cerebral Hemisphere for Certain Tumors with Hemiplegia*. Journal of the American Medical Association, 1928. **90**(11): p. 823-825.
94. Marienhagen, K., et al., *Interactions between fetal rat brain cells and mature brain tissue in vivo and in vitro*. Neuropathol Appl Neurobiol, 1994. **20**(2): p. 130-43.
95. Sakariassen, P.O., et al., *Angiogenesis-independent tumor growth mediated by stem-like cancer cells*. Proc Natl Acad Sci U S A, 2006. **103**(44): p. 16466-71.
96. Wang, J., et al., *A reproducible brain tumour model established from human glioblastoma biopsies*. BMC Cancer, 2009. **9**: p. 465.
97. Panková, K., et al., *The molecular mechanisms of transition between mesenchymal and amoeboid invasiveness in tumor cells*. Cell Mol Life Sci, 2010. **67**(1): p. 63-71.
98. Watkins, S. and H. Sontheimer, *Hydrodynamic cellular volume changes enable glioma cell invasion*. J Neurosci, 2011. **31**(47): p. 17250-9.
99. Schiapparelli, P., et al., *NKCC1 Regulates Migration Ability of Glioblastoma Cells by Modulation of Actin Dynamics and Interacting with Cofilin*. EBioMedicine, 2017. **21**: p. 94-103.

100. Friedl, P. and K. Wolf, *Plasticity of cell migration: a multiscale tuning model*. J Cell Biol, 2010. **188**(1): p. 11-9.
101. Taddei, M.L., et al., *Microenvironment and tumor cell plasticity: An easy way out*. Cancer Letters, 2013. **341**(1): p. 80-96.
102. Friedl, P., et al., *Classifying collective cancer cell invasion*. Nature Cell Biology, 2012. **14**(8): p. 777-783.
103. Osswald, M., et al., *Brain tumour cells interconnect to a functional and resistant network*. Nature, 2015. **528**(7580): p. 93-98.
104. McCutcheon, S. and D.C. Spray, *Glioblastoma-Astrocyte Connexin 43 Gap Junctions Promote Tumor Invasion*. Mol Cancer Res, 2021.
105. Gritsenko, P.G., et al., *p120-catenin-dependent collective brain infiltration by glioma cell networks*. Nature Cell Biology, 2020. **22**(1): p. 97-107.
106. Weil, S., et al., *Tumor microtubules convey resistance to surgical lesions and chemotherapy in gliomas*. Neuro-Oncology, 2017. **19**(10): p. 1316-1326.
107. Joseph, J.V., et al., *TGF- β promotes microtube formation in glioblastoma through thrombospondin 1*. Neuro-Oncology, 2021.
108. de Gooijer, M.C., et al., *An Experimenter's Guide to Glioblastoma Invasion Pathways*. Trends in Molecular Medicine, 2018. **24**(9): p. 763-780.
109. Cuddapah, V.A., et al., *A neurocentric perspective on glioma invasion*. Nature reviews. Neuroscience, 2014. **15**(7): p. 455-465.
110. Gritsenko, P.G., O. Ilina, and P. Friedl, *Interstitial guidance of cancer invasion*. J Pathol, 2012. **226**(2): p. 185-99.
111. Giese, A., et al., *Cost of migration: invasion of malignant gliomas and implications for treatment*. J Clin Oncol, 2003. **21**(8): p. 1624-36.
112. Bellail, A.C., et al., *Microregional extracellular matrix heterogeneity in brain modulates glioma cell invasion*. The International Journal of Biochemistry & Cell Biology, 2004. **36**(6): p. 1046-1069.
113. Daubon, T., et al., *Deciphering the complex role of thrombospondin-1 in glioblastoma development*. Nature communications, 2019. **10**(1): p. 1146-1146.
114. Xia, S., et al., *Tumor microenvironment tenascin-C promotes glioblastoma invasion and negatively regulates tumor proliferation*. Neuro Oncol, 2016. **18**(4): p. 507-17.
115. Bowman, R.L., et al., *GlioVis data portal for visualization and analysis of brain tumor expression datasets*. Neuro Oncol, 2017. **19**(1): p. 139-141.
116. Piao, Y., L. Lu, and J. de Groot, *AMPA receptors promote perivascular glioma invasion via $\beta 1$ integrin-dependent adhesion to the extracellular matrix*. Neuro-Oncology, 2009. **11**(3): p. 260-273.
117. Zagzag, D., et al., *Molecular events implicated in brain tumor angiogenesis and invasion*. Pediatr Neurosurg, 2000. **33**(1): p. 49-55.
118. Chen, W., et al., *Human astrocytes secrete IL-6 to promote glioma migration and invasion through upregulation of cytomembrane MMP14*. Oncotarget; Vol 7, No 38, 2016.
119. Markovic, D.S., et al., *Gliomas induce and exploit microglial MT1-MMP expression for tumor expansion*. Proc Natl Acad Sci U S A, 2009. **106**(30): p. 12530-5.

120. Le, D.M., et al., *Exploitation of Astrocytes by Glioma Cells to Facilitate Invasiveness: A Mechanism Involving Matrix Metalloproteinase-2 and the Urokinase-Type Plasminogen Activator–Plasmin Cascade*. The Journal of Neuroscience, 2003. **23**(10): p. 4034.
121. Gilder, A.S., et al., *Soluble Urokinase Receptor Is Released Selectively by Glioblastoma Cells That Express Epidermal Growth Factor Receptor Variant III and Promotes Tumor Cell Migration and Invasion*. The Journal of biological chemistry, 2015. **290**(24): p. 14798-14809.
122. Mentlein, R., K. Hattermann, and J. Held-Feindt, *Lost in disruption: Role of proteases in glioma invasion and progression*. Biochimica et Biophysica Acta (BBA) - Reviews on Cancer, 2012. **1825**(2): p. 178-185.
123. Held-Feindt, J., et al., *Matrix-degrading proteases ADAMTS4 and ADAMTS5 (disintegrins and metalloproteinases with thrombospondin motifs 4 and 5) are expressed in human glioblastomas*. International Journal of Cancer, 2006. **118**(1): p. 55-61.
124. Liu, D., et al., *Tie2/TEK modulates the interaction of glioma and brain tumor stem cells with endothelial cells and promotes an invasive phenotype*. Oncotarget, 2010. **1**(8): p. 700-9.
125. Reardon, D.A., et al., *Phase 2 and biomarker study of trebananib, an angiopoietin-blocking peptibody, with and without bevacizumab for patients with recurrent glioblastoma*. Cancer, 2018. **124**(7): p. 1438-1448.
126. El Andaloussi, A. and M.S. Lesniak, *An increase in CD4+CD25+FOXP3+ regulatory T cells in tumor-infiltrating lymphocytes of human glioblastoma multiforme*. Neuro-oncology, 2006. **8**(3): p. 234-243.
127. Garcia, J.H., S. Jain, and M.K. Aghi, *Metabolic Drivers of Invasion in Glioblastoma*. Frontiers in cell and developmental biology, 2021. **9**: p. 683276-683276.
128. Labak, C.M., et al., *Glucose transport: meeting the metabolic demands of cancer, and applications in glioblastoma treatment*. American journal of cancer research, 2016. **6**(8): p. 1599-1608.
129. Libby, C.J., et al., *A role for GLUT3 in glioblastoma cell invasion that is not recapitulated by GLUT1*. Cell Adh Migr, 2021. **15**(1): p. 101-115.
130. Ye, Z.C. and H. Sontheimer, *Glioma cells release excitotoxic concentrations of glutamate*. Cancer Res, 1999. **59**(17): p. 4383-91.
131. Behrens, P.F., et al., *Extracellular glutamate and other metabolites in and around RG2 rat glioma: an intracerebral microdialysis study*. J Neurooncol, 2000. **47**(1): p. 11-22.
132. Fack, F., et al., *Altered metabolic landscape in IDH-mutant gliomas affects phospholipid, energy, and oxidative stress pathways*. EMBO Molecular Medicine, 2017. **9**(12): p. 1681-1695.
133. van Lith, S.A.M., et al., *Tumor cells in search for glutamate: an alternative explanation for increased invasiveness of IDH1 mutant gliomas*. Neuro-oncology, 2014. **16**(12): p. 1669-1670.
134. Takano, T., et al., *Glutamate release promotes growth of malignant gliomas*. Nat Med, 2001. **7**(9): p. 1010-5.

135. Lefranc, F., et al., *Glioblastoma quo vadis: Will migration and invasiveness reemerge as therapeutic targets?* *Cancer Treat Rev*, 2018. **68**: p. 145-154.
136. Venkataramani, V., et al., *Glutamatergic synaptic input to glioma cells drives brain tumour progression*. *Nature*, 2019. **573**(7775): p. 532-538.
137. Venkatesh, H.S., et al., *Electrical and synaptic integration of glioma into neural circuits*. *Nature*, 2019. **573**(7775): p. 539-545.
138. Osuka, S. and E.G. Van Meir, *Overcoming therapeutic resistance in glioblastoma: the way forward*. *J Clin Invest*, 2017. **127**(2): p. 415-426.
139. Molina, J.R., et al., *Invasive glioblastoma cells acquire stemness and increased Akt activation*. *Neoplasia*, 2010. **12**(6): p. 453-63.
140. Baker, G.J., et al., *Mechanisms of Glioma Formation: Iterative Perivascular Glioma Growth and Invasion Leads to Tumor Progression, VEGF-Independent Vascularization, and Resistance to Antiangiogenic Therapy*. *Neoplasia*, 2014. **16**(7): p. 543-561.
141. Scribner, E. and H.M. Fathallah-Shaykh, *Single Cell Mathematical Model Successfully Replicates Key Features of GBM: Go-Or-Grow Is Not Necessary*. *PLOS ONE*, 2017. **12**(1): p. e0169434.
142. Levin, V.A., et al., *Randomized, double-blind, placebo-controlled trial of marimastat in glioblastoma multiforme patients following surgery and irradiation* ★. *Journal of Neuro-Oncology*, 2006. **78**(3): p. 295-302.
143. Levin, V., et al., *Randomized phase II study of temozolomide (TMZ) with and without the matrix metalloprotease (MMP) inhibitor prinomastat in patients (pts) with glioblastoma multiforme (GBM) following best surgery and radiation therapy*. *Proceed ASCO*, 2002. **21**: p. 26a.
144. Wick, A., et al., *Phase 1b/2a study of galunisertib, a small molecule inhibitor of transforming growth factor-beta receptor I, in combination with standard temozolomide-based radiochemotherapy in patients with newly diagnosed malignant glioma*. *Investigational New Drugs*, 2020. **38**(5): p. 1570-1579.
145. Martínez, A. and E. Soriano, *Functions of ephrin/Eph interactions in the development of the nervous system: Emphasis on the hippocampal system*. *Brain Research Reviews*, 2005. **49**(2): p. 211-226.
146. Nakada, M., et al., *The phosphorylation of ephrin-B2 ligand promotes glioma cell migration and invasion*. *International journal of cancer*, 2010. **126**(5): p. 1155-1165.
147. Nabors, L.B., et al., *A safety run-in and randomized phase 2 study of cilengitide combined with chemoradiation for newly diagnosed glioblastoma (NABTT 0306)*. *Cancer*, 2012. **118**(22): p. 5601-7.
148. Stupp, R., et al., *Cilengitide combined with standard treatment for patients with newly diagnosed glioblastoma with methylated MGMT promoter (CENTRIC EORTC 26071-22072 study): a multicentre, randomised, open-label, phase 3 trial*. *The Lancet Oncology*, 2014. **15**(10): p. 1100-1108.
149. Nandhu, M.S., et al., *Development of a Function-Blocking Antibody Against Fibulin-3 as a Targeted Reagent for Glioblastoma*. *Clinical cancer research : an official journal of the American Association for Cancer Research*, 2018. **24**(4): p. 821-833.

-
150. Pencheva, N., et al., *Identification of a Druggable Pathway Controlling Glioblastoma Invasiveness*. Cell Rep, 2017. **20**(1): p. 48-60.
 151. Jung, E., et al., *Emerging intersections between neuroscience and glioma biology*. Nat Neurosci, 2019. **22**(12): p. 1951-1960.
 152. Holdhoff, M., et al., *Timed sequential therapy of the selective T-type calcium channel blocker mibefradil and temozolomide in patients with recurrent high-grade gliomas*. Neuro-Oncology, 2017. **19**(6): p. 845-852.
 153. Berges, R., et al., *A tubulin binding peptide targets glioma cells disrupting their microtubules, blocking migration, and inducing apoptosis*. Mol Ther, 2012. **20**(7): p. 1367-77.
 154. Karim, R., et al., *Enhanced and preferential internalization of lipid nanocapsules into human glioblastoma cells: effect of a surface-functionalizing NFL peptide*. Nanoscale, 2018. **10**(28): p. 13485-13501.
 155. Phillips, A.C., et al., *ABT-414, an Antibody-Drug Conjugate Targeting a Tumor-Selective EGFR Epitope*. Mol Cancer Ther, 2016. **15**(4): p. 661-9.
 156. Van Den Bent, M., et al., *INTELLANCE 2/EORTC 1410 randomized phase II study of Depatux-M alone and with temozolomide vs temozolomide or lomustine in recurrent EGFR amplified glioblastoma*. Neuro-Oncology, 2020. **22**(5): p. 684-693.
 157. Balchin, D., M. Hayer-Hartl, and F.U. Hartl, *In vivo aspects of protein folding and quality control*. Science, 2016. **353**(6294): p. aac4354.
 158. Flick, K. and P. Kaiser, *Protein degradation and the stress response*. Semin Cell Dev Biol, 2012. **23**(5): p. 515-22.
 159. Teicher, B.A. and J.E. Tomaszewski, *Proteasome inhibitors*. Biochemical Pharmacology, 2015. **96**(1): p. 1-9.
 160. Rajendra, J., et al., *Enhanced proteasomal activity is essential for long term survival and recurrence of innately radiation resistant residual glioblastoma cells*. Oncotarget, 2018. **9**(45): p. 27667-27681.
 161. Ciechanover, A. and P. Brundin, *The Ubiquitin Proteasome System in Neurodegenerative Diseases: Sometimes the Chicken, Sometimes the Egg*. Neuron, 2003. **40**(2): p. 427-446.
 162. Ciechanover, A. and A.L. Schwartz, *The ubiquitin system: pathogenesis of human diseases and drug targeting*. Biochimica et Biophysica Acta (BBA) - Molecular Cell Research, 2004. **1695**(1): p. 3-17.
 163. Ciechanover, A., *The ubiquitin-proteasome pathway: on protein death and cell life*. Embo j, 1998. **17**(24): p. 7151-60.
 164. Kumar, S., et al., *Autophagy and the Lysosomal System in Cancer*. Cells, 2021. **10**(10): p. 2752.
 165. Galluzzi, L., et al., *Molecular definitions of autophagy and related processes*. The EMBO journal, 2017. **36**(13): p. 1811-1836.
 166. Quinet, G., et al., *Mechanisms Regulating the UPS-ALS Crosstalk: The Role of Proteaphagy*. Molecules, 2020. **25**(10).
 167. Zaffagnini, G. and S. Martens, *Mechanisms of Selective Autophagy*. Journal of Molecular Biology, 2016. **428**(9, Part A): p. 1714-1724.

-
168. Bhattacharyya, S., et al., *Regulated protein turnover: snapshots of the proteasome in action*. Nature reviews. Molecular cell biology, 2014. **15**(2): p. 122-133.
 169. Larrue, C., et al., *Proteasome inhibitors induce FLT3-ITD degradation through autophagy in AML cells*. Blood, 2016. **127**(7): p. 882-92.
 170. Nedelsky, N.B., P.K. Todd, and J.P. Taylor, *Autophagy and the ubiquitin-proteasome system: collaborators in neuroprotection*. Biochimica et biophysica acta, 2008. **1782**(12): p. 691-699.
 171. Lim, J. and Z. Yue, *Neuronal aggregates: formation, clearance, and spreading*. Developmental cell, 2015. **32**(4): p. 491-501.
 172. Marshall, Richard S., et al., *Autophagic Degradation of the 26S Proteasome Is Mediated by the Dual ATG8/Ubiquitin Receptor RPN10 in Arabidopsis*. Molecular Cell, 2015. **58**(6): p. 1053-1066.
 173. Landis-Piowar, K.R., et al., *The proteasome as a potential target for novel anticancer drugs and chemosensitizers*. Drug Resistance Updates, 2006. **9**(6): p. 263-273.
 174. Yang, H., et al., *Repurposing old drugs as new inhibitors of the ubiquitin-proteasome pathway for cancer treatment*. Seminars in Cancer Biology, 2021. **68**: p. 105-122.
 175. Asano, S., et al., *A molecular census of 26S proteasomes in intact neurons*. Science, 2015. **347**(6220): p. 439-442.
 176. Kleiger, G. and T. Mayor, *Perilous journey: a tour of the ubiquitin-proteasome system*. Trends Cell Biol, 2014. **24**(6): p. 352-9.
 177. Clague, M.J., C. Heride, and S. Urbé, *The demographics of the ubiquitin system*. Trends Cell Biol, 2015. **25**(7): p. 417-26.
 178. Schwartz, A.L. and A. Ciechanover, *Targeting proteins for destruction by the ubiquitin system: implications for human pathobiology*. Annu Rev Pharmacol Toxicol, 2009. **49**: p. 73-96.
 179. Ciechanover, A., A. Orian, and A.L. Schwartz, *Ubiquitin-mediated proteolysis: biological regulation via destruction*. Bioessays, 2000. **22**(5): p. 442-51.
 180. Akutsu, M., I. Dikic, and A. Bremm, *Ubiquitin chain diversity at a glance*. J Cell Sci, 2016. **129**(5): p. 875-80.
 181. Thrower, J.S., et al., *Recognition of the polyubiquitin proteolytic signal*. Embo j, 2000. **19**(1): p. 94-102.
 182. Erpapazoglou, Z., O. Walker, and R. Haguenaue-Tsapis, *Versatile roles of k63-linked ubiquitin chains in trafficking*. Cells, 2014. **3**(4): p. 1027-88.
 183. Collins, G.A. and A.L. Goldberg, *The Logic of the 26S Proteasome*. Cell, 2017. **169**(5): p. 792-806.
 184. Jin, W.L., X.Y. Mao, and G.Z. Qiu, *Targeting Deubiquitinating Enzymes in Glioblastoma Multiforme: Expectations and Challenges*. Med Res Rev, 2017. **37**(3): p. 627-661.
 185. Scholz, N., et al., *Targeting the Ubiquitin System in Glioblastoma*. Front Oncol, 2020. **10**: p. 574011.

186. Lee, C., et al., *ATP-Dependent Proteases Degrade Their Substrates by Processively Unraveling Them from the Degradation Signal*. *Molecular Cell*, 2001. **7**(3): p. 627-637.
187. Peth, A., T. Uchiki, and A.L. Goldberg, *ATP-dependent steps in the binding of ubiquitin conjugates to the 26S proteasome that commit to degradation*. *Mol Cell*, 2010. **40**(4): p. 671-81.
188. Lee, B.H., et al., *USP14 deubiquitinates proteasome-bound substrates that are ubiquitinated at multiple sites*. *Nature*, 2016. **532**(7599): p. 398-401.
189. Crosas, B., et al., *Ubiquitin chains are remodeled at the proteasome by opposing ubiquitin ligase and deubiquitinating activities*. *Cell*, 2006. **127**(7): p. 1401-13.
190. Peth, A., et al., *Ubiquitinated proteins activate the proteasomal ATPases by binding to Usp14 or Uch37 homologs*. *The Journal of biological chemistry*, 2013. **288**(11): p. 7781-7790.
191. Fulda, S., et al., *Cellular stress responses: cell survival and cell death*. *International journal of cell biology*, 2010. **2010**: p. 214074-214074.
192. Ackerman, D. and M.C. Simon, *Hypoxia, lipids, and cancer: surviving the harsh tumor microenvironment*. *Trends in Cell Biology*, 2014. **24**(8): p. 472-478.
193. Anderson, P., N. Kedersha, and P. Ivanov, *Stress granules, P-bodies and cancer*. *Biochim Biophys Acta*, 2015. **1849**(7): p. 861-70.
194. Luo, J., N.L. Solimini, and S.J. Elledge, *Principles of Cancer Therapy: Oncogene and Non-oncogene Addiction*. *Cell*, 2009. **136**(5): p. 823-837.
195. Tameire, F., et al., *ATF4 couples MYC-dependent translational activity to bioenergetic demands during tumour progression*. *Nature cell biology*, 2019. **21**(7): p. 889-899.
196. Chen, M. and S. Xie, *Therapeutic targeting of cellular stress responses in cancer*. *Thorac Cancer*, 2018. **9**(12): p. 1575-1582.
197. McConkey, D.J., *The integrated stress response and proteotoxicity in cancer therapy*. *Biochemical and Biophysical Research Communications*, 2017. **482**(3): p. 450-453.
198. Tian, X., et al., *Targeting the Integrated Stress Response in Cancer Therapy*. *Frontiers in Pharmacology*, 2021. **12**(2621).
199. Anderson, P. and N. Kedersha, *Stressful initiations*. *Journal of Cell Science*, 2002. **115**(16): p. 3227-3234.
200. Chatterjee, D. and O. Chakrabarti, *Role of stress granules in modulating senescence and promoting cancer progression: special emphasis on glioma*. *Int J Cancer*, 2021.
201. Matsuki, H., et al., *Both G3BP1 and G3BP2 contribute to stress granule formation*. *Genes Cells*, 2013. **18**(2): p. 135-46.
202. Kedersha, N., P. Ivanov, and P. Anderson, *Stress granules and cell signaling: more than just a passing phase?* *Trends Biochem Sci*, 2013. **38**(10): p. 494-506.
203. Wolozin, B. and P. Ivanov, *Stress granules and neurodegeneration*. *Nature reviews. Neuroscience*, 2019. **20**(11): p. 649-666.

-
204. Shin, Y. and C.P. Brangwynne, *Liquid phase condensation in cell physiology and disease*. Science, 2017. **357**(6357).
 205. Somasekharan, S.P., et al., *YB-1 regulates stress granule formation and tumor progression by translationally activating G3BP1*. The Journal of cell biology, 2015. **208**(7): p. 913-929.
 206. Panas, M.D., P. Ivanov, and P. Anderson, *Mechanistic insights into mammalian stress granule dynamics*. J Cell Biol, 2016. **215**(3): p. 313-323.
 207. Attwood, K.M., et al., *Raloxifene prevents stress granule dissolution, impairs translational control and promotes cell death during hypoxia in glioblastoma cells*. Cell Death Dis, 2020. **11**(11): p. 989.
 208. Kedersha, N.L., et al., *RNA-binding proteins TIA-1 and TIAR link the phosphorylation of eIF-2 alpha to the assembly of mammalian stress granules*. J Cell Biol, 1999. **147**(7): p. 1431-42.
 209. Alberti, S., et al., *Granulostasis: Protein Quality Control of RNP Granules*. Front Mol Neurosci, 2017. **10**: p. 84.
 210. Tourrière, H., et al., *The RasGAP-associated endoribonuclease G3BP assembles stress granules*. The Journal of cell biology, 2003. **160**(6): p. 823-831.
 211. Kedersha, N., et al., *Dynamic shuttling of TIA-1 accompanies the recruitment of mRNA to mammalian stress granules*. J Cell Biol, 2000. **151**(6): p. 1257-68.
 212. Yang, P., et al., *G3BP1 Is a Tunable Switch that Triggers Phase Separation to Assemble Stress Granules*. Cell, 2020. **181**(2): p. 325-345.e28.
 213. Gilks, N., et al., *Stress granule assembly is mediated by prion-like aggregation of TIA-1*. Mol Biol Cell, 2004. **15**(12): p. 5383-98.
 214. Markmiller, S., et al., *Context-Dependent and Disease-Specific Diversity in Protein Interactions within Stress Granules*. Cell, 2018. **172**(3): p. 590-604.e13.
 215. Wheeler, J.R., et al., *Distinct stages in stress granule assembly and disassembly*. Elife, 2016. **5**.
 216. Jain, S., et al., *ATPase-Modulated Stress Granules Contain a Diverse Proteome and Substructure*. Cell, 2016. **164**(3): p. 487-98.
 217. Hofmann, S., et al., *Translation suppression promotes stress granule formation and cell survival in response to cold shock*. Molecular Biology of the Cell, 2012. **23**(19): p. 3786-3800.
 218. Turakhiya, A., et al., *ZFAND1 Recruits p97 and the 26S Proteasome to Promote the Clearance of Arsenite-Induced Stress Granules*. Mol Cell, 2018. **70**(5): p. 906-919.e7.
 219. Riggs, C.L., et al., *Mammalian stress granules and P bodies at a glance*. J Cell Sci, 2020. **133**(16).
 220. Dalton, L.E., et al., *Chapter 8 - Phosphoproteins in Stress-Induced Disease*, in *Progress in Molecular Biology and Translational Science*, S. Shenolikar, Editor. 2012, Academic Press. p. 189-221.
 221. Buchan, J.R., et al., *Eukaryotic stress granules are cleared by autophagy and Cdc48/VCP function*. Cell, 2013. **153**(7): p. 1461-1474.












-
222. Gwon, Y., et al., *Ubiquitination of G3BP1 mediates stress granule disassembly in a context-specific manner*. *Science*, 2021. **372**(6549): p. eabf6548.
 223. Dubinski, A. and C. Vande Velde, *Altered stress granule disassembly: links to neurodegenerative disease?* *Trends Neurosci*, 2021.
 224. Ganassi, M., et al., *A Surveillance Function of the HSPB8-BAG3-HSP70 Chaperone Complex Ensures Stress Granule Integrity and Dynamism*. *Molecular Cell*, 2016. **63**(5): p. 796-810.
 225. Buchberger, A., *Roles of Cdc48 in regulated protein degradation in yeast*. *Subcell Biochem*, 2013. **66**: p. 195-222.
 226. Meyer, H., M. Bug, and S. Bremer, *Emerging functions of the VCP/p97 AAA-ATPase in the ubiquitin system*. *Nature Cell Biology*, 2012. **14**(2): p. 117-123.
 227. van den Boom, J. and H. Meyer, *VCP/p97-Mediated Unfolding as a Principle in Protein Homeostasis and Signaling*. *Molecular Cell*, 2018. **69**(2): p. 182-194.
 228. Ju, J.-S., et al., *Valosin-containing protein (VCP) is required for autophagy and is disrupted in VCP disease*. *Journal of Cell Biology*, 2009. **187**(6): p. 875-888.
 229. Papadopoulos, C., et al., *VCP/p97 cooperates with YOD1, UBXD1 and PLAA to drive clearance of ruptured lysosomes by autophagy*. *The EMBO Journal*, 2017. **36**(2): p. 135-150.
 230. Wang, B., et al., *ULK1 and ULK2 Regulate Stress Granule Disassembly Through Phosphorylation and Activation of VCP/p97*. *Mol Cell*, 2019. **74**(4): p. 742-757.e8.
 231. Tolay, N. and A. Buchberger, *Comparative profiling of stress granule clearance reveals differential contributions of the ubiquitin system*. *Life Sci Alliance*, 2021. **4**(5).
 232. Schuster, A., et al., *ANI-type zinc finger protein 3 (ZFAND3) is a transcriptional regulator that drives Glioblastoma invasion*. *Nat Commun*, 2020. **11**(1): p. 6366.
 233. Puchalski, R.B., et al., *An anatomic transcriptional atlas of human glioblastoma*. *Science*, 2018. **360**(6389): p. 660-663.
 234. Schuster, A., et al., *RNAi/CRISPR Screens: from a Pool to a Valid Hit*. *Trends Biotechnol*, 2019. **37**(1): p. 38-55.
 235. Bartha, I., et al., *Human gene essentiality*. *Nat Rev Genet*, 2018. **19**(1): p. 51-62.
 236. Przybyla, L. and L.A. Gilbert, *A new era in functional genomics screens*. *Nature Reviews Genetics*, 2021.
 237. Prolo, L.M., et al., *Targeted genomic CRISPR-Cas9 screen identifies MAP4K4 as essential for glioblastoma invasion*. *Sci Rep*, 2019. **9**(1): p. 14020.
 238. Yang, J., et al., *Genome-wide RNAi screening identifies genes inhibiting the migration of glioblastoma cells*. *PLoS One*, 2013. **8**(4): p. e61915.
 239. Hart, T., et al., *High-Resolution CRISPR Screens Reveal Fitness Genes and Genotype-Specific Cancer Liabilities*. *Cell*, 2015. **163**(6): p. 1515-26.
 240. Mitsunobu, H., et al., *Beyond Native Cas9: Manipulating Genomic Information and Function*. *Trends in Biotechnology*, 2017. **35**(10): p. 983-996.

-
241. Gilbert, Luke A., et al., *Genome-Scale CRISPR-Mediated Control of Gene Repression and Activation*. Cell, 2014. **159**(3): p. 647-661.
 242. Sack, L.M., et al., *Profound Tissue Specificity in Proliferation Control Underlies Cancer Drivers and Aneuploidy Patterns*. Cell, 2018. **173**(2): p. 499-514.e23.
 243. Pontén, F., K. Jirström, and M. Uhlen, *The Human Protein Atlas--a tool for pathology*. J Pathol, 2008. **216**(4): p. 387-93.
 244. Stanhill, A., et al., *An arsenite-inducible 19S regulatory particle-associated protein adapts proteasomes to proteotoxicity*. Mol Cell, 2006. **23**(6): p. 875-85.
 245. Yun, C., et al., *Proteasomal adaptation to environmental stress links resistance to proteotoxicity with longevity in *Caenorhabditis elegans**. Proc Natl Acad Sci U S A, 2008. **105**(19): p. 7094-9.
 246. Lee, D., S. Takayama, and A.L. Goldberg, *ZFAND5/ZNF216 is an activator of the 26S proteasome that stimulates overall protein degradation*. Proc Natl Acad Sci U S A, 2018. **115**(41): p. E9550-e9559.
 247. Digregorio, M., et al., *Relevance of Translation Initiation in Diffuse Glioma Biology and its Therapeutic Potential*. Cells, 2019. **8**(12): p. 1542.
 248. Fhu, C.W. and A. Ali, *Dysregulation of the Ubiquitin Proteasome System in Human Malignancies: A Window for Therapeutic Intervention*. Cancers, 2021. **13**(7): p. 1513.
 249. Vlachostergios, P.J., I.A. Voutsadakis, and C.N. Papandreou, *The shaping of invasive glioma phenotype by the ubiquitin-proteasome system*. Cell Commun Adhes, 2013. **20**(5): p. 87-92.
 250. Taniuchi, K., I. Nishimori, and M.A. Hollingsworth, *The N-Terminal Domain of G3BP Enhances Cell Motility and Invasion by Posttranscriptional Regulation of BART*. Molecular Cancer Research, 2011. **9**(7): p. 856-866.
 251. Wang, Y., et al., *G3BP1 promotes tumor progression and metastasis through IL-6/G3BP1/STAT3 signaling axis in renal cell carcinomas*. Cell death & disease, 2018. **9**(5): p. 501-501.
 252. Bittencourt, L.F.F., et al., *G3BP1 knockdown sensitizes U87 glioblastoma cell line to Bortezomib by inhibiting stress granules assembly and potentializing apoptosis*. J Neurooncol, 2019. **144**(3): p. 463-473.
 253. Zhang, Y., et al., *Repression of the stress granule protein G3BP2 inhibits immune checkpoint molecule PD-L1*. Mol Oncol, 2021.
 254. Brigelius-Flohé, R. and A. Kipp, *Glutathione peroxidases in different stages of carcinogenesis*. Biochim Biophys Acta, 2009. **1790**(11): p. 1555-68.
 255. Wei, P.-C., et al., *Loss of the oxidative stress sensor NPGPx compromises GRP78 chaperone activity and induces systemic disease*. Molecular cell, 2012. **48**(5): p. 747-759.
 256. Gan, X., et al., *High GPX1 expression promotes esophageal squamous cell carcinoma invasion, migration, proliferation and cisplatin-resistance but can be reduced by vitamin D*. International journal of clinical and experimental medicine, 2014. **7**(9): p. 2530-2540.

-
257. Lee, E., et al., *Glutathione peroxidase-1 regulates adhesion and metastasis of triple-negative breast cancer cells via FAK signaling*. Redox Biology, 2020. **29**: p. 101391.
 258. Banning, A., et al., *Glutathione Peroxidase 2 Inhibits Cyclooxygenase-2-Mediated Migration and Invasion of HT-29 Adenocarcinoma Cells but Supports Their Growth as Tumors in Nude Mice*. Cancer Res, 2008. **68**(23): p. 9746-53.
 259. Zhu, X., et al., *GPX3 suppresses tumor migration and invasion via the FAK/AKT pathway in esophageal squamous cell carcinoma*. American journal of translational research, 2018. **10**(6): p. 1908-1920.
 260. Peng, G., et al., *Glutathione peroxidase 4 maintains a stemness phenotype, oxidative homeostasis and regulates biological processes in Panc-1 cancer stem-like cells*. Oncol Rep, 2019. **41**(2): p. 1264-1274.
 261. Zhao, H., et al., *Gpx 4 is involved in the proliferation, migration and apoptosis of glioma cells*. Pathology - Research and Practice, 2017. **213**(6): p. 626-633.
 262. Zhang, J., et al., *GPX8 promotes migration and invasion by regulating epithelial characteristics in non-small cell lung cancer*. Thorac Cancer, 2020. **11**(11): p. 3299-3308.
 263. Khatib, A., et al., *The glutathione peroxidase 8 (GPX8)/IL-6/STAT3 axis is essential in maintaining an aggressive breast cancer phenotype*. Proceedings of the National Academy of Sciences, 2020. **117**(35): p. 21420-21431.
 264. Nguyen, V.D., et al., *Two endoplasmic reticulum PDI peroxidases increase the efficiency of the use of peroxide during disulfide bond formation*. J Mol Biol, 2011. **406**(3): p. 503-15.
 265. Limia, C.M., et al., *Emerging Roles of the Endoplasmic Reticulum Associated Unfolded Protein Response in Cancer Cell Migration and Invasion*. Cancers, 2019. **11**(5): p. 631.
 266. Urra, H., et al., *Endoplasmic Reticulum Stress and the Hallmarks of Cancer*. Trends in Cancer, 2016. **2**(5): p. 252-262.
 267. Fang, J., et al., *Metformin alleviates human cellular aging by upregulating the endoplasmic reticulum glutathione peroxidase 7*. Aging Cell, 2018. **17**(4): p. e12765.
 268. Joseph, J.V., et al., *Hypoxia enhances migration and invasion in glioblastoma by promoting a mesenchymal shift mediated by the HIF1 α -ZEB1 axis*. Cancer Letters, 2015. **359**(1): p. 107-116.

I

AN1-type zinc finger protein 3 (ZFAND3) is a transcriptional regulator that drives Glioblastoma invasion

Anne Schuster¹, Eliane Klein¹, Virginie Neirinckx ¹, Arnon Møldrup Knudsen ^{2,3}, Carina Fabian^{1,4}, Ann-Christin Hau ¹, Monika Dieterle ¹, Anais Oudin¹, Petr V. Nazarov ⁵, Anna Golebiewska ¹, Arnaud Muller⁵, Daniel Perez-Hernandez⁵, Sophie Rodius⁵, Gunnar Dittmar ⁵, Rolf Bjerkgvig ^{1,4}, Christel Herold-Mende ⁶, Barbara Klink ^{7,8}, Bjarne Winther Kristensen^{2,3} & Simone P. Niclou ^{1,4}✉

The infiltrative nature of Glioblastoma (GBM), the most aggressive primary brain tumor, critically prevents complete surgical resection and masks tumor cells behind the blood brain barrier reducing the efficacy of systemic treatment. Here, we use a genome-wide interference screen to determine invasion-essential genes and identify the AN1/A20 zinc finger domain containing protein 3 (ZFAND3) as a crucial driver of GBM invasion. Using patient-derived cellular models, we show that loss of ZFAND3 hampers the invasive capacity of GBM, whereas ZFAND3 overexpression increases motility in cells that were initially not invasive. At the mechanistic level, we find that ZFAND3 activity requires nuclear localization and integral zinc-finger domains. Our findings indicate that ZFAND3 acts within a nuclear protein complex to activate gene transcription and regulates the promoter of invasion-related genes such as *COL6A2*, *FN1*, and *NRCAM*. Further investigation in ZFAND3 function in GBM and other invasive cancers is warranted.

¹NORLUX Neuro-Oncology Laboratory, Department of Oncology, Luxembourg Institute of Health, Luxembourg, Luxembourg. ²Department of Pathology, Odense University Hospital, Odense, Denmark. ³Department of Clinical Research, University of Southern Denmark, Odense, Denmark. ⁴Department of Biomedicine, University of Bergen, Bergen, Norway. ⁵Quantitative Biology Unit, Luxembourg Institute of Health, Luxembourg, Luxembourg. ⁶Division of Neurosurgical Research, Department of Neurosurgery, University of Heidelberg, Heidelberg, Germany. ⁷National Center of Genetics, Laboratoire National de Santé, Dudelange, Luxembourg. ⁸Functional Tumor Genetics, Department of Oncology, Luxembourg Institute of Health, Luxembourg, Luxembourg. ✉email: simone.niclou@lih.lu

Cancer cell invasion and ensuing metastasis are a leading cause of death. Malignant tumors of the brain, including Glioblastoma (GBM), are characterized by a high invasive capacity leading to a spread throughout the brain parenchyma¹, a growth pattern which is largely accountable for the current therapeutic failure and poor patient outcome. Invasive cells that migrate away from the tumor core escape surgical resection, are partially sheltered from radio- and chemotherapy and are not detected by standard imaging techniques. Furthermore it was recently shown that glial tumors form multicellular networks through ultra-long membrane protrusions, so-called tumor microtubules, that facilitate brain invasion and contribute to treatment resistance^{2,3}.

Due to the specific structure of the adult brain, GBM invasion differs from vascular or lymphatic pathways classically associated with peripheral metastatic cancer. GBM cells insinuate themselves in the interstitial space of the neural tissue or migrate along blood vessels and white matter tracts, relying on basal membranes and extracellular matrix (ECM) components⁴. Although significant efforts were carried out to elucidate the mechanisms underlying GBM cell invasion (e.g., cytoskeleton remodeling, secretion of proteases, intracellular signaling)⁵, therapeutic approaches targeting GBM invasion have not heralded any benefit so far and novel targets regulating the invasive process are actively being pursued^{6–8}.

RNA interference screens are powerful tools to uncover gene function and their contribution to specific cellular phenotypes⁹. Such approaches allowed e.g., the identification of genes involved in cell migration and invasion in various cancer models^{10,11} including GBM¹². Here, we applied genome-wide RNA interference in GBM and identified AN1-Type Zinc Finger protein 3 (ZFAND3) as a key regulator of GBM cell invasion. Zinc finger (ZF) proteins are involved in nucleic acid recognition, transcriptional activation, protein folding and assembly, however the function of ZFAND3 remains unknown. ZFAND3 (also known as testis expressed sequence 27, *Tex27*) was initially characterized during mouse sperm maturation^{13,14} and was associated with susceptibility for development of type 2 diabetes in humans^{15,16}. We find that ZFAND3 strongly potentiates invasiveness of GBM patient-derived cells in vitro, ex vivo and in vivo. We show that nuclear ZFAND3 expression is increased in the infiltrative compartment in GBM patient biopsies and that nuclear localization is essential for ZFAND3 activity. Finally we identify ZFAND3 as a transcription factor that regulates expression of adhesion and invasion-related genes.

Results

RNA interference screen identifies ZFAND3 as a candidate gene involved in GBM invasion. Although GBMs in patients are invariably invasive, not all patient-derived GBM cells display the same invasion capacity. Inter-patient differences can be observed when patient-derived GBM stem-like cells (GSCs) are implanted into the mouse brain: Non-invasive (NI) cells grow as circumscribed tumors displaying aberrant blood vessels and necrosis; low invasive (LI) cells partially invade into the cortex and traverse the corpus callosum to the contralateral hemisphere and highly invasive cells (HI) completely colonize the brain parenchyma of both hemispheres (Fig. 1a, additional examples on Supplementary Fig. 1a, b). We have previously described similar histological phenotypes with differential invasive potential in GBM patient-derived orthotopic xenografts based on organotypic tumor spheroids¹⁷. Interestingly the distinct invasive behavior of GSCs could be recapitulated in vitro, e.g., using 3D-Boyden chamber assays (Fig. 1b, c, Supplementary Fig. 1a, b) or sphere sprouting assays (Fig. 1d, e). We further confirmed the differential invasive

phenotypes in ex vivo invasion assays in organotypic brain slice cultures, which allowed to determine differences in single cell velocity (Fig. 1f–i). The invasion capacity was correlated to the expression of some (*CDH2*, *MMP2*, *SNAIL1*, *ZEB1*) but not all known invasion markers in vitro and in vivo (Supplementary Fig. 1c–h), but did not correlate to transcriptional GBM subtypes (proneural, mesenchymal, classical) as defined by Wang et al.¹⁸ (Supplementary Fig. 1i). Taken together these data indicate that patient-derived GSCs faithfully reflect the heterogeneity and invasion capacity of GBM in vivo, ex vivo and in vitro.

Using highly invasive (HI) GBM GSCs, we performed a genome-wide loss-of-function shRNA screen to uncover novel key drivers of GBM invasion. Invasion-defective and invasion-competent cells were specifically isolated using the Boyden chamber assay (Fig. 2a). In highly aneuploid cancer cells, such as GBM GSCs, RNA interference may be more reliable than CRISPR based knockout screens, because the transcripts rather than the DNA are targeted⁹. Focusing on the invasion-defective cells, barcoded shRNAs were sequenced and a stringent bioinformatic analysis pipeline was applied by combining four of the most common analysis methods: RSA¹⁹, RIGER²⁰, MAGECK^{21,22}, and HiTSelect²³ (Supplementary Fig. 2a, b). Only the gene candidates in common between all four methods were selected, resulting in a set of 17 invasion-essential candidate genes within the 2% top hits (Fig. 2b). This included Colony stimulating factor 1 (*CSF1*), a known cytokine involved in invasion and metastasis. To further reduce the number of gene candidates of interest, we analysed the expression of the 17 genes in NI, LI, and HI cells in vitro and when grown as xenografts in vivo. Compared to other candidate genes, the AN1-Type Zinc Finger protein 3 (*ZFAND3*) gene showed higher expression in HI cells compared to NI and LI cells, in vitro as well as in vivo, and corresponding knockdown clones were enriched in the analysis (Supplementary Fig. 2b–d), we therefore focused on *ZFAND3* for further analysis. Quantitative real time PCR (qPCR) confirmed a higher expression of *ZFAND3* in HI cells, compared to LI and NI (Fig. 2c). Immunohistochemistry of corresponding GBM xenografts in the mouse brain showed more ZFAND3 positive cells in HI tumors in comparison to LI tumors (Fig. 2d). Analysis of TCGA data via the GlioVis platform²⁴ revealed strong *ZFAND3* expression in all classes of diffuse glioma compared to nontumor controls (Supplementary Fig. 2e), in line with the high invasive potential of these tumors. There was no correlation with transcriptional GBM subtypes (Supplementary Fig. 2f). Pan-tumor studies based on TCGA and GTEx databases (via GEPIA platform)^{25,26} also highlighted increased *ZFAND3* expression in diverse cancers compared to control tissue, in particular in pancreatic adenocarcinoma and melanoma (Supplementary Fig. 2g). Next we analysed ZFAND3 protein expression in 21 fresh GBM patient biopsies. ZFAND3 protein was detected in the majority of GBM (17/21) and throughout different tumor compartments, including central, intermediate and peripheral areas (Fig. 2e). By immunofluorescence, we found that ZFAND3 was present in the cytoplasm and the nucleus of GBM cells (identified by P53 staining) and we analysed the fraction of ZFAND3 positive tumor cells based on subcellular localization (Fig. 2f and Supplementary Fig. 3a, b). The fraction of positive cells was similar throughout different tumor compartments, both for cytoplasmic and nuclear staining (Supplementary Fig. 3c, d). However, in contrast to cytoplasmic ZFAND3 staining (Fig. 2g), we found that both the staining intensity and the ratio of nuclear/cytoplasmic ZFAND3 staining were increased in peripheral tumor cells compared to central cells, indicating that the relative fraction of tumor cells with nuclear ZFAND3 is higher in the tumor periphery, and that nuclear ZFAND3 is expressed to a higher extent in these cells (Fig. 2h, i). Since ZFAND3 appeared also in nontumor cells, we

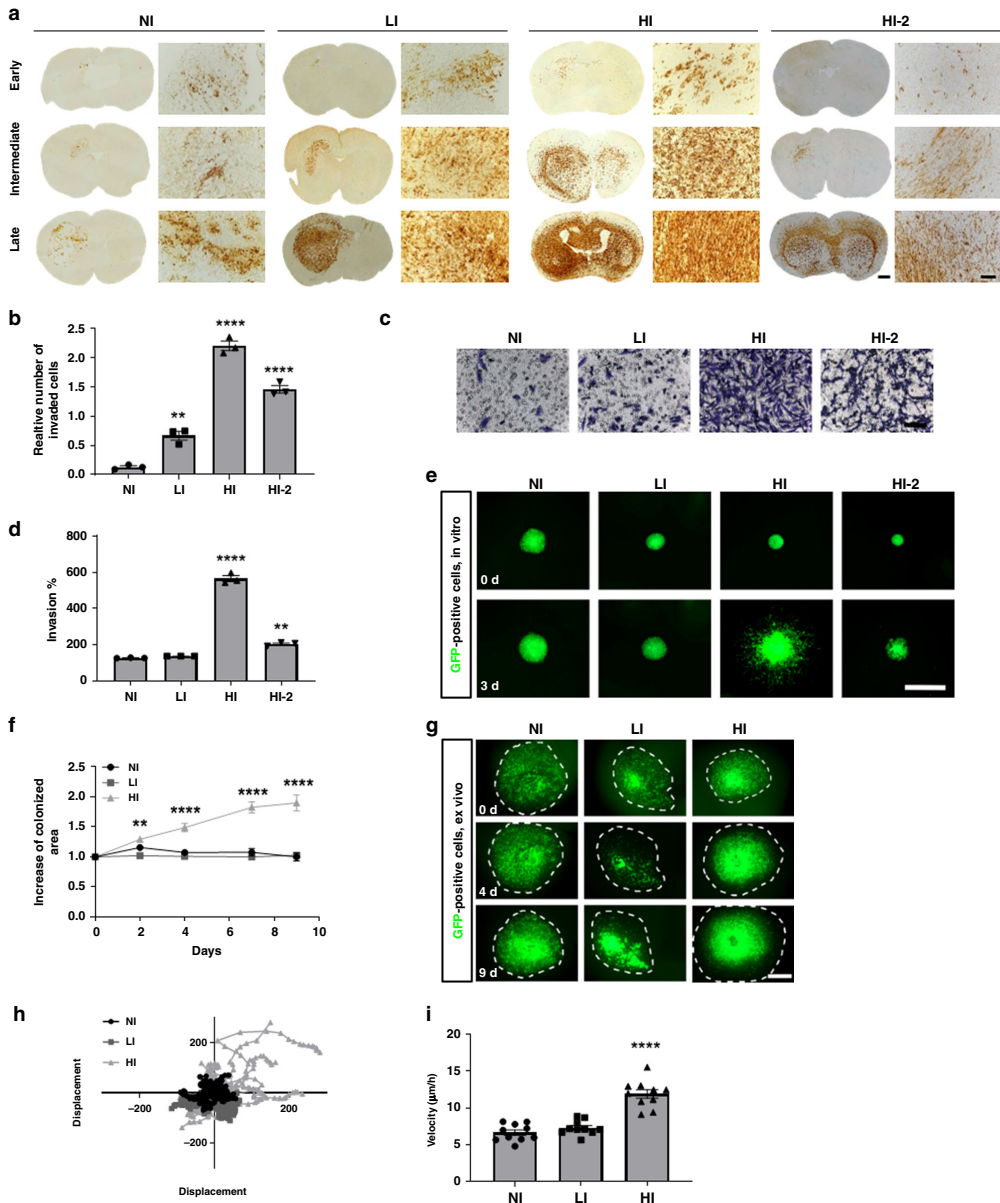
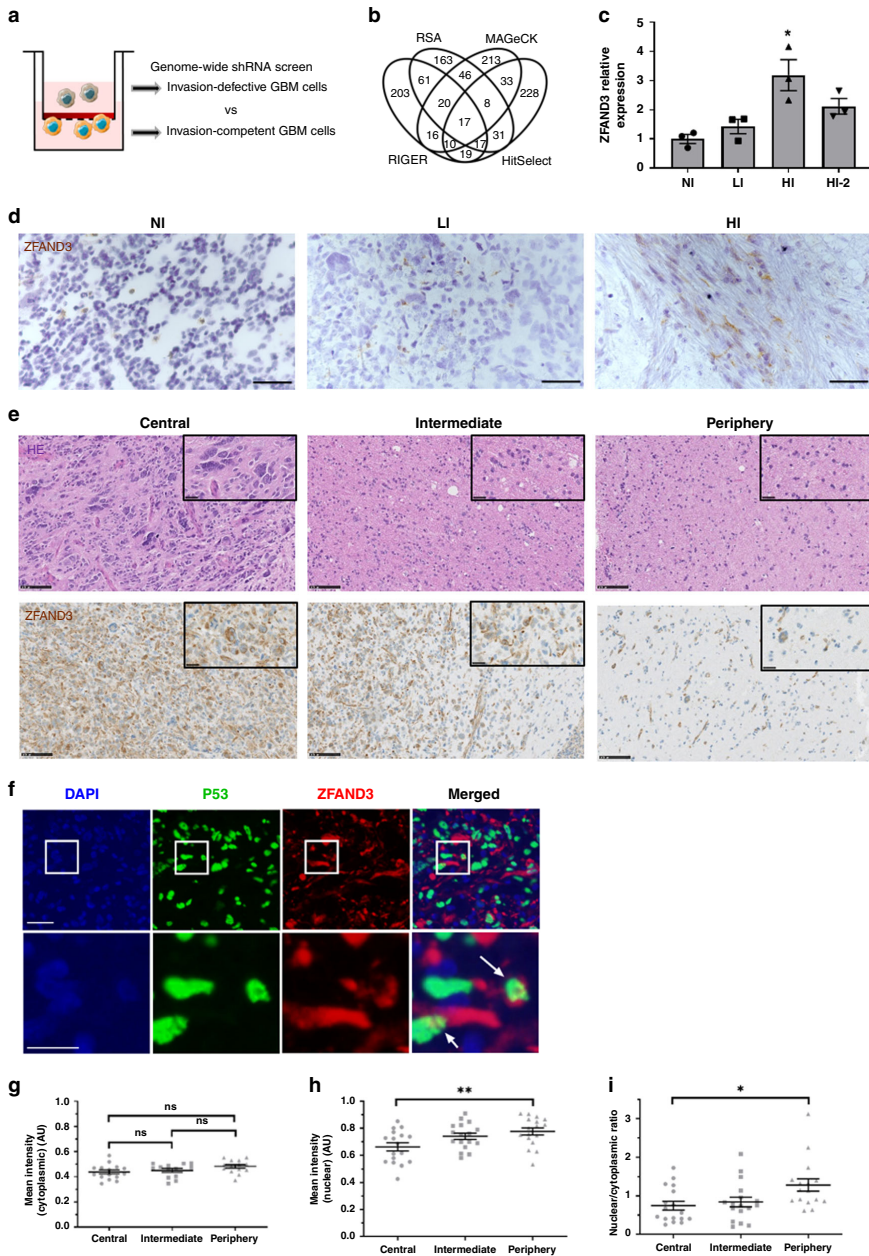


Fig. 1 Patient-derived GBM stem-like cells (GSCs) display different invasion phenotypes in vivo, which are recapitulated in in vitro and ex vivo assays.

a Early, intermediate and late time point of different GSC orthotopic xenografts in mice displaying non invasive (NI), low invasive (LI) and highly invasive (HI, HI-2) phenotypes. Respective tumor development times were 5 weeks (NI), 8 weeks (LI) and 25 weeks (HI, HI-2). Anti-human vimentin staining was used to visualize tumor cells (Scale bars = 100 µm and 1000 µm for overview). ($n = 2$ mice for each tumor and time point with $n = 3$ –4 sections per mouse). **b** In vitro Boyden Chamber invasion assay, displaying the relative number of invaded cells ($n = 3$). **c** Representative pictures of in vitro Boyden chamber invasion assay reflecting the different invasion phenotypes. Scale bar 100 µm. **d** Quantification of invasion of GSCs in 3D sprouting assay ($n = 3$). **e** Representative pictures of sprouting assay of different GFP-positive GSCs ($n = 3$) (Scale bar = 1000 µm). GFP: Green fluorescent protein. **f** Quantification of increase of colonized area of GSCs in ex vivo brain slice cultures, 9 days after tumor implantation ($n = 10$). **g** Representative pictures of GSCs in ex vivo brain slice cultures at day 0, 4, and 9 (Scale bar = 1000 µm). **h** Displacement of GSCs injected into ex vivo brain slice cultures ($n = 10$). **i** Velocity of GSCs in ex vivo brain slice cultures. Results of (**b**, **d**, **f** and **i**) displayed as average \pm SEM and were analyzed with one-way ANOVA. ** $p_{\text{value}} < 0.01$, **** $p_{\text{value}} < 0.0001$.



performed colabeling for Iba1 (microglia marker) and NeuN (neuronal marker). We observed some colocalization with Iba1, but not with NeuN, both in clinical samples (Supplementary Fig. 3e) and in xenografts (Supplementary Fig. 3f), indicating that ZFAND3 is expressed by a subpopulation of microglial cells. The majority of staining was found in the tumor area rather than in the neuropil (Supplementary Fig. 3f lower panel). In conclusion,

we identified ZFAND3 as an invasion-related gene that displays increased nuclear expression in the infiltrative tumor compartment of clinical GBM specimen.

ZFAND3 knockdown impairs GBM cell invasion in vitro, ex vivo and in vivo. To confirm the functional screen data,

Fig. 2 Expression of ZFAND3 is associated with GBM cell invasion. **a** Set up of genome-wide shRNA pooled screen selecting for invasion-defective and invasion-competent cells in ECM-collagen coated transwell chambers. **b** Loss-of-function screen focused on shRNAs significantly enriched in invasion-defective cells. Results were analysed with RSA, RIGER, MAGeCK and HitSelect methods, identifying 17 genes as the top 2% common hits. **c** qPCR showed higher ZFAND3 expression in highly invasive GSCs (HI, HI-2) compared to non-invasive (NI) ($n = 3$; $p = 0.007$) and low-invasive (LI) cells ($n = 3$ biologically independent samples). Results are displayed as average \pm SEM and were analysed with one-way ANOVA. $^*p_{\text{value}} < 0.1$. **d** IHC for ZFAND3 in intracranial GBM xenografts in mice generated from respected patient-derived GSCs (NI, LI HI) (Scale bars = 50 μm , hematoxylin counterstaining). **e** IHC revealed ZFAND3 protein in GBM patient biopsies in the tumor core (central), intermediate area (intermediate) and tumor margin with diffuse infiltration (periphery) (Scale bars = 100 μm). Representative images are shown ($n = 21$). **f** Triple immunofluorescence identified ZFAND3 staining in cytoplasm and nucleus of positive tumor cells: ZFAND3 (red), P53 (green) and DAPI (blue) (Scale bar upper row = 50 μm , lower row = 15 μm). ($n = 17$ different patient samples). Mean intensity of cytoplasmic (**g**) and nuclear (**h**) ZFAND3+ tumor cells in central, intermediate, and peripheral tumor areas, the latter being increased in the periphery ($n = 17$). Data were analyzed as matched data with one-way ANOVA and Tukey's multiple comparison test. ($p = 0.009$) **i** Ratio of nuclear/cytoplasmic ZFAND3 staining is increased in the periphery compared to the central tumor area ($n = 17$ patient samples). Data were analysed as matched data with Kruskal-Wallis test and Dunn's multiple comparison test ($p = 0.012$). $^*p_{\text{value}} < 0.05$, $^{**}p_{\text{value}} < 0.01$.

shRNA-mediated knockdown (KD) of ZFAND3 was performed in two highly invasive GSCs (HI and HI-2). Efficient KD with two different shRNAs was achieved at RNA and protein level (Fig. 3a, b and Supplementary Fig. 4a–e). Similar to patient samples, endogenous ZFAND3 protein displayed cytoplasmic and nuclear localization, while KD cells only retained minor cytoplasmic staining (Fig. 3c). ZFAND3 KD had no significant impact on cell proliferation (Fig. 3d). Using Boyden chamber assays on the same cells, ZFAND3 KD significantly reduced invasion compared to shCtrl in HI cells (Fig. 3e, f). This was confirmed in the HI-2 cell line (Supplementary Fig. 4a–e).

To better imitate invasion in a brain microenvironment, we implanted GBM HI cells into ex vivo brain slices. In ZFAND3 KD cells the area of colonization of the brain slice was decreased in contrast to shCtrl (Fig. 3g, h) and cellular velocity, as determined by single cell tracking, was reduced accordingly (Fig. 3i, j). Finally, we evaluated the invasion potential of ZFAND3 KD cell in vivo: eight weeks after intracranial tumor implantation, the mice were sacrificed and cell invasion to the contralateral hemisphere was quantified. We found significantly less cells in ZFAND3 KD tumors compared to control (Fig. 3k, l and Supplementary Fig. 4j). Taken together these data validate the result of the screen and indicate that loss of ZFAND3 strongly impairs GBM cell invasion in vitro, ex vivo and in vivo.

Expression of ZFAND3 confers invasion potential to non-invasive patient-derived GBM cells. Given that ZFAND3 downregulation considerably decreased the invasion potential of invasive GSCs, we asked if ZFAND3 overexpression was able to bestow invasion capacity to non-invasive (NI) GSCs. We therefore expressed ZFAND3 in NI GSCs, as shown by qPCR (Fig. 4a) and western blot analysis (Fig. 4b). Upon overexpression, ZFAND3 protein mostly accumulated in the nucleus (Fig. 4c) and did not affect proliferation of the cells (Fig. 4d). Instead we found that ZFAND3 increased invasion in vitro (Fig. 4e, f) and ex vivo in brain slice cultures. ZFAND3 expressing cells colonized a larger area (Fig. 4g, h) and displayed higher velocity (Fig. 4i, j). Upon transplantation in the mouse brain, ZFAND3 expressing tumors lost the circumscribed growth pattern of control NI cells (Fig. 4k and Supplementary Fig. 4k). The number of cells escaping the tumor mass was significantly increased for ZFAND3 expressing cells, compared to controls (Fig. 4l). These data indicate that ZFAND3 expression confers invasion potential to GBM cells that were initially not invasive.

Nuclear localization of ZFAND3 is required for GBM cell invasion. ZFAND3 contains two ZF domains, a N-terminal A20 domain and a C-terminal AN1 domain separated by a linker region (Fig. 5a). As we found ZFAND3 immunostaining in the

nucleus and nuclear localization was increased in the infiltrative tumor compartment, we asked whether nuclear localization was needed for ZFAND3 activity. A ZFAND3 construct with a mutated nuclear localization signal (NLS) (ZFAND3-mutNLS) was expressed in NI cells (Fig. 5a–c and Supplementary Fig. 5a–c). This resulted in ZFAND3 accumulation in the cytoplasm (Fig. 5d) and prevented ZFAND3-induced invasion (Fig. 5f, g). The addition of a second NLS sequence to the mutant construct rescued both nuclear localisation and the invasion phenotype (Fig. 5a–g), indicating that ZFAND3 was active in the nucleus. No impact on proliferation was observed (Fig. 5e). In summary, these data demonstrate that nuclear localization is required for ZFAND3-induced invasion.

Deletion of zinc-finger domains leads to loss of invasion phenotype. In an attempt to further uncover the molecular basis of its activity, we generated ZFAND3 mutants with deletion of individual or both ZF domains (ZFAND3- $\Delta 1$, $\Delta 2$, and $\Delta 1\Delta 2$) (Fig. 5a and Supplementary Fig. 5a), and expressed them in NI GSCs (Fig. 5h, i). None of the variants exhibited proliferation defects (Fig. 5j). In contrast to full length ZFAND3, no increase in invasion was observed in cells expressing ZFAND3- $\Delta 1$, ZFAND3- $\Delta 2$ or ZFAND3- $\Delta 1\Delta 2$ (Fig. 5k, l), suggesting that both ZF domains are required for induction of invasion. Of note, while the double deletion construct accumulated in the cytoplasm, ZFAND3- $\Delta 1$ and ZFAND3- $\Delta 2$ correctly translocated to the nucleus (Fig. 5m). To further pinpoint the active residues, we generated point mutations in putative zinc-complexing amino acids (M1, M2, and M1-M2) (Supplementary Fig. 5a). These constructs retained nuclear localization, but also full activity with regard to the invasive phenotype (Supplementary Fig. 5b–g). In conclusion, although the exact residues conferring nuclear ZFAND3 activity remain elusive, our data hint to the need of both ZF domains to trigger invasion in GBM cells, suggesting that ZFAND3 may act as a transcriptional regulator.

ZFAND3 is involved in transcriptional regulation of invasion-related genes. To address whether ZFAND3 correlates with the expression of genes involved in migration and epithelial-mesenchymal transition, we analysed expression of *CDH2* (coding for N-cadherin), *MMP2*, *SNAI2* and *ZEB1* in GSCs with various ZFAND3 expression levels. Surprisingly, the modulation of ZFAND3 expression (KD or overexpression) or function (mutation constructs) did not affect expression of these genes (Supplementary Fig. 6). We therefore performed RNA sequencing on shCtrl, shZFAND3-1 and shZFAND3-2 HI cells to gain broader insight into the transcriptional landscape upon ZFAND3 knockdown. Among the differentially expressed genes (DEGs), 58 genes were significantly downregulated in both shZFAND3-1 and shZFAND3-2 versus

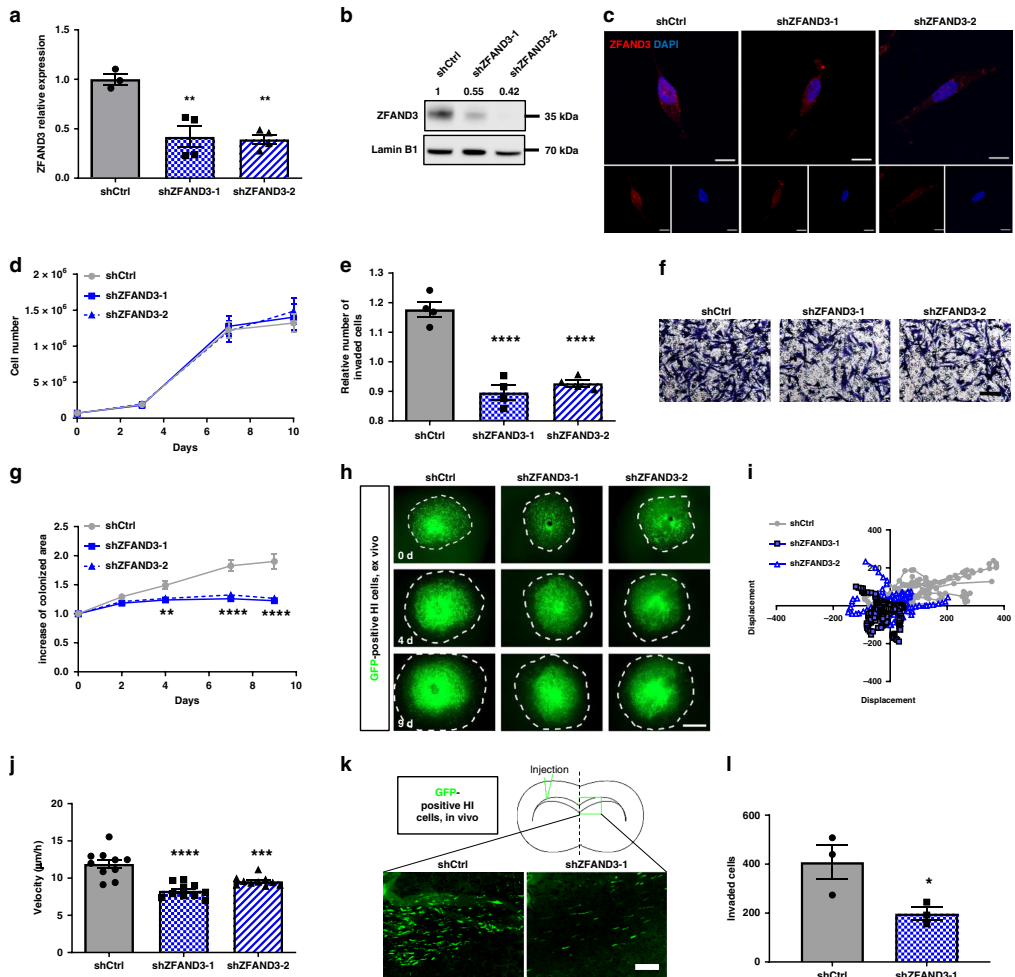


Fig. 3 Knockdown of ZFAND3 decreases invasion capacity of highly-invasive GBM cells. **a** qPCR confirming knockdown (KD) of ZFAND3 in highly invasive GCSs (HI) using two ZFAND3 shRNAs ($n \geq 3$ biologically independent samples). Results are displayed as average \pm SEM and were analysed with one-way ANOVA. **b, c** Decrease of ZFAND3 protein in ZFAND3 KD by western blot ($n = 3$) and IF staining (red: ZFAND3, blue: DAPI. Scale bars = 10 μ m) ($n = 2$). In analogy to patient samples, ZFAND3 protein is present in the nucleus and cytoplasm. **d** Growth curves of control and ZFAND3 KD cells show no defect in cell proliferation ($n = 3$ biologically independent experiments). **e, f** Boyden chamber invasion assay showing reduced invasion in ZFAND3 KD cells compared to control ($n = 4$ biologically independent experiments) (Scale bar = 100 μ m). Results are displayed as average \pm SEM and were analysed with one-way ANOVA. **g, h** ZFAND3 KD cells implanted in ex vivo brain slice cultures showed reduced colonization compared to control cells, 9 days after tumor implantation ($n = 10$ biologically independent samples) (Scale bar = 1000 μ m). Results are displayed as average \pm SEM and were analysed with a two-way ANOVA. **i, j** Visualization and quantification of single cell displacement of ZFAND3 KD cells in ex vivo brain slice cultures showing reduced velocity compared to control ($n = 15$ cells over 10 biologically independent samples). Results are displayed as average \pm SEM and were analysed with one-way ANOVA. **k, l** Upon intracranial implantation ($n = 3$ biologically independent animals), ZFAND3 KD cell invasion toward the contralateral hemisphere was decreased compared to control tumors. GBM xenografts were analyzed at 2 months post-surgery (3 sections per mouse) (Scale bar = 100 μ m). Results are displayed as average \pm SEM and were analysed with an unpaired, two-sided t test. * $p_{\text{value}} < 0.05$, ** $p_{\text{value}} < 0.01$, *** $p_{\text{value}} < 0.001$, **** $p_{\text{value}} < 0.0001$.

shCtrl HI cells (FDR < 0.05, logFC < -0.5) (Fig. 6a, b, Supplementary Fig. 7a, b). Gene ontology analysis associated these DEGs with adhesion and motility-related pathways, such as migration, integrin complex, ECM and cell adhesion (Fig. 6c). Among these DEGs, we selected genes reportedly linked to GBM cell invasion including

COL6A2 (alpha-2 subunit of type VI collagen), EGFR (epidermal growth factor receptor), FNI (fibronectin 1), NRCAM (neuronal cell adhesion molecule) and NRPI (neuropilin 1), and confirmed their downregulation upon ZFAND3 KD (Fig. 6d–h), thus supporting a role for ZFAND3 in transcriptional regulation. To further address

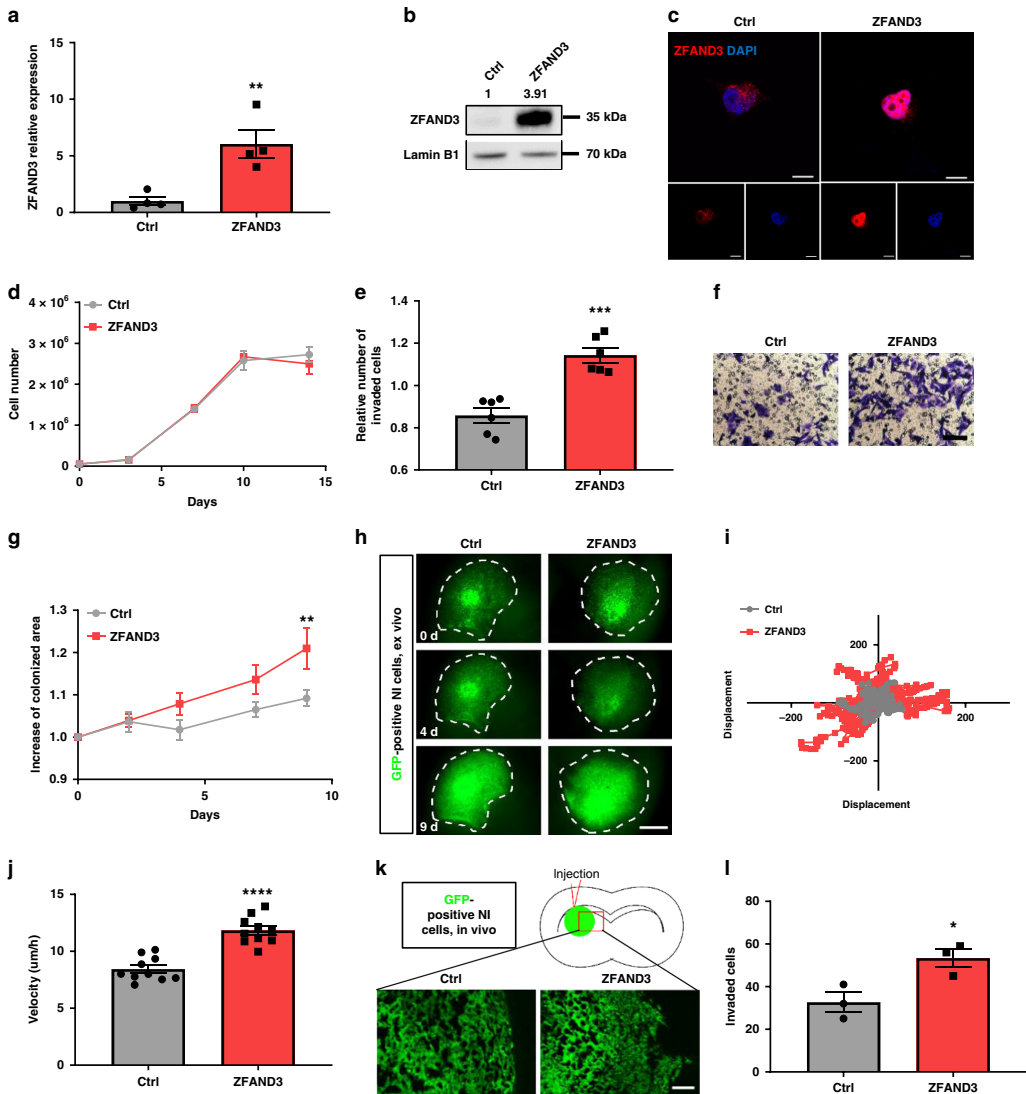
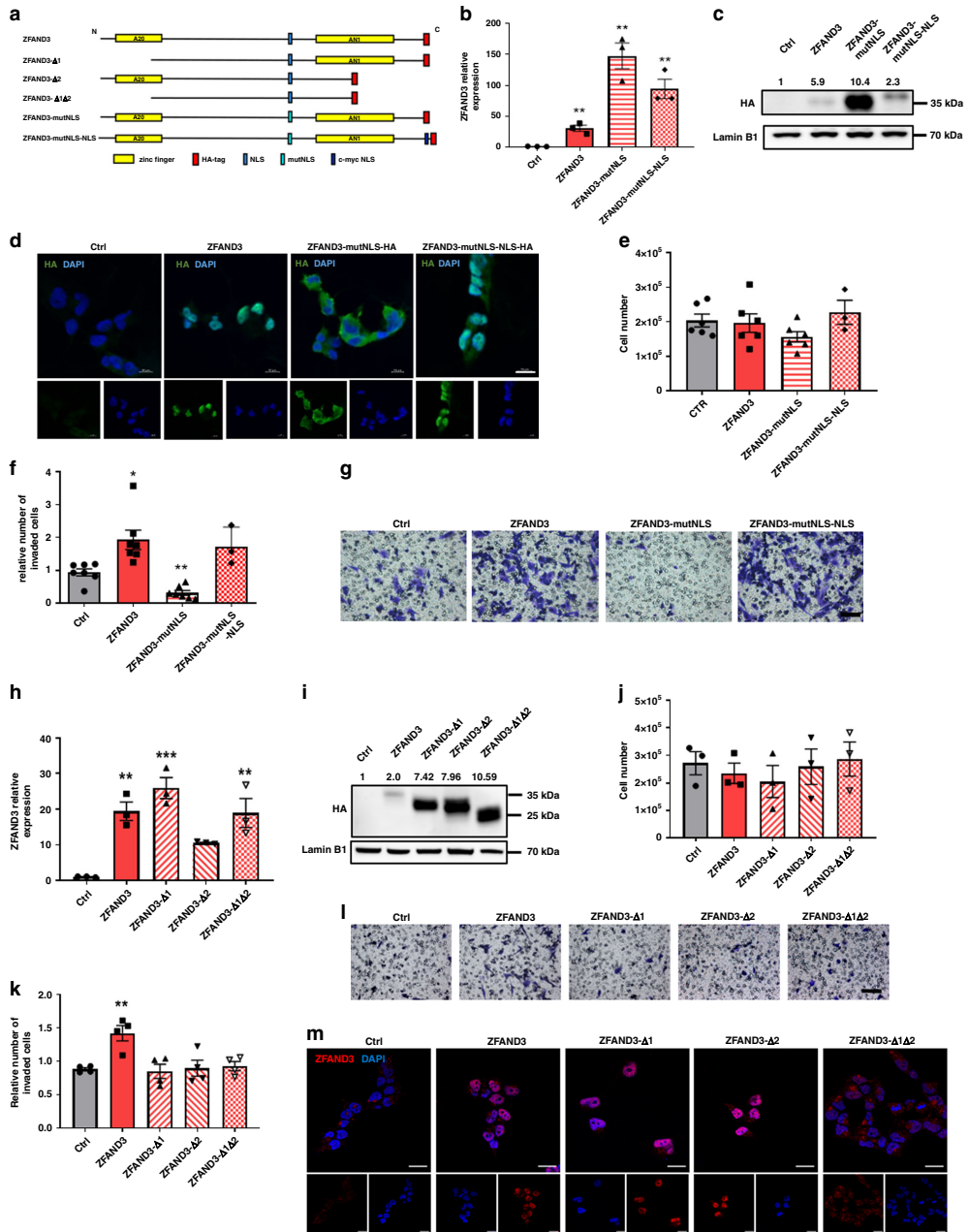


Fig. 4 Overexpression of ZFAND3 in non-invasive GBM cells confers invasion potential. ZFAND3 overexpression in non-invasive GSCs (NI) ($n = 4$ biologically independent samples) confirmed by qPCR (**a**), Western blot ($n = 3$) (**b**) and with IF staining (**c**) (red: ZFAND3, blue: DAPI. Scale bars = 10 μm). **d** ZFAND3-overexpression did not affect cell proliferation ($n = 3$ biologically independent experiments). **e, f** Boyden chamber invasion assay indicating increased invasion potential in ZFAND3-overexpressing cells ($n = 6$ biologically independent experiments) (Scale bar = 100 μm). **g, h** ZFAND3-overexpressing cells implanted in ex vivo brain slice cultures showed augmented colonization compared to control cells, 9 days after tumor implantation ($n = 10$ biologically independent samples) (Scale bar = 1000 μm). **i** Velocity of ZFAND3-overexpressing cells in ex vivo brain slice cultures was improved compared to control cells ($n = 10$, $p < 0.0001$). **j** Visualization of single cell displacement for control and ZFAND3-overexpressing cells in ex vivo brain slice cultures ($n = 15$ cells over 10 biologically independent samples). **k, l** Upon orthotopic xenografting in mice ($n = 3$), an increased number of ZFAND3-overexpressing cells invaded out of the tumor border into the surrounding tissue, compared to control cells (analysis done at 4 weeks after implantation) (3 sections per mouse) (Scale bar = 100 μm). Results of (**a, e, g, j, l**) are displayed as average \pm SEM, results of (**a, e, j, l**) were analysed with an unpaired, two-sided *t* test, results of **g** were analysed with a two-way ANOVA. * $p_{\text{value}} < 0.05$, ** $p_{\text{value}} < 0.01$, *** $p_{\text{value}} < 0.001$, **** $p_{\text{value}} < 0.0001$.



this, we interrogated the ZFAND3 neighboring interactome, using the BioID screening technology²⁷. Briefly, we expressed ZFAND3 fused with a biotin ligase (ZFAND3-BirA) in GSCs, which allowed the biotinylation of proteins in close proximity (~10 nm) (Fig. 6i). After streptavidin-based purification, biotinylated proteins were analysed by mass spectrometry, and statistical analysis revealed

143 significantly enriched proteins in ZFAND3-BirA cells compared to control (adj. *p* value < 0.05, FC > 2) (Fig. 6j). Gene ontology analysis indicated candidate interactors to be involved in RNA regulation and transcriptional processes (Fig. 6k, Supplementary Fig. 7c), reinforcing our hypothesis. To validate these results we performed ZFAND3-FLAG coimmunoprecipitation (FLAG Co-IP)

Fig. 5 ZFAND3-induced invasion requires nuclear localization and presence of zinc-finger domains. **a** Structural overview of ZFAND3 protein and corresponding mutants with zinc finger domain deletions ($\Delta 1$, $\Delta 2$, $\Delta 1\Delta 2$), mutated nuclear localization signal (mutNLS) and NLS rescue with c-myc NLS (mutNLS-NLS). HA-tag: hemagglutinin tag. N: N-terminus, C: C-terminus. **b** Expression of NLS constructs in NI GSCs as confirmed by qPCR ($n = 3$ biologically independent samples), results were analysed with a two-tailed, unpaired *t* test, and **(c)** by Western blot ($n = 3$). **d** IF staining showing that ZFAND3-mutNLS does not translocate to the nucleus, while mutNLS-NLS rescue does (green: HA, blue: DAPI. Scale bars = 10 μm). ($n = 2$) **e** Proliferation assay of cells with indicated constructs control (measurements done at day 3; $n = 7$ biologically independent experiments for Ctr, ZFAND3 and ZFAND3-mutNLS, $n = 3$ biologically independent experiments for ZFAND3-mutNLS-NLS). **f, g** Boyden chamber invasion assay showing loss of invasion phenotype with ZFAND3-mutNLS and rescue with ZFAND3-mutNLS-NLS in NI GSC ($n = 6$ biologically independent experiments for Ctr, ZFAND3 and ZFAND3-mutNLS, $n = 3$ biologically independent experiments for ZFAND3-mutNLS-NLS) (Scale bar = 100 μm). Results were analysed with a two-tailed, unpaired *t* test. **h** Expression of deletion constructs in NI GSCs by qPCR ($n = 3$ biologically independent samples). Results were analysed with one-way ANOVA **(h)** Western blot **(i)** ($n = 3$). **j** Proliferation of cells overexpressing respective constructs ($n = 3$ biologically independent experiments). Results were analysed with a two-way ANOVA. **k, l** Boyden chamber invasion assay indicating loss of invasion induction with deletion constructs ($n = 4$ biologically independent experiments) (Scale bar = 100 μm). Results were analysed with one-way ANOVA. **m** IF staining showing that ZFAND3 $\Delta 1$ and ZFAND3 $\Delta 2$ mutants localize to the nucleus, whereas ZFAND3 $\Delta 1\Delta 2$ does not (red: ZFAND3, blue: DAPI. Scale bars = 20 μm) ($n = 2$) All results are displayed as average \pm SEM. * $p_{\text{value}} < 0.05$, ** $p_{\text{value}} < 0.01$, *** $p_{\text{value}} < 0.001$, **** $p_{\text{value}} < 0.0001$.

and subsequent mass spectrometry analysis (Supplementary Fig. 7d–f). Among the 143 proteins identified as ZFAND3 interactome, 22 proteins were also pulled-down by FLAG Co-IP supporting these as ZFAND3 interactors (Fig. 6). These included several proteasome-associated proteins (PSMD1, PSMD8, PSMC3), nuclear importins (KPNA3, KPNA4), and splicing factors (e.g., PUF60, SF1, PPI4) (Supplementary Fig. 7g). Since we found the invasion-related activity of ZFAND3 to be localized to the nucleus, we focused on nuclear proteins. Database-driven analysis of protein complexes (via the Dragon Database for Human Transcription Co-Factors and Transcription Factor Interacting Proteins (TcoF-DB)²⁸ revealed interacting proteins PUF60, Pontin and Treacle (respectively encoded by *PUF60*, *RUVBL1* and *TCOF1* genes) as common binding partners within a GPN-loop GTPase 1 (GPN1) complex. To investigate if the interaction with ZFAND3 could be further confirmed by western blot, FLAG-tagged ZFAND3 from overexpressing cells (NI-ZFAND3 OE) was immunoprecipitated and analysed. PUF60 co-immunoprecipitated with ZFAND3 thereby validating it as a ZFAND3 interaction partner (Supplementary Fig. 7h), a weak background detected in control cells was not present when using isotype-specific IgG control in overexpressing cells. Technical reasons prevented confirmation of direct interaction with TCOF1 or Pontin by WB Co-IP.

Next, we aimed to relate these findings to events taking place at the promoter regions of potential target genes. We in-silico analysed the promoters of *COL6A2*, *NRCAM* and *FNI* with the Genomatix tool and identified a multitude of GC-rich target sequences, preferentially recognized by ZF containing DNA-binding proteins (Fig. 7a–c). We thus performed dual-luciferase reporter assays in U87 or HEK293T cells with the promoter sequences of *COL6A2*, *NRCAM* or *FNI* and detected an increased luciferase signal upon ZFAND3 co-expression, demonstrating that ZFAND3 was able to activate the promoter region of the genes of interest and induce their transcription (Fig. 7d–f). As expected the effect was not seen with ZFAND3- $\Delta 1\Delta 2$ (lacking both ZF domains). We also assessed expression of *COL6A2*, *NRCAM* and *FNI* genes in NI GSCs stably expressing ZFAND3 (Supplementary Fig. 8a–d) or ZFAND3 mutant constructs (Supplementary Fig. 8e–j) with no marked change in expression of target genes. Although unexpected, the latter might be related to adaptation to long term overexpression. Finally, we performed ChIP-qPCR experiments in NI GSCs overexpressing FLAG-tagged ZFAND3 or FLAG-tag alone. We observed association of ZFAND3 with in silico predicted ZF consensus sites in the promoter regions of *COL6A2*, *NRCAM*, and *FNI* in ZFAND3 overexpressing cells compared to controls (Fig. 7g–i). In line, point mutations introduced into ZF consensus sites contained within respective promoter regions failed to comparably induce

luminescence in reporter assays for target genes (Fig. 7d–f). In summary, we propose that ZFAND3 induces the expression of invasion-related genes through activation of a transcriptional complex involving PUF60, ultimately boosting the invasive behavior of GBM cells (Fig. 7j).

Discussion

ZFAND3 is a member of the ZFAND family of proteins, which contain a ZF domain of the AN1 type. ZF proteins ensure a plethora of cellular functions in health and disease, such as DNA recognition, RNA packaging, transcriptional regulation, and are involved in many aspects of cancer progression²⁹. In humans, there are eight ZFAND family members, of which only ZFAND2a and ZFAND4 have recently been implicated in cancer^{30–33}. Members of the ZFAND family are associated with stress response and proteasomal degradation through recruitment of the 26S proteasome, e.g., ZFAND1³⁴, ZFAND2A/B^{30,35}, ZFAND5³⁶, and ZFAND6³⁷. ZFAND3 has so far only been associated to type 2 diabetes susceptibility¹⁵, but nothing is known about its cellular function or its role in tumor biology. Here, we have identified and validated ZFAND3 as a modulator of GBM cell invasion, and demonstrate that it acts through regulation of transcriptional activity. We find that in patient samples ZFAND3 expression is increased in infiltrative cells from the tumor margin.

At the mechanistic level, we show that ZFAND3-induced invasion activity relies on its nuclear localization and requires integral AN1 and A20 ZF domains. The prevention of nuclear translocation and invasive phenotype through removal of the NLS signal and rescue of localization and activity by addition of a new NLS demonstrates that ZFAND3 acts in the nucleus. This is in contrast to other ZFAND proteins that are primarily located in the cytoplasm and associated to the ubiquitin-proteasome system (UPS), which may also explain the differences observed with ZF domain mutant constructs. While single deletion of either the AN1 (ZFAND3 $\Delta 1$) or the A20 domain (ZFAND3 $\Delta 2$) did not impair nuclear translocation, the invasion phenotype was lost. This might be explained by a conformational change in the protein structure, interfering with DNA or protein binding hence affecting its activity. Functional studies of other members of the ZFAND protein family employing similar deletions have shown that proteins with deletion of one of the two domains retain certain functions. e.g., in ZFAND5 the AN1 domain is required for the stimulation of peptidase activity whereas the A20 domain is needed for the binding of polyubiquitinated proteins³⁶ and both ZFAND5 AN1 and A20 domains were found to be essential for RNA stabilization³⁸. Also, the AN1 domain and UBL domains of ZFAND1 were found to be required for its binding to PSMD1 and p97/Cdc48, respectively^{34,39}. In an attempt to further nail down

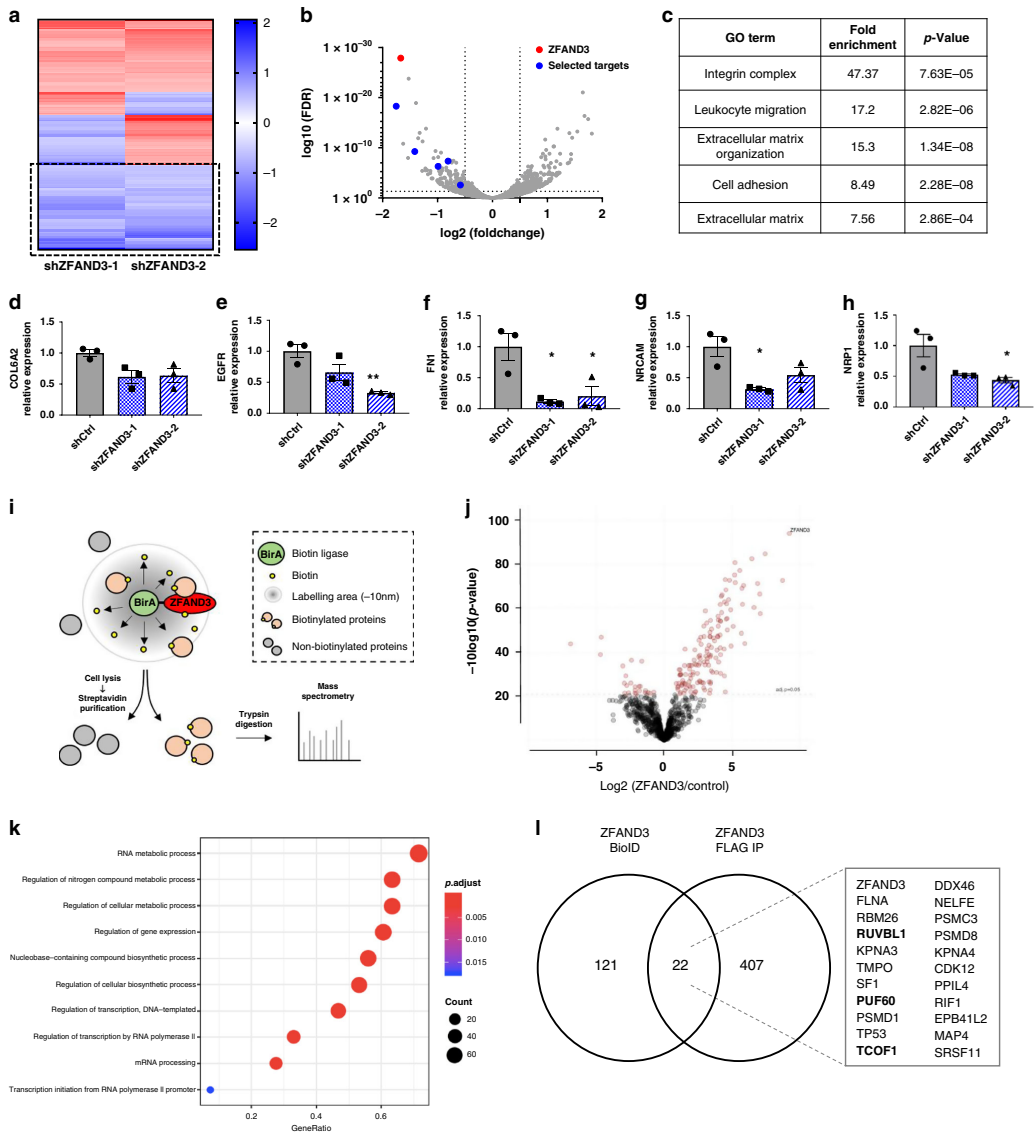


Fig. 6 ZFAND3 regulates gene expression and is part of a nucleus-specific protein interactome involved in RNA metabolism, processing, and transcription. **a** RNAseq analysis of HI GSCs ($n = 3$ per condition) identified 58 common DEGs from two KD clones (shZFAND3-1 and shZFAND3-2) vs shCtrl cells ($FDR \leq 0.05$, $\log_2FC \leq -0.5$ and ≥ 0.5). **b** Volcano plot showing DEGs in shZFAND3-2 compared to Ctrl. Among these, 5 downregulated DEGs were selected for further investigation. **c** Gene ontology analysis (David database) associated the 58 DEGs to invasion-related GO terms. qPCR confirmed reduced expression of *COL6A2* (**d**), *EGFR* (**e**), *FNI* (**f**), *NRCAM* (**g**) and *NR1P1* (**h**) in HI GSCs with shZFAND3-1 or shZFAND3-2 compared to shCtrl ($n = 3$ biologically independent samples). Results are displayed as average \pm SEM. **i** Bio-ID approach applied to unveil the interactome of ZFAND3 (adapted from Vernaite et al.⁵⁹) ($n = 4$). **j** Volcano plot showing 143 proteins significantly enriched in ZFAND3-BirA expressing cells. Two-sample t test was performed with a Benjamini-Hodgberg based $FDR < 0.01$. **k** Gene ontology analysis demonstrated that these 143 proteins are involved in RNA metabolism, processing, and transcription. **l** Co-IP/MS in ZFAND3-FLAG expressing cells confirming 22 proteins from the Bio-ID experiment as candidate ZFAND3 interactors. Gene names of identified proteins are indicated, with Pontin (*RUVBL1*), PUF60 (*PUF60*) and Treacle (*TCOF1*) highlighted in bold. * $p_{value} < 0.05$, ** $p_{value} < 0.01$.

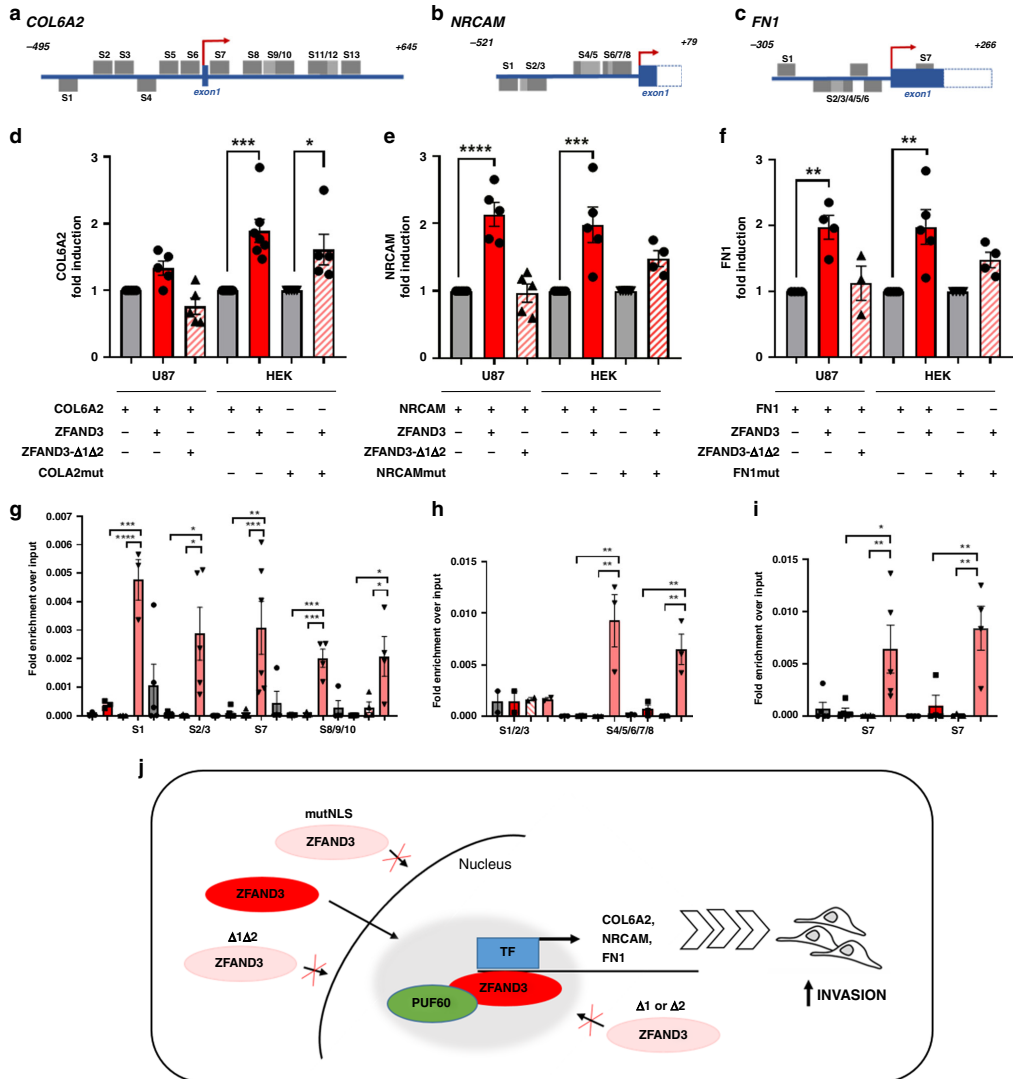


Fig. 7 ZFAND3 binds to and induces promoter activity on COL6A2, NRCAM and FN1 genes. Transcription factor consensus site analysis (via Genomatix) identified several putative ZF binding sites (GC-rich regions, hereafter named S1-S13) in the promoter regions of *COL6A2* (a), *NRCAM* (b) and *FN1* (c). Dual-luciferase reporter assays carried out in U87 or HEK293T cells showed that transiently coexpressed ZFAND3 binds to the promoter regions of *COL6A2* ($n \geq 5$) (d), *NRCAM* ($n \geq 4$) (e) and *FN1* ($n \geq 4$) (f) inducing luciferase expression, whereas deletion mutant ZFAND3-Δ1Δ2 did not. Luciferase activation was compromised on promoters with mutated GC-rich regions (COLA2mut, NRCAMmut, FN1mut) ($n \geq 4$ biologically independent experiments $^*p_{\text{value}} < 0.05$, $^{**}p_{\text{value}} < 0.01$, $^{***}p_{\text{value}} < 0.001$, $^{****}p_{\text{value}} < 0.0001$). ZFAND3 binding to GC-rich regions in the promoter regions of *COL6A2* ($n \geq 3$) (g), *NRCAM* ($n \geq 2$) (h) and *FN1* ($n \geq 4$) (i) in HI cells overexpressing ZFAND3 as determined by ChIP qPCR ($n \geq 2$ biologically independent experiments $^*p_{\text{value}} < 0.05$, $^{**}p_{\text{value}} < 0.01$, $^{***}p_{\text{value}} < 0.001$, $^{****}p_{\text{value}} < 0.0001$). j Proposed model of ZFAND3 activity in a nuclear protein complex that regulates a gene expression program to trigger cell invasion.

the active residues, we introduced missense mutations in the zinc-complexing amino acids of both domains (constructs M1, M2, M1-M2) similar to what was reported for ZFAND5³⁶. The equivalent mutation in the A20 domain of ZFAND5 (M1)

abolished its ubiquitin-binding activity^{36,40}, whereas the missense mutations in the AN1 domain (M2) resulted in a loss of its ability to stimulate the proteasome³⁶. In our hands ZFAND3 with either mutated domain (M1 or M2) or both (M1-M2) did not diminish

its ability to promote invasion (Supplementary Fig. 5b–f), suggesting that these specific residues are not relevant for the observed nuclear ZFAND3 activity.

In line with its nuclear activity, we identify a nucleus-specific ZFAND3 interactome, including DNA/RNA binding proteins, splicing factors and helicases generally involved in RNA metabolic processes and transcription. Based on our proteomics data and on available database-knowledge, we propose a ZFAND3 containing protein complex including PUF60 (*PUF60*) and possibly Pontin (*RUVBL1*) and Treacle (*TCOF1*) that regulates gene transcription (Fig. 7j). Of interest, these three proteins have been previously involved in cell motility in cancer or during development^{41–43}. Binding sites for ZF containing DNA-binding proteins are enriched in the promoter regions of *COL6A2*, *NRCAM*, or *FNI*, which were previously described in specific invasive signatures in GBM^{44,45}. We demonstrate binding of ZFAND3 to the promoter regions of these genes and confirm ZFAND3-induced transcription by dual-reporter gene assays, indicating a role for ZFAND3 in a transcriptional invasion program. In analogy to other ZFAND members, several UPS-associated proteins i.e., PSM1, PSM3, and PSM8, were also identified in our ZFAND3 interactome, which may point to additional cellular functions in the cytoplasm. In this context, it has been reported that the UPS plays an essential role in transcription by maintaining a fine-tuned equilibrium of protein synthesis and degradation⁴⁶. Whether ZFAND3's transcriptional activity is linked to a proteasomal function remains to be determined.

Collectively, these studies identify ZFAND3 as a transcriptional regulator of invasion-related genes, thereby boosting the infiltrative phenotype of GBM cells. We show that ZFAND3 requires nuclear translocation and functional ZF domains for displaying gene regulatory activity. The specific ZFAND3 interactome points to a role in transcriptional complex regulation, although an involvement in proteolysis cannot be excluded. These data expand our knowledge on the cellular functions and tumorigenic potential of ZFAND family members thus far largely known for their role in protein degradation. Further elucidation of the molecular determinants of ZFAND3 activity in oncogenic pathways may provide opportunities for targeting cancers, including GBM, prone to locoregional invasion or metastasis.

Methods

Cell culture. Patient-derived GSC lines were generated in the laboratories of Christel Herold-Mende and Rolf Bjerkvig. They were characterized as non invasive (NI: NCH644; NI-2: GG6), low invasive (LI: NCH421k), and highly invasive (HI: NCH601; HI-2: NCH465; HI-3: NCH660h and HI-4: BG7) (Fig. 1 and Supplementary Fig. 1). NCH421k, NCH601, NCH465 and NCH660h were cultured as nonadherent spheres in DMEM-F12 medium (Lonza) containing 1x BIT100 (Provitro), 2 mM Ultralutamine, 30 U/ml Pen-Strep, 1 U/ml Heparin (Sigma), 20 ng/ml bFGF (Miltenyi, 130-093-841) and 20 ng/ml EGF (Provitro, 1325950500). NCH644, BG7 and GG6 were grown in Neurobasal base medium (Life Technologies) supplemented with 1x B27 without vitamine A (Life Technologies) 2mM L-Glutamine, 30 U/ml Pen-Strep, 1 U/ml heparin, 20 ng/ml bFGF and 20 ng/ml EGF. Human embryonic kidney 293 (HEK293T) cells and U87 GBM cells were cultured in DMEM (Lonza) supplemented with 10% fetal bovine serum (FBS), 2 mM Ultralutamine, and 30 U/ml Pen-Strep. Since GSCs were exposed to 7% FBS in the Boyden chamber assay, we verified expression of ZFAND3 and stem cell markers under these conditions (Supplementary Fig. 4f–i). No significant change in ZFAND3 expression was observed, except for HI cells (NCH601) where expression was slightly increased. Stem cell markers showed variable expression across cell lines and in response to FBS, in line with previous reports⁴⁷ (Supplementary Fig. 4f–i).

GBM intracranial xenografts in mice. GSCs were implanted in the brain of NOD/SCID mice (3 mice/group) (Charles River). Mice were anesthetized with a mixture of ketamine (100 mg/kg) and xylazine (10 mg/kg) and placed in a stereotaxic frame (Narishige Group, Tokyo, Japan). Tumor cells were implanted into the right frontal cortex using a Hamilton syringe (Hamilton, Reno, NV, USA) (NI, LI, NI ctrl, NI ZFAND3; 50'000 cells, HI, HI-2, HI shCtrl, HI shZFAND3; 300'000 cells). All tumor cells were GFP-labeled. Mice were sacrificed at defined time points and brains were extracted and either frozen for cryosections or embedded in paraffin. All

procedures were in accordance with national legislation and the European Directive on animal experimentation (2010/63/EU) and were approved by the responsible authorities in Luxembourg (protocol: LUPA2017/15).

Invasion assays

In vitro. For Boyden chamber assays, GSCs were plated on transwell chambers (1500 or 3000 cells/mm²) (Thincert, Greiner), previously coated with a 1:1 mixture of 0.05 mg/ml collagen type I (Sigma-Aldrich) and 0.5 mg/ml protein of ECM gel (Sigma-Aldrich) in 1:1 PBS-DMEM-F12, for 2 h at 37 °C. Medium with 10% FBS was added as a chemoattractant to the lower chamber. After 3 days, cells were fixed with 4% PFA and stained with 0.05% crystal violet solution for 15 min. Non-invading cells were removed, and invasion was evaluated by counting the cells on the lower side of the membrane under light microscope and ×20 magnification (5 representative fields per membrane). Experiments were conducted in at least 3 biological replicates (each with 2 technical replicates). To account for the variability between separate assays, the data are represented as number of invaded cells relative to the global mean (total number of invading cells) of each experiment, allowing to combine biological replicates and apply appropriate statistics. The effect of Boyden chamber conditions on ZFAND3 expression and stem cell markers were verified by qPCR (Supplementary Fig. 4f–i). For the sprouting assay, 5 × 10³ cells/well were plated in an agar-coated well for 3 days to form a sphere. The sphere was transferred to an ECM/collagen-coated well, and covered with ECM. Pictures were taken using EVOS microscope, and invasion was calculated by the ratio of the sphere area at 48 h to 0 h. Analysis was corrected for the expansion of the sphere core.

Ex vivo. Brain slices were prepared from adult NOD/SCID mice. Briefly, mice were sacrificed by cervical dislocation, and brains were rapidly harvested and placed in ice-cold cutting solution (0.1% GlutaMax, 25 mM HEPES, 50U/ml Pen-Strep in DMEM). Brain slices (400 μm thick) were generated with a McIlwain Tissue Chopper and cultured on transwell chambers (1 μm pore size) in a 1:1 mixture of HibernateTM-A medium (ThermoFisher) supplemented with 20% BIT-100 and 100U/ml Pen-Strep with DMEM-F12 supplemented with 20% BIT-100, 100U/ml Pen-Strep, 200 mM ultralutamine and 1U/ml heparin.

Brain slices were cultured 4 days prior to GSC implantation. For this, 5 × 10⁴ GFP-labeled cells in 1 μl of ECM were injected in the cortex, above the corpus callosum, by gently punching a hole in the tissue and slowly releasing the cell/gel mixture. For the quantification of colonized area, pictures were taken every 2–3 days using the EVOS microscope and analysed with ImageJ. After 9 days, live cell imaging using Incucyte was performed, and the velocity of GFP positive invading cells in the brain slices were assessed with ImageJ (15 cells per condition and 10 replicates per cell line).

In vivo. For invasion analysis of HI and NI cells in orthotopic xenografts ($n = 3$), 8 μm cryosections were used. For each xenograft 3 sections were counted (in total 9 per condition). Sections at the level of the injection side were chosen and all GFP positive HI cells were counted manually in the contralateral hemisphere as shown in Supplementary Fig. 4j. For invasion analysis of NI cells, all GFP positive NI cells escaping the tumor mass were manually marked and counted (example shown in Supplementary Fig. 4k, l). Imaging was performed on a Ni-E microscope (Nikon) with the NIS Elements Software.

For invasion assays, data were analyzed using the GraphPad Prism 8 software. Results are reported as mean ± standard error of the mean, and n is described as the number of biological replicates. Data were analyzed with two-tailed Student t test. Statistical significance was set at $p < 0.05$.

Genome-wide shRNA library screen. A lentiviral-based genome-wide shRNA pooled library contained 95'700 shRNAs targeting 18.205 human genes (5 shRNAs/gene) (RHS6083, Dharmacon). Loss-of-function screen was performed in triplicates starting with 4 × 10⁷ HI cells (MOI 0.3, fold representation of shRNAs 100x). After 3 days of puromycin selection (1.5 μg/ml), a reference sample (baseline control) was collected (2 × 10⁷ cells). Next, 5 × 10⁷ HI cells were plated per transwell chambers (in total 24 transwell chambers per replicate to ensure 100x fold representation of shRNAs) (see protocol below) and after 3 days, invasion-deficient and invasion-competent cells were harvested, genomic DNA was extracted and shRNA sequencing libraries were prepared by PCR amplification according to the manufacturers protocol (RHS6083, Dharmacon). Libraries were pooled and 50 bp single-end sequencing was performed on an Illumina HiSeq 2500 platform (Illumina, Inc). The number of reads per sample were adapted according to the manufacturers protocol depending on the numbers of cells initially used for library preparation (per 10⁶ cells, about 10⁷ reads were sequenced). The protocol followed standard procedures and library representation rules of shRNA pooled screens⁹. The comparison of shRNA representation in invasion-deficient and invasion-competent cells was performed using the combination of four standard analysis methods: redundant siRNA activity (RSA)¹⁹, RNAi gene enrichment ranking (RIGER)²⁰, Model-based Analysis of Genome-wide CRISPR-Cas9 Knockout^{21,22} and HiTSelect²³. The analysis focused on shRNAs significantly enriched in invasion-deficient cells. Baseline reference was used to verify shRNA representation after transduction. Only gene candidates with significant differential

shRNA representation in all four analysis methods were considered as hits. The total screen was performed in three independent biological replicates.

Immunohistochemistry on GBM xenografts. Coronal sections (8 μm) from paraffin-embedded mouse brains were pretreated for 5 min with Proteinase K (Dako) followed by 20 min incubation at 95 °C in retrieval solution (Dako). The Dako Envision + System-HRP was used following the manufacturer's instructions. Primary antibodies were incubated for 2 h at RT, and secondary antibodies for 1 h at RT (list of antibodies in Supplementary Table 3). Signal was developed with 3,3'-diaminobenzidine (DAB) chromogen in 5–10 min, and pictures were acquired using a Ni-E microscope (Nikon).

For immunofluorescent staining, cells plated on ECM coated coverslips and cryosections of orthotopic xenografts were fixed and permeabilized in TBS with 0.1% Triton (TBST), followed by blocking with 10% FBS for 1 h. Primary antibodies were incubated overnight at 4 °C (list of antibodies in Supplementary Table 3). Secondary antibodies were applied with DAPI for 1 h at RT. The cells and cryosections were then washed and mounted with Fluoromount (Sigma). Imaging was performed on a Ni-E microscope (Nikon) with the NIS Elements Software or LSM880 confocal microscope (Zeiss) with the Zeiss Zen Software. Data were analyzed using the GraphPad Prism 8 software. Results are reported as mean \pm standard error of the mean, and *n* is described as the number of biological replicates. Data were analyzed with two-tailed Student *t* tests or ANOVA. Statistical significance was set at $p < 0.05$. Immunofluorescent staining for ZFAND3, IBA1 and NeuN was done as described below for clinical samples.

Immunohistochemistry on GBM clinical samples. Human tissue samples for immunohistochemistry were collected at Odense University Hospital, Odense, Denmark between 2010 and 2014 with approval from the Danish Data Inspection Authority (approval number 16/11065) and the Regional Scientific Ethical Committee of the Region of Southern Denmark (approval number S-20150148). All samples were diagnosed as GBM according to the 2016 WHO classification. 21 GBM with $\geq 60\%$ P53-positive cells in central tumor areas and simultaneously including areas with diffuse tumor cell infiltration and tumor periphery were subject to double immunofluorescence stainings for P53 and ZFAND3. P53 protein expression was used to localize tumor cells, and thereby enable measurement of ZFAND3 protein expression in both tumor cells and nontumor cells throughout the different tumor regions. Tissue sections of 3 μm were cut on a microtome, and subject to deparaffinization and heat-induced-epitope retrieval with CCI-buffer (Ventana Medical Systems). Tissue sections were then stained with primary ZFAND3 antibody (clone: HPA016755, Atlas antibodies, 1:600 for regular immunohistochemistry, 1:1000 for immunofluorescence) for 32 minutes on the Ventana Discovery Ultra platform (Ventana Medical Systems). Antibody detection was performed with the Optiview-DAB detection system for regular immunohistochemistry and DISCOVERY OmniMap anti-Rb HRP coupled with the DISCOVERY Cy5 Kit for immunofluorescence. For double-fluorescence stainings, tissue sections were subject to a second heat-induced epitope retrieval and then incubated with either primary P53 antibody (clone: DO7, Ventana Medical Systems, ready-to-use) for 4 min, Iba1 antibody (Wako Pure Chemical Industries, 1:3000) for 16 minutes or NeuN (clone: A60, Chemicon, 1:500) for 32 min. Detection was performed with DISCOVERY OmniMap anti-Ms/anti-Rb HRP coupled with the DISCOVERY FAM Kit. Nuclei were counterstained with DISCOVERY QD DAPI and slides mounted with VECTASHIELD mounting medium without DAPI.

Fluorescence images were acquired with a Leica DM6000B microscope with an Olympus DP72 camera. Regions of interest including central tumor area, areas with intermediate tumor infiltration and peripheral tumor areas were manually outlined for each slide using the Visiopharm software V6.6.1 (Visiopharm, Hoersholm, Denmark). The software was set to randomly sample 10 images from each defined region of interest on each slide at 20X magnification. A software based cell-classifier was programmed to identify P53-positive tumor cells, DAPI-positive cells and ZFAND3-staining. Finally, the fractions and mean intensities of ZFAND3-positive tumor- and nontumor cells, including tumor cells stratified by nuclear/cytoplasmic ZFAND3 staining were measured by the classifier (Supplementary Fig. 3a, b). Four tumors did not have ZFAND3 protein expression and were excluded from data analysis. Comparison of multiple groups was performed with ANOVA and Tukey's post-test for data with Gaussian distribution and Kruskal-Wallis test with Dunn's post-test for data without Gaussian distribution. Comparison of two groups was performed with T-tests for data with Gaussian distribution and Mann Whitney tests for non-Gaussian distributed data.

ZFAND3 constructs. ZFAND3 deletion constructs included deletion of ZF domain AN1, A20 or both. In the mutant constructs putative Zinc complexing amino acids (AAs) were mutated to alanine: C32A + C35A (M1); C176A + C181A (M2); all four (M1-M2). For the mutant NLS constructs, the three amino acids K132, R133 and R135 were mutated to Alanine (wildtype NLS peptide: SPVKKRPRLL, mutNLS peptide: SPVAAPALL). The NLS sequence PAAKRVKLDG (coding for the c-Myc NLS) was added to the C-terminus of the ZFAND3mutNLS N-terminal of the HA-tag. Mutant constructs are shown in Supplementary Fig. 5

and listed in Supplementary Table 4. shRNAs against ZFAND3 are shown in Supplementary Table 2.

All constructs were transduced in different patient-derived GSCs using lentiviral vectors. Lentiviral particles were produced in HEK cells by co-transfection of the plasmid of interest with the viral core packaging construct pCMVdeltaR8.74 and the VSV-G envelope protein vector pMD.G.2 as previously described⁴⁸. Supernatant containing viral particles was used to transduce 4×10^5 GSCs and puromycin selection (1 $\mu\text{g}/\text{ml}$) was applied to obtain stably transduced cells.

Quantitative real-time PCR. 1 μg of total RNA was extracted using Qiagen RNeasy Mini Kit (Qiagen) and reverse transcribed to cDNA using the iScript cDNA Synthesis Kit (Bio-Rad) or SuperScriptIII with random primers (Invitrogen), according to the manufacturer's protocol. qPCR was carried out using Fast SYBR Green Master Mix and the Viia 7 Real Time PCR System (Life Technologies; Ta = 60 °C). qPCR reaction was performed in 5 μL volume. Fold-change (FC) was calculated using the ΔCt method and normalized to the expression of EF1 α . See Supplementary Table 1 for the list of primers. CT-values were determined using the QuantStudio real time software and data were analyzed using Microsoft Excel and the GraphPad Prism 8 software. Results are reported as mean \pm standard error of the mean, and *n* is described as the number of biological replicates. Data were analyzed with two-tailed Student *t* tests or ANOVA. Statistical significance was set at $p < 0.05$.

Western blot. Total proteins from GSCs with ZFAND3 manipulations were extracted in RIPA lysis buffer and quantified using Bradford reagent (BioRad). After SDS-PAGE electrophoresis, proteins were transferred on nitrocellulose membrane (iBlot, Life Technologies). Primary antibodies were diluted in blocking solution (milk 5%) and incubated overnight at 4 °C (list of antibodies in Supplementary Table 3). After incubation with HRP-conjugated secondary antibodies, the chemiluminescent signal was recorded using the Pierce ECL Western blot detection kit (ThermoFisher), and the ImageQuant LAS4010 imaging station and software (GE Healthcare) and Image J.

Microarray analysis. Genome-wide expression profiles of NI, LI, and HI were determined using the GeneChip Human Gene 1.0ST Arrays (Affymetrix), as described⁴⁹. Briefly, total RNA was extracted using QIAGEN RNeasy Mini Kit (Qiagen), processed using the Affymetrix WT Expression kit before being hybridized on Affymetrix GeneChip Human Gene 1.0 ST arrays, according to the manufacturer's instructions (protocol P/N 702808 Rev.6). Upon hybridization, microarrays were washed, stained and scanned according to manufacturer's standard procedures. Microarray data are available in the Gene Expression Omnibus (GEO) repository under accession number GSE134470.

RNA sequencing. For RNA sequencing, total RNA was extracted from shCtrl, shZFAND3-1 and shZFAND3-2 highly invasive cells using RNeasy Plus Mini Kit (Qiagen) according to manufacturer's protocol. RNA purity was assessed using the Agilent 2100 Bioanalyzer. 500 ng total RNA with a RIN of at least 9.7 were used for RNA sequencing. TruSeq library preparation on 9 samples (3 replicates per group) was performed according to the Illumina standard protocol. Paired end of 2x 75 bp reads was performed using the NextSeq500 (Illumina). Raw sequencing data was mapped to human genome (assembly version Genome Reference Consortium Human build 38, GRCh38) using Bowtie v2-2.3.2⁵⁰. Transcript abundance was evaluated with HTSeq v0.6.1⁵¹. The normalization and transcripts differential expression analyses of count data were performed using the DESeq2 package⁵². Comparisons of shZFAND3-1 vs. shCtrl and shZFAND3-2 vs. shCtrl were assessed with the following parameters: fold change $> \log_2 -0.5$ fold, false discovery rate 0.05. Common differentially expressed genes in both comparisons were considered as hits (Supplementary Table 6). RNASeq data are available in the GEO repository under accession number GSE138618.

Streptavidin enrichment of biotinylated proteins and on-bead digestion (Bio-ID). For the analysis of ZFAND3 interactions, NI GBM GSCs (NCH644) were stably transduced with the myc-BioID-ZFAND3 construct (Supplementary Table 4), nontransduced cells were used as control. To activate the biotin ligase, cells were incubated in complete media supplemented with 100 μM D-Biotin (Carl Roth) for 48 h. After two PBS washes, cell pellets were lysed in 1% sodium deoxycholate in 50 mM ammonium bicarbonate pH8 and protease inhibitor cocktail, sonicated, incubated 30 min on ice and centrifuged at 11,000 $\times g$ and 4 °C for 30 min. Supernatant was recovered and proteins were quantified using PierceTM BCA Protein Assay Kit (Thermo Scientific). PierceTM Streptavidin Magnetic Beads (Thermo Scientific) were washed once in cold lysis buffer, and 1.8 mg of protein per sample was incubated with 50 μL of beads for 3 h at 4 °C with gentle end-over-end rotation. Beads were captured with a magnetic stand, washed 3 times in cold lysis buffer and 3 times in cold 50 mM ammonium bicarbonate pH8. Proteins were digested overnight on beads at 37 °C and 60 $\times g$ with 1 μg of trypsin (Promega). Fresh trypsin (0.5 μg) was added to the beads and incubation was extended for 2 h at 37 °C and 60 $\times g$. Beads were captured with a magnetic stand and peptides were transferred to a new tube. Beads were rinsed twice with 100 μL

of 50 mM ammonium bicarbonate and these 2 rinses were pooled to the previously eluted peptides. Samples were further reduced with 10 mM DTT for 45 min at 37 °C and 60 xg, and carbamidomethylated with 25 mM iodoacetamide for 30 min at RT and 60 xg in the dark. Peptides were finally centrifuged 15 min at 11,000 × g at 4 °C to remove any insoluble material.

ZFAND3-FLAG Coimmunoprecipitation for mass spectrometry. Co-Immunoprecipitation (Co-IP) for mass spectrometry (MS) was done on whole cell lysate using the Dynabeads™ Co-IP Kit (Invitrogen, 14321D). For antibody coupling, 1.5 mg Dynabeads™ M-270 Epoxy were incubated with 8 µg of FLAG M2 antibody (Sigma F1804) at 37 °C on a mixing roller for 16 h. Beads were washed according to manufacturer's instructions and diluted to a concentration of 10 mg/ml and left at 4 °C until further processing. NI GBM GSCs overexpressing ZFAND3 with a FLAG-tag were incubated in complete media supplemented and while harvesting washed twice in ice-cold PBS. Cells were lysed with 1x IP Buffer containing NaCl 100 mM, DTT 1 mM and one cComplete™ EDTA-free Protease Inhibitor Cocktail for 15 min on ice, and sonicated. The lysates were quantified using the Bradford Reagent (Bio-Rad). Proteins of interest were captured by incubating 1 mg of protein lysate with 1.5 mg of antibody-coupled beads at 4 °C for 30 min. Beads were resuspended in cold ammonium bicarbonate 50 mM, reduced with DTT 10 mM for 45 min at 37 °C and 60 xg, and carbamidomethylated with iodoacetamide 25 mM for 30 min at RT and 60 xg in the dark. Proteins were digested with 1 µg of trypsin (V5111, Promega) overnight on beads at 37 °C and 60 xg. Fresh trypsin (0.5 µg) was added to the beads and incubation was extended for 2 h at 37 °C and 60 xg. Dynabeads were captured with a magnetic stand, peptides were recovered and transferred to a new tube. Beads were rinsed twice with 100 µL of ammonium bicarbonate 50 mM and these 2 rinses were pooled to the previous eluate. Peptides were centrifuged 15 min at 11,000 × g at 4 °C to remove any insoluble material, acidified in 1% formic acid, desalted on Sep-Pak C18 Elution Plates (Waters, 186002318), dried by vacuum centrifugation and reconstituted in 12 µL of 1% Acetonitrile/0.05% trifluoroacetic acid. Samples were quantified by Nanodrop and further analysed by mass spectrometry (see below).

Mass spectrometry analysis and data analysis. Peptides were acidified in 1% formic acid, desalted on Sep-Pak C18 µElution Plates (Waters, 186002318), dried by vacuum centrifugation and reconstituted in 20 µL of 1% Acetonitrile / 0.1% formic acid. 1 µL of each sample was measured by LC-MS/MS on a Q-Exactive Plus mass spectrometer (Thermo) connected to a Dionex Ultimate 3000 (Thermo), run in trap mode using a Acclaim Pepmap 100 trap column (Dionex). The peptides were separated on a 15 cm Acclaim pepmap RSLC column (Dionex) using a 89 min gradient (2% to 50% acetonitrile) with a flow rate of 0.3 µL/min. MS acquisition was performed with an MS1 resolution of 70,000 and a scan range from 375 to 1500 m/z with an AGC target of 3 × 10⁶. The top 12 peaks were selected for fragmentation in data-dependent mode using an MS2 resolution of 17,500 and a maximum injection time of 45 ms and an isolation window of 1.2 m/z and an AGC target of 10⁵. Dynamic exclusion was set to 20 s and the normalized collision energy was specified to 28.

For analysis, the MaxQuant software package version 1.6.5.0⁵³ was used. Carbamidomethylation on cysteine was set as a fixed modification and oxidized methionine and acetylated N-termini as variable modifications. Peptide tolerance was 20 ppm and the minimum ratio for LFQ was set to 2. An FDR <1% was applied for peptides and proteins and the Andromeda search⁵⁴ was performed using a human Uniprot database (July 2018). MS intensities were normalized by the MaxLFQ algorithm implemented in MaxQuant⁵⁵ while using the match-between-runs feature.

Only protein groups that were not marked as potential contaminants nor detected by MaxQuant using reverse database were kept for the analysis. LFQ-normalized intensities were log₂-transformed. Statistical analysis of the dataset was performed using R-statistical software package (version 3.4.1). For data analysis, first, proteins that were only identified by site or were potential contaminants were excluded. Only the proteins that were found in at least three biological replicates for every condition were used for column wise imputation from a normal distribution and subsequent statistical analysis. Significantly differentially expressed protein groups were detected by R-package limma⁵⁶. For this, a two-sample *t* test was performed with a Benjamini-Hodgberg based FDR <0.01. Abundance changes with a *p* value <0.05 and a minimum fold change of 2 were considered significant (Supplementary Table 7 for BioID experiment, Supplementary Table 8 for IP experiment). The GO analysis was carried out by R software, *p* value and *q* value cutoff 5%, *n* and minimum 3 proteins per category as threshold; significantly, differentially regulated proteins (corresponding Uniprot IDs) were used as targets and all other proteins captured by proteomics experiment were considered as a background. Protein IDs that matched several gene IDs were removed from the analysis.

ZFAND3-FLAG coimmunoprecipitation for western blot analysis. Co-IP with subsequent Western blot analysis was performed on nuclear extracts following Agoston and Schulte⁵⁷. For antibody coupling, 1 mg Dynabeads™ M-270 Epoxy were incubated with 5 µg of FLAG M2 antibody (Sigma F1804) or Mouse IgG at 37 °C on a mixing roller for 16 h. Fresh nuclear proteins extracts from NI GBM

GSCs overexpressing ZFAND3 with a FLAG-tag and Ctrl-FLAG expressing cells were prepared as following. 2 × 10⁶ were used to prepare cytoplasmic lysates in 300 µL Buffer A + (10 mM HEPES, 10 mM KCl, 1 mM DTT, 1x cComplete™ EDTA free), followed by 15 min incubation on ice 30 µL IGEPAL/PBS solution was added and cells were briefly vortexed. The nuclei were pelleted by centrifugation for 1 min at 9000 × g at 4 °C. Nuclear extract lysis was done by adding 180 µL Buffer B + (10 mM HEPES, 10 mM KCl, 1 mM DTT, 400 mM NaCl, 1% IGEPAL, 1x cComplete™ EDTA free) and incubated for 15 min on a rotating wheel. To obtain isotonic salt concentration 300 µL Buffer A + was added. Lysates were treated with DNase 1 (Ambion) with 50U for 30 min at 4 °C. Nuclear protein extracts were pre-cleared for 2 h using 0.3 mg Dynabeads™ M-270 Epoxy at 4 °C on a rotating wheel. 30 µL of each lysate was kept as input control for later. Dynabeads were equilibrated in 900 µL Buffer BP + (3:1.8 ratio of Buffer A and B) before adding the lysates. Nuclear protein extracts were divided into two (FLAG and IgG) to use equal amount of lysate per IP. Dynabeads-antibody containing lysates were incubated for 2 h at 4 °C on a rotating wheel. After magnetic separation of precipitate and supernatant, supernatant was removed and kept for later as supernatant control. Dynabeads-bound precipitates were washed four times with Buffer BP + and once with 1x LBW 0.1% Tween-20. After the washing steps, 30 µL 4x LDS (50 mM DTT) was added to each sample and incubated for 10 min at 70 °C. After magnetic separation, supernatants were transferred into a fresh tube. Samples were directly loaded on a SDS-PAGE for Western Blot analysis.

Dual luciferase reporter assay. Plasmids encoding the Firefly Luciferase reporter gene under the control of the candidate gene promoters, and a Renilla Luciferase plasmid under the control of an SV-40 Promoter were purchased from Vector-Builder®. Plasmid DNA was purified using NucleoBond Xtra Midi Kit (Macherey-Nagel). Reporter cells (U87 or HEK293T) were seeded into 24-well plates at a density of 7.5 × 10⁴ per well and transfected the next day, using 1.5 µL Lipofectamine 2000 (Thermo Fisher), with the selected Luciferase reporter plasmids (COL6A2, FN1 and NRCAM) and co-transfected with either empty control, ZFAND3 or ZFAND3 A1Δ2. A Renilla Luciferase Reporter was co-transfected with a 1:10 ratio of luciferase reporter plasmids as a reference control. Luciferase activity was recorded 30 h post-transfection using Dual-Glo® Luciferase Assay System (Promega) according to the manufacturer's instructions, using ClarioStar plate reader (BMG LabTech). The ratio of the Firefly:Renilla luminescence was calculated and normalized to the ratio of the empty control. Data were analyzed using the GraphPad Prism 8 software. Results are reported as mean ± standard error of the mean, and *n* is described as the number of biological replicates. Data were analyzed by ANOVA. Statistical significance was set at *p* < 0.05.

Chromatin immunoprecipitation (ChIP) qPCR. ChIP was performed as described previously⁵⁸ with the following changes: cells were cross-linked for 30 min at 4 °C in 2% PFA made from freshly prepared 18.5% PFA. Chromatin was sheared to a mean length of 100–500 bp with a Bioruptor UCD-200 in a cold room at 4 °C (Diagenode). Immunoprecipitation was performed with the antibodies listed in S3. ChIP precipitates were assessed by quantitative real-time PCR with the primers listed in Supplementary Table 1 and PowerUp™ SYBR™ Green master mix reagents (Thermo Fisher Scientific) on a QuantStudio™ 1M 5 Real-Time PCR detection system (Thermo Fisher Scientific). Enrichment of the precipitated DNA was determined relative to the input (1:100 as 100 × 2^(Ct adjusted input – Ct immunoprecipitate)). Results are reported as mean ± standard error of the mean, and *n* is described as the number of biological replicates. Statistical significance was determined using ANOVA in the GraphPad Prism 8 software.

Reporting summary. Further information on research design is available in the Nature Research Reporting Summary linked to this article.

Data availability

All data generated or analysed during this study are included in this published article (and its Supplementary Data files). RNAseq data are available in the GEO repository under accession number GSE138618; DNA microarray data under accession number GSE134470.

Raw proteomics data have been deposited in the The MassIVE site repository of the University of California San Diego (ProteomeXchange consortia) under <http://massive.ucsd.edu/MSV000086247>. The constructs generated during the current study are available from the corresponding author on reasonable request.

Received: 14 February 2020; Accepted: 4 November 2020;

Published online: 11 December 2020

References

1. Claes, A., Idema, A. J. & Wesseling, P. Diffuse glioma growth: a guerilla war. *Acta Neuropathol.* **114**, 443–458 (2007).

2. Osswald, M. et al. Brain tumour cells interconnect to a functional and resistant network. *Nature* **528**, 93–98 (2015).
3. Weil, S. et al. Tumor microtubules convey resistance to surgical lesions and chemotherapy in gliomas. *Neuro Oncol.* **19**, 1316–1326 (2017).
4. Cuddapah, V. A., Robel, S., Watkins, S. & Sontheimer, H. A neurocentric perspective on glioma invasion. *Nat. Rev. Neurosci.* **15**, 455–465 (2014).
5. de Gooijer, M. C. et al. Experimenter's guide to glioblastoma invasion pathways. *Trends Mol. Med.* **24**, 763–780 (2018).
6. Lefranc, F. et al. Glioblastoma quo vadis: will migration and invasiveness reemerge as therapeutic targets? *Cancer Treat. Rev.* **68**, 145–154 (2018).
7. Picariello, H. S. et al. Myosin IIA suppresses glioblastoma development in a mechanically sensitive manner. *Proc. Natl Acad. Sci. USA* **116**, 15550–15559 (2019).
8. Tome-Garcia, J. et al. Analysis of chromatin accessibility uncovers TEAD1 as a regulator of migration in human glioblastoma. *Nat. Commun.* **9**, 4020 (2018).
9. Schuster, A. et al. RNAi/CRISPR screens: from a pool to a valid hit. *Trends Biotechnol.* **37**, 38–55 (2019).
10. Seo, M. et al. RNAi-based functional selection identifies novel cell migration determinants dependent on PI3K and AKT pathways. *Nat. Commun.* **5**, 5217 (2014).
11. Agaesse, G. et al. A large-scale RNAi screen identifies LCMR1 as a critical regulator of Tspan8-mediated melanoma invasion. *Oncogene* **36**, 446–457 (2017).
12. Prolo, L. M. et al. Targeted genomic CRISPR-Cas9 screen identifies MAP4K4 as essential for glioblastoma invasion. *Sci. Rep.* **9**, 14020 (2019).
13. Lopez-Fernandez, L. A. & del Mazo, J. Characterization of genes expressed early in mouse spermatogenesis, isolated from a subtractive cDNA library. *Mamm. Genome* **7**, 698–700 (1996).
14. de Luis, O., Lopez-Fernandez, L. A. & del Mazo, J. Tex27, a gene containing a zinc-finger domain, is up-regulated during the haploid stages of spermatogenesis. *Exp. Cell Res.* **249**, 320–326 (1999).
15. Ndiaye, F. K. et al. Expression and functional assessment of candidate type 2 diabetes susceptibility genes identify four new genes contributing to human insulin secretion. *Mol. Metab.* **6**, 459–470 (2017).
16. Cho, Y. S. et al. Meta-analysis of genome-wide association studies identifies eight new loci for type 2 diabetes in east Asians. *Nat. Genet.* **44**, 67–72 (2011).
17. Bougnaud, S. et al. Molecular crosstalk between tumour and brain parenchyma instructs histopathological features in glioblastoma. *Oncotarget* **7**, 31955–31971 (2016).
18. Wang, Q. et al. Tumor evolution of glioma-intrinsic gene expression subtypes associates with immunological changes in the microenvironment. *Cancer Cell* **32**, 42–56 (2017). e46.
19. Konig, R. et al. A probability-based approach for the analysis of large-scale RNAi screens. *Nat. Methods* **4**, 847–849 (2007).
20. Luo, B. et al. Highly parallel identification of essential genes in cancer cells. *Proc. Natl Acad. Sci. USA* **105**, 20380–20385 (2008).
21. Li, W. et al. Quality control, modeling, and visualization of CRISPR screens with MAGeCK-VISPR. *Genome Biol.* **16**, 281 (2015).
22. Li, W. et al. MAGeCK enables robust identification of essential genes from genome-scale CRISPR/Cas9 knockout screens. *Genome Biol.* **15**, 554 (2014).
23. Diaz, A. A., Qin, H., Ramalho-Santos, M. & Song, J. S. HiTSelect: a comprehensive tool for high-complexity-pooled screen analysis. *Nucleic Acids Res.* **43**, e16 (2015).
24. Bowman, R. L., Wang, Q., Carro, A., Verhaak, R. G. & Squatrito, M. GliOVis data portal for visualization and analysis of brain tumor expression datasets. *Neuro Oncol.* **19**, 139–141 (2017).
25. Tang, Z. et al. GEPIA: a web server for cancer and normal gene expression profiling and interactive analyses. *Nucleic Acids Res.* **45**, W98–W102 (2017).
26. Consortium, G. T. The genotype-tissue expression (GTEx) project. *Nat. Genet.* **45**, 580–585 (2013).
27. Roux, K. J., Kim, D. I. & Burke, B. BioID: a screen for protein-protein interactions. *Curr. Protoc. Protein Sci.* **74**, 23 (2013). Unit 19.
28. Schaefer, U., Schmeier, S. & Bajic, V. B. TcoF-DB: dragon database for human transcription co-factors and transcription factor interacting proteins. *Nucleic Acids Res.* **39**, D106–D110 (2011).
29. Cassandri, M. et al. Zinc-finger proteins in health and disease. *Cell Death Discov.* **3**, 17071 (2017).
30. Osorio, F. G. et al. Loss of the proteostasis factor AIRAPL causes myeloid transformation by deregulating IGF-1 signaling. *Nat. Med.* **22**, 91–96 (2016).
31. Kurihara-Shimomura, M. et al. Zinc finger AN1-type containing 4 is a novel marker for predicting metastasis and poor prognosis in oral squamous cell carcinoma. *J. Clin. Pathol.* **71**, 436–441 (2018).
32. Suarez-Canto, J. et al. Distinct expression and clinical significance of zinc finger AN1-type containing 4 in oral squamous cell carcinomas. *J. Clin. Med.* **7** (2018).
33. Pizzato Scomazzon, S. et al. The zinc-finger AN1-type domain 2a gene acts as a regulator of cell survival in human melanoma: role of E3-ligase cIAP2. *Mol. Cancer Res.* **17**, 2444–2456 (2019).
34. Turakhiya, A. et al. ZFAND1 recruits p97 and the 26S proteasome to promote the clearance of arsenite-induced stress granules. *Mol. Cell* **70**, 906–919 (2018). e907.
35. Rossi, A. et al. The proteasome inhibitor bortezomib is a potent inducer of zinc finger AN1-type domain 2a gene expression: role of heat shock factor 1 (HSF1)-heat shock factor 2 (HSF2) heterocomplexes. *J. Biol. Chem.* **289**, 12705–12715 (2014).
36. Lee, D., Takayama, S. & Goldberg, A. L. ZFAND5/ZNF216 is an activator of the 26S proteasome that stimulates overall protein degradation. *Proc. Natl. Acad. Sci. USA* **115**, E9550–E9559 (2018).
37. Fenner, B. J., Scannell, M. & Pohn, J. H. Identification of polyubiquitin binding proteins involved in NF-kappaB signaling using protein arrays. *Biochim Biophys. Acta* **1794**, 1010–1016 (2009).
38. He, G., Sun, D., Ou, Z. & Ding, A. The protein Zfand5 binds and stabilizes mRNAs with AU-rich elements in their 3'-untranslated regions. *J. Biol. Chem.* **287**, 24967–24977 (2012).
39. Sa-Moura, B. et al. A conserved protein with AN1 zinc finger and ubiquitin-like domains modulates Cdc48 (p97) function in the ubiquitin-proteasome pathway. *J. Biol. Chem.* **288**, 33682–33696 (2013).
40. Hishiyama, A. et al. A novel ubiquitin-binding protein ZNF216 functioning in muscle atrophy. *EMBO J.* **25**, 554–564 (2006).
41. Sun, D., Lei, W., Hou, X., Li, H. & Ni, W. PUF60 accelerates the progression of breast cancer through downregulation of PTEN expression. *Cancer Manag. Res.* **11**, 821–830 (2019).
42. Mao, Y. Q. & Houry, W. A. The role of pontin and reptin in cellular physiology and cancer etiology. *Front Mol. Biosci.* **4**, 58 (2017).
43. Serrano, F. et al. A novel human pluripotent stem cell-derived neural crest model of treacher collins syndrome shows defects in cell death and migration. *Stem Cells Dev.* **28**, 81–100 (2019).
44. Gollapalli, K. et al. Subventricular zone involvement in Glioblastoma - A proteomic evaluation and clinicoradiological correlation. *Sci. Rep.* **7**, 1449 (2017).
45. Machado, R. A. C. et al. CHD7 promotes glioblastoma cell motility and invasiveness through transcriptional modulation of an invasion signature. *Sci. Rep.* **9**, 3952 (2019).
46. Geng, F., Wenzel, S. & Tansey, W. P. Ubiquitin and proteasomes in transcription. *Annu Rev. Biochem.* **81**, 177–201 (2012).
47. Dirkse, A. et al. Stem cell-associated heterogeneity in Glioblastoma results from intrinsic tumor plasticity shaped by the microenvironment. *Nat. Commun.* **10**, 1787 (2019).
48. Naldini, L. et al. In vivo gene delivery and stable transduction of nondividing cells by a lentiviral vector. *Science* **272**, 263–267 (1996).
49. Abdul Rahim, S. A. et al. Regulation of hypoxia-induced autophagy in glioblastoma involves ATG9A. *Br. J. Cancer* **117**, 813–825 (2017).
50. Langmead, B., Wilks, C., Antonescu, V. & Charles, R. Scaling read aligners to hundreds of threads on general-purpose processors. *Bioinformatics* **35**, 421–432 (2019).
51. Anders, S., Pyl, P. T. & Huber, W. HTSeq—a python framework to work with high-throughput sequencing data. *Bioinformatics* **31**, 166–169 (2015).
52. Love, M. I., Huber, W. & Anders, S. Moderated estimation of fold change and dispersion for RNA-seq data with DESeq2. *Genome Biol.* **15**, 550 (2014).
53. Cox, J. & Mann, M. MaxQuant enables high peptide identification rates, individualized p.p.b.-range mass accuracies and proteome-wide protein quantification. *Nat. Biotechnol.* **26**, 1367–1372 (2008).
54. Cox, J. et al. Andromeda: a peptide search engine integrated into the MaxQuant environment. *J. Proteome Res.* **10**, 1794–1805 (2011).
55. Cox, J. et al. Accurate proteome-wide label-free quantification by delayed normalization and maximal peptide ratio extraction, termed MaxLFQ. *Mol. Cell Proteom.* **13**, 2513–2526 (2014).
56. Ritchie, M. E. et al. limma powers differential expression analyses for RNA-seq and microarray studies. *Nucleic Acids Res.* **43**, e47 (2015).
57. Agoston, Z. & Schulte, D. Meis2 competes with the Groucho co-repressor Tle4 for binding to Otx2 and specifies target fate without induction of a secondary midbrain-hindbrain boundary organizer. *Development* **136**, 3311–3322 (2009).
58. Hau, A. C. et al. MEIS homeodomain proteins facilitate PARP1/ARTD1-mediated eviction of histone H1. *J. Cell Biol.* **216**, 2715–2729 (2017).
59. Varnaite, R. & MacNeill, S. A. Meet the neighbors: mapping local protein interactomes by proximity-dependent labeling with BioID. *Proteomics* **16**, 2503–2518 (2016).

Acknowledgements

We thank Virginie Baus and Vanessa Barthelemy for technical assistance and are grateful for the financial support of the Fondation Cancer Luxembourg (INVGBM and Pan-RTK Targeting), Télévie-FNRS (GBModImm no 7.8513.18 and TETHER no 7.4615.18) and the Luxembourg National Research Fund (FNRS; CORE Junior C17/BM/11664971/DEMICS).

Author contributions

A.S., V.N., E.K., A.M.K., A.O., M.D., C.F., A.C.H., A.G., D.P.H., S.R., B.K. performed experiments and analyzed data. P.V.N., A.M., D.P.H. performed statistical and bioinformatic analyses. C.H.M., R.B., B.W.K. provided material. G.D., B.W.K., S.P.N. supervised experiments. S.P.N., A.S. designed project. A.S., V.N., E.K., S.P.N. wrote manuscript. S.P.N. supervised project and provided funds. All authors edited and approved the manuscript.

Competing interests

The authors declare no competing interests.

Additional information

Supplementary information is available for this paper at <https://doi.org/10.1038/s41467-020-20029-y>.

Correspondence and requests for materials should be addressed to S.P.N.

Peer review information *Nature communications* thanks Harald Sontheimer, Nadejda Tsankova and the other, anonymous, reviewer(s) for their contribution to the peer review of this work. Peer reviewer reports are available.

Reprints and permission information is available at <http://www.nature.com/reprints>

Publisher's note Springer Nature remains neutral with regard to jurisdictional claims in published maps and institutional affiliations.



Open Access This article is licensed under a Creative Commons Attribution 4.0 International License, which permits use, sharing, adaptation, distribution and reproduction in any medium or format, as long as you give appropriate credit to the original author(s) and the source, provide a link to the Creative Commons license, and indicate if changes were made. The images or other third party material in this article are included in the article's Creative Commons license, unless indicated otherwise in a credit line to the material. If material is not included in the article's Creative Commons license and your intended use is not permitted by statutory regulation or exceeds the permitted use, you will need to obtain permission directly from the copyright holder. To view a copy of this license, visit <http://creativecommons.org/licenses/by/4.0/>.

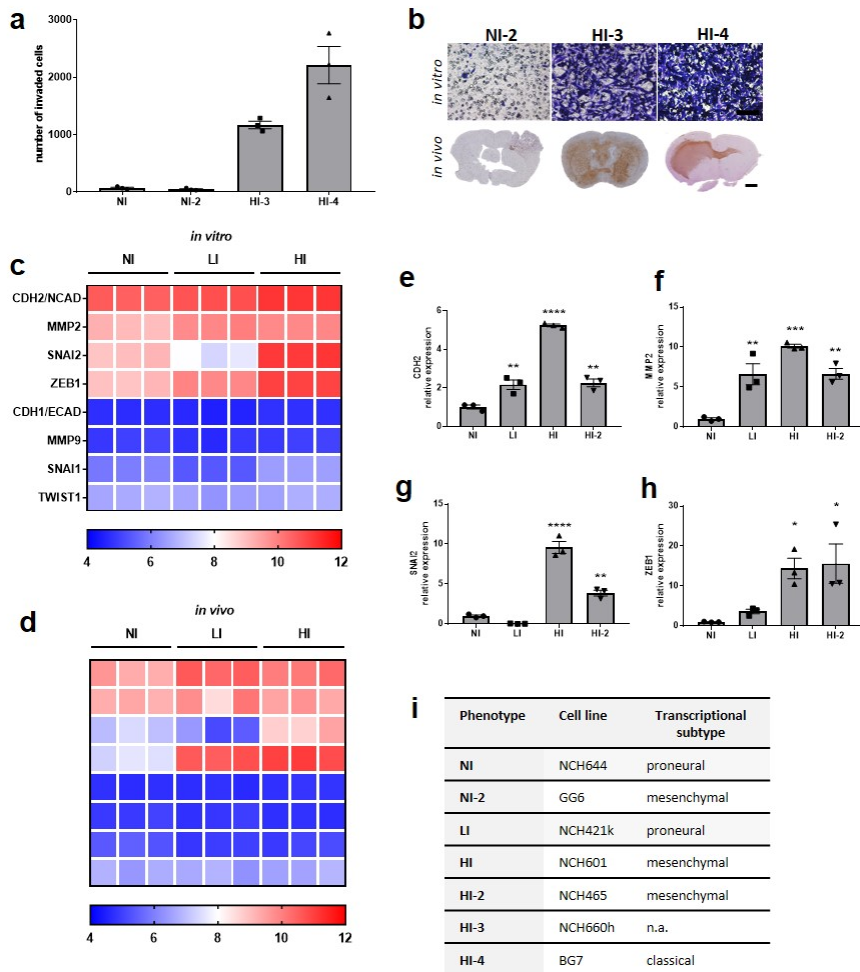
© The Author(s) 2020

Supplementary files - Schuster et al.

AN1-type zinc finger protein 3 (ZFAND3) is a transcriptional regulator that drives Glioblastoma invasion

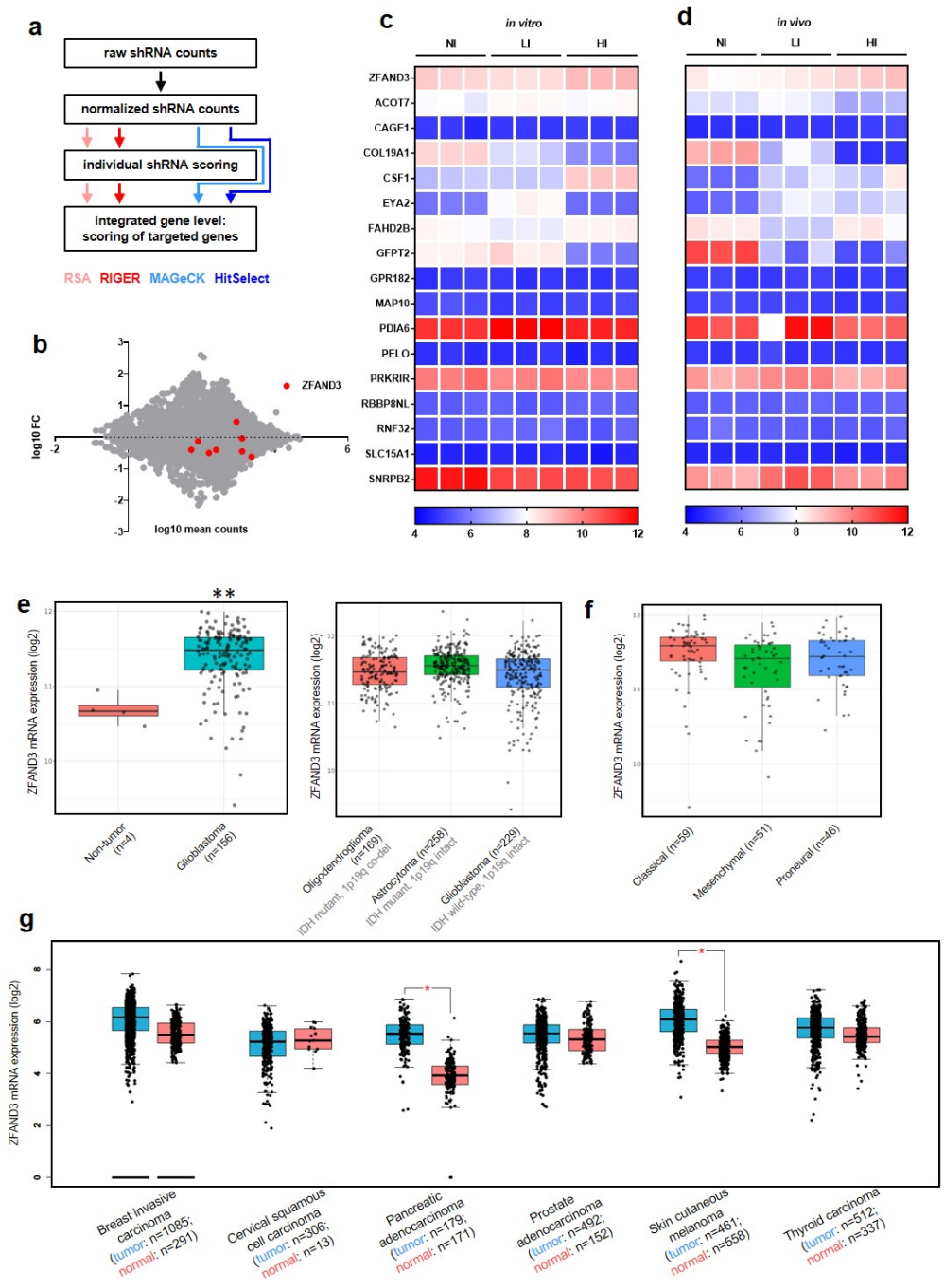
Supplementary Figures

Supplementary Figure 1



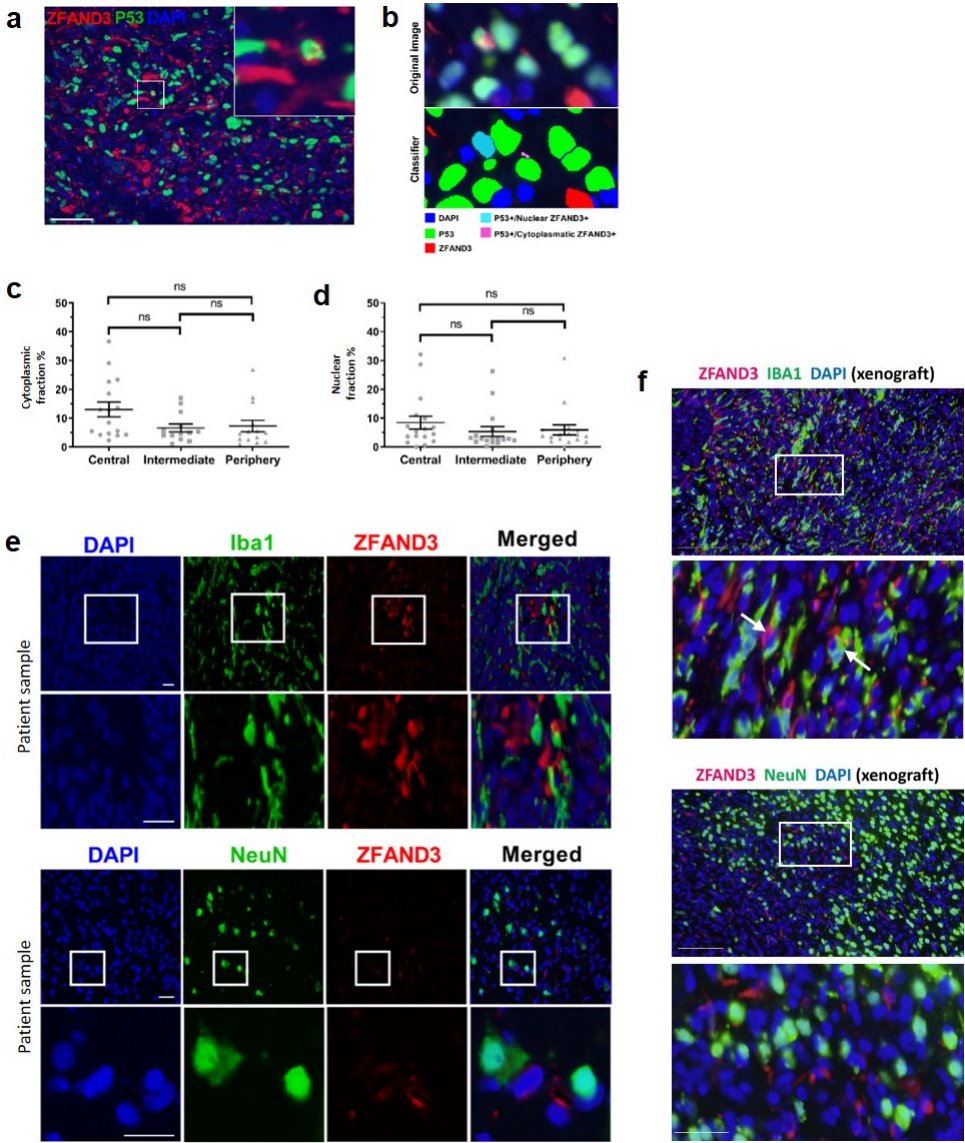
Supplementary Figure 1: Characterization of patient-derived GSC lines. a-b) Invasion capacities of additional GSC lines: (a) Quantification of *in vitro* invasion in Boyden chamber assays (n=3 biologically independent experiments) of 2 non-invasive (NI, NI-2) and two highly invasive (HI-3, HI-4) GSC lines. (NI line is shown as comparison to Fig. 1). Results are displayed as average number of invaded cells +/- SEM. (b) Representative pictures of *in vitro* invasion (Boyden chamber assays) and *in vivo* invasion in orthotopic mouse xenografts (except NI-2 in rat). Scale bar = 1000 μ m. c-h) The expression of general invasion markers reflects the status of non invasive (NI), invasive (LI), highly invasive (HI, HI-2) GSCs. Genome-wide expression analysis revealed differential expression of *CDH2*, *MMP2*, *SNAI2*, *ZEB1*, but absence of expression of *CDH1*, *MMP9*, *SNAI1*, *TWIST1* in GSCs *in vitro* (c) and at endpoint of tumor development (d) in orthotopic xenografts *in vivo*. qPCR showing expression of *CDH2* (n=3) (e), *MMP2* (n=3) (f), *SNAI2* (n=3) (g) and *ZEB1* (n=3) (h) in different types of GSCs. Results are displayed as average +/- SEM and were analysed with an ordinary one-way ANOVA * $p_{\text{value}} < 0.05$; ** $p_{\text{value}} < 0.01$; *** $p_{\text{value}} < 0.001$; **** $p_{\text{value}} < 0.0001$. i) List of human GSC lines indicating their invasive phenotype (left panel) and transcriptional GBM subtype (right panel) based on gene expression and/or methylation profiling.

Supplementary Figure 2



Supplementary Figure 2: Genome-wide shRNA analysis identifying ZFAND3 as top candidate. a) Analysis pipeline of genome-wide shRNA interference screen. b) shRNA distribution based on RSA analysis shows that shRNAs targeting *ZFAND3* appear enriched (7 out of 8) in invasion-defective cells ($\log_{10}FC < 0$). Genome-wide expression analysis shows the expression of the 17 genes identified by the shRNA screen in different types of GSCs c) *in vitro* and d) *in vivo* at endpoint of tumor development in orthotopic xenografts. e) Analysis of *ZFAND3* expression in patients from TCGA database, via the Gliovis platform (GBM and GBM/LGG cohort, RNAseq data) ¹. Data were analysed with Tukey's Honest Significance Difference, after one-way ANOVA. ** $p_{value} < 0.01$ f) *ZFAND3* expression in GBM patients from TCGA database according to GBM transcriptional subtype. Whiskers of dot plots represent extreme low and high values as long as they are within the 1.5 times interquartile range (IQR), meaning that whiskers are limited to 1.5 IQR. Dots above and below whiskers display outlying data points. Centres represent the medians and the box limits show the 25th and 75th percentiles. g) *ZFAND3* expression among different cancer types (tumor in blue, normal tissue in red). Data collected from GEPIA ² based on TCGA normal and GTEx data. Data were analysed with one-way ANOVA, using disease state as variable for calculating differential expression. * $p_{value} < 0.05$. The boxes of the box plot display data from the 25th to 75th percentile, while the whiskers show the 10th and 90th percentile. The centres represent the medians of the data.

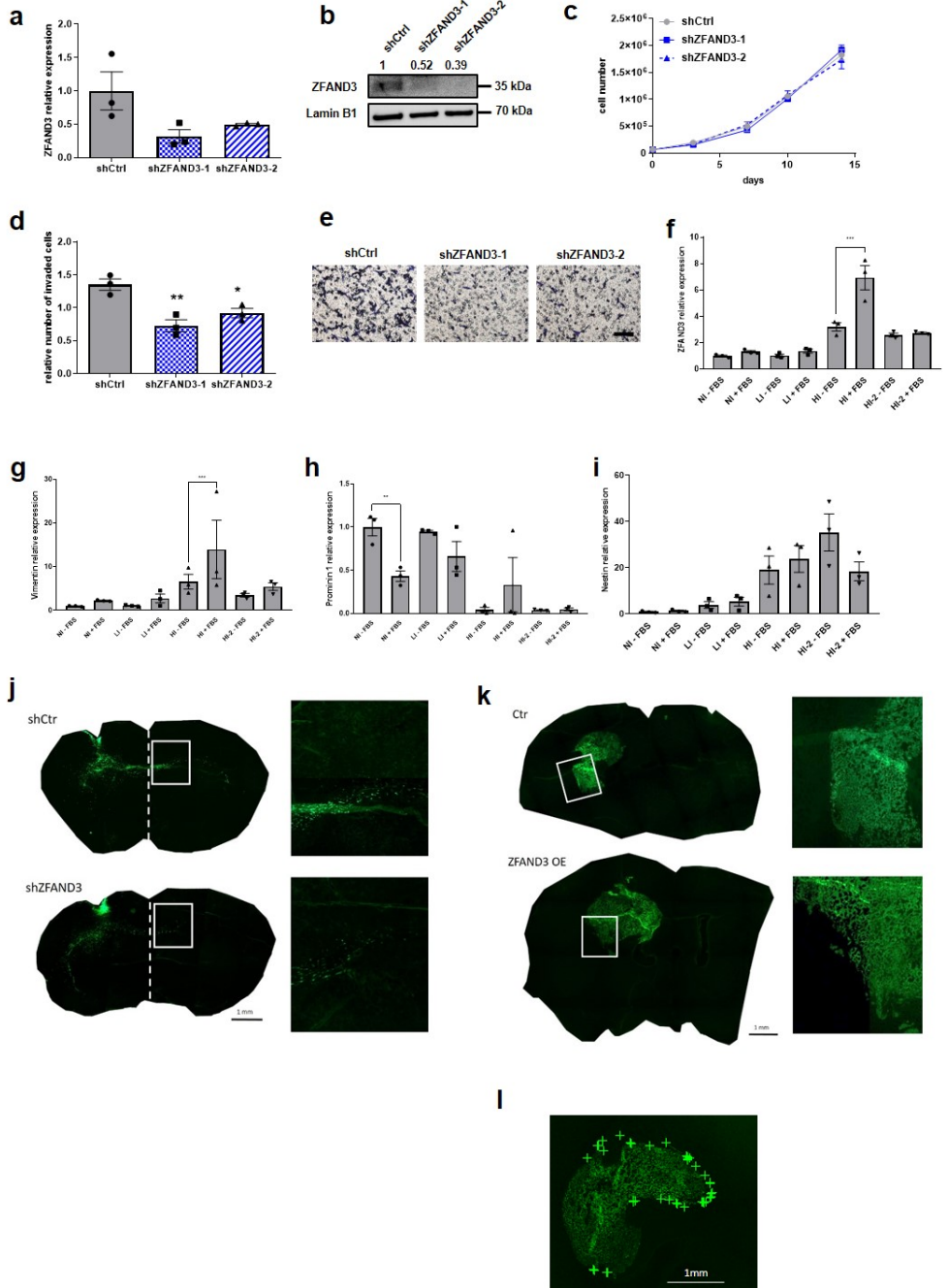
Supplementary Figure 3



Supplementary Figure 3: ZFAND3 protein expression in GBM patient samples and xenografts. a) Representative picture of P53/ZFAND3 double-fluorescence stainings in GBM patients. (Scale bar = 50µm). (n=17 patient samples) b) Representative picture of a central tumor region with and without the application of a software based cell-classifier. Identification of DAPI-positive nuclei (blue), P53-positive nuclei (green),

ZFAND3 staining (red), cells with P53+/ZFAND3+ cytoplasmic expression (pink) and cells with P53-/ZFAND3+ nuclear expression (turquoise). Scale bar = 10 μm c-d) Quantification of tumor cell fraction with cytoplasmic (c) or nuclear (n=17 patient samples) (d) ZFAND3 positivity on three tumor regions (central, intermediate, peripheral). e) Double-immunofluorescence of ZFAND3 with Iba1 (upper panel) or NeuN (lower panel) in GBM patients (Scale bar upper rows = 25 μm , lower rows = 15 μm). (n=9 different patient samples) f) Double-immunofluorescence of ZFAND3 with Iba1 (upper panel) or NeuN (lower panel) in HI GSC xenograft. Scale bar = 100 μm on overview images and 25 μm on magnified images(n=4 mice). For c and d results are displayed as average \pm SEM and data were analysed as matched data with one-way ANOVA and Tukey's multiple comparison test,

Supplementary Figure 4



Supplementary Figure 4: ZFAND3 knockdown in 2nd HI cells, gene expression during invasion assay and overview images of xenografts. a) qPCR showing ZFAND3 expression upon knockdown (KD) in highly invasive GBM cells (HI-2) (n=3 biologically independent samples). Results are displayed as average +/- SEM and were analysed with an ordinary one-way ANOVA b) Western-blot showing protein expression upon ZFAND3 KD (n=3). c) Growth curves of control and ZFAND3 KD cells (n=3). d) *In vitro* Boyden chamber invasion assays of control and ZFAND3 KD cells (n=3 biologically independent experiments). Results are displayed as average +/- SEM and were analysed with an ordinary one-way ANOVA.e) Representative pictures of *in vitro* Boyden chamber invasion assays. Scale bar = 100 μ m. f) ZFAND3 expression in different GSC models under *in vitro* invasion conditions (7% FBS in medium) (n=3). Results are displayed as average fold change +/- SEM and were analysed with an ordinary one-way ANOVA. g-i) Expression of stem cell markers in different GSC models under *in vitro* invasion conditions (n=3). Results are displayed as average fold change +/- SEM and were analysed with an ordinary one-way ANOVA. j) Overview image of HI GSC xenograft with control (shCtr) and ZFAND3 knockdown (shZFAND3). GFP positive tumor cells invading to the contralateral brain hemisphere were counted (boxed area and blow up). k) Overview image of NI GSC xenograft of control (ctr) or ZFAND3 overexpressing cells. GFP positive tumor cells at the edge of the tumor area were counted as shown in (l). *p_{value}<0.05; **p_{value}<0.01; ***p_{value}<0.001.

Supplementary Figure 5

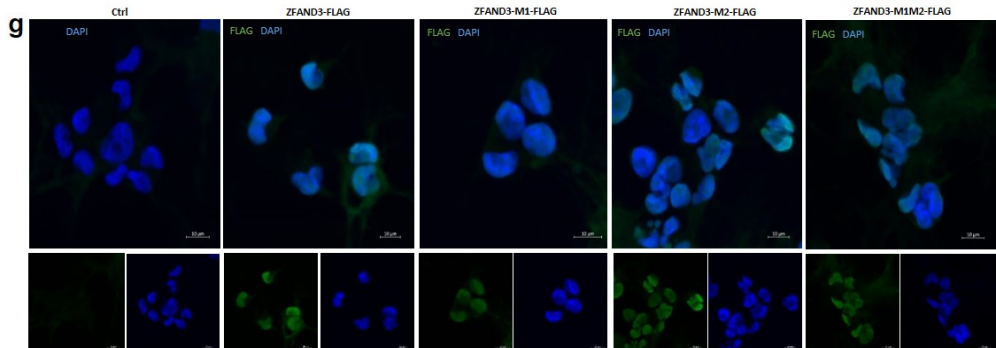
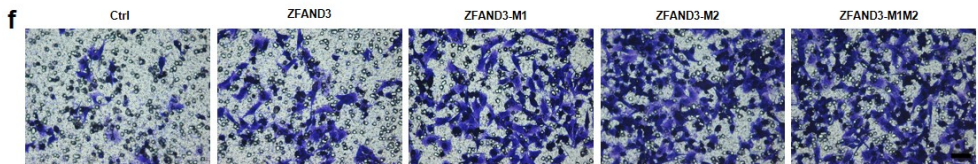
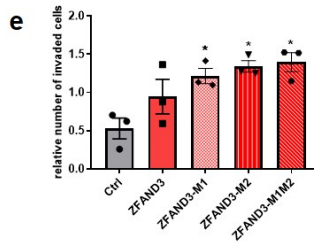
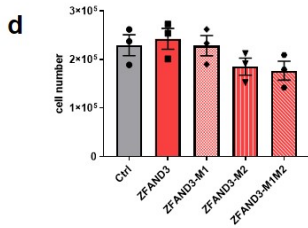
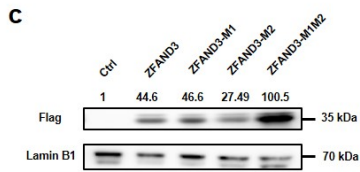
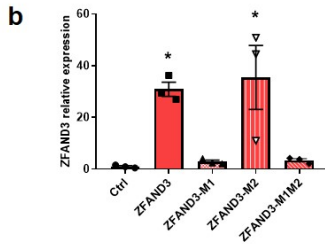
a MGDAGSERSKAPSL**PPRCPCGFWGSSKTMNLC**SKCFADFQKKQPDDDSAPSTSNSSQSDLFSEETSDNNNTSITTP
 TLPSPQQPLPTELNVTSPSKEECGPCTDTAHVSLITPTKRSCGTDSSQSENA**SPVKKRPLI**ENTERSEETSRSKQK
 SR**RRRCFCQCOTKLELVQQLGSCR**CGYVF**CM**LRHLPEQ**HDCTFDHMR**RGREEAIMRMVKLDRKVGRRSCQRIGEGCS

NLS site, AAs mutated to Alanine in ZFAND3mutNLS in bold/underlined (K132A, R133A and R135A)

Zinc finger_A20-type (AA 15-44) deleted in ZFAND3-Δ1

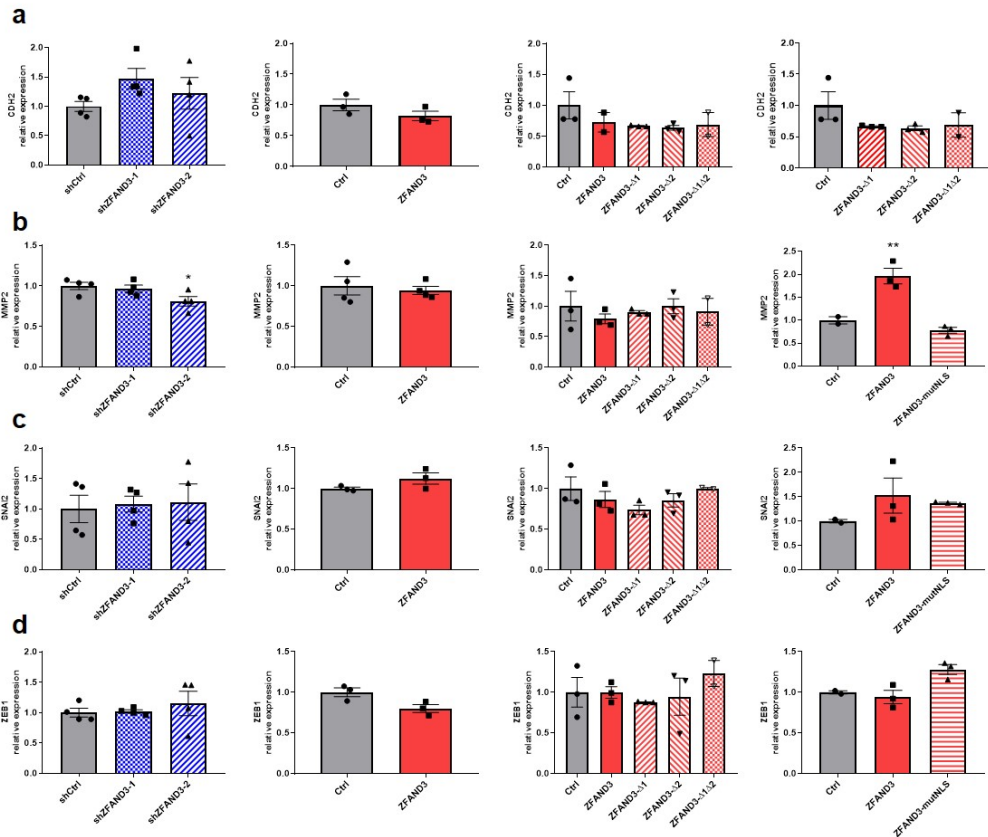
Zinc Finger_AN1-type (AA 155-198) deleted in ZFAND3-Δ2

AA: Zinc complexing amino acids. AAs mutated to Alanine are underlined (C32A + C35A in ZFAND3 M1; C176A + C181A in ZFAND3 M2; all four in ZFAND3 M1-M2)



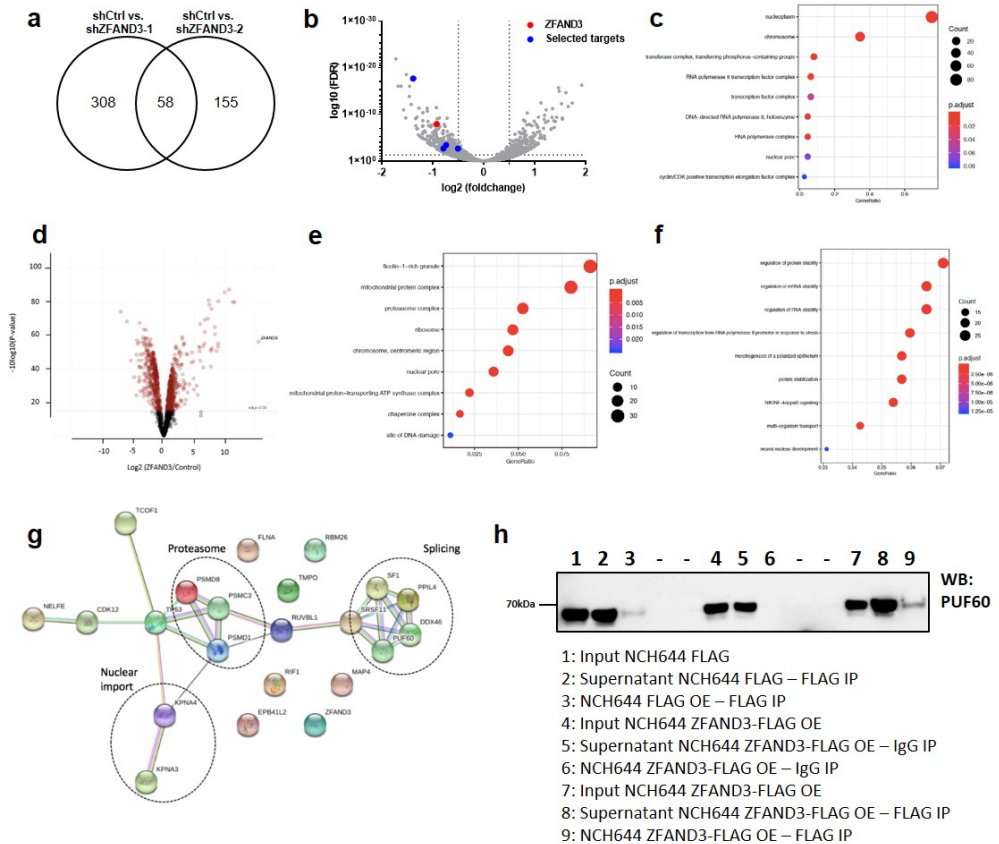
Supplementary Figure 5: ZFAND3 mutant constructs. a) ZFAND3 protein sequence indicating domain areas and mutant constructs used in this manuscript. b) Validation of expression of ZFAND3 wildtype and point mutation constructs (M1, M2, M1-M2) in NI GSCs by qPCR (n=3 biologically independent samples) (b) and Western blot (n=2) (c). Note that for M1, primers in qPCR did not bind efficiently because of overlapping point mutations. d) No effect on proliferation was seen with respective constructs (day 3, n=3 biologically independent experiments). e) *In vitro* Boyden chamber invasion assays of control cells and cells harboring mutations in the ZFAND3 zinc finger domains (n=3 biologically independent experiments). (f) Representative pictures of *in vitro* Boyden chamber invasion assays. Scale bar = 100 μ m. (g) Nuclear localization of ZFAND3 in cells with mutations in zinc finger domains was maintained (n=3). (green: FLAG, blue: DAPI. Scale bars = 10 μ m). Results are displayed as average +/- SEM and for b) and e) results were analysed with an ordinary one-way ANOVA. * $p_{\text{value}} < 0.05$.

Supplementary Figure 6



Supplementary Figure 6: qPCRs showing gene expression of general invasion markers upon ZFAND3 knockdown, overexpression, zinc-finger deletions and mutation in nuclear localization signal. a-d) qPCR showing expression of invasion-related genes (*CDH2*, *MMP-2*, *SNAI2*, *ZEB1*) in NI GSCs upon modulation of ZFAND3 expression by knockdown (blue) or overexpression of either wildtype ZFAND3 or mutant constructs (red). Results are displayed as average +/- SEM and were analysed with an ordinary one-way ANOVA (n= 2-4). **pvalue<0.01.

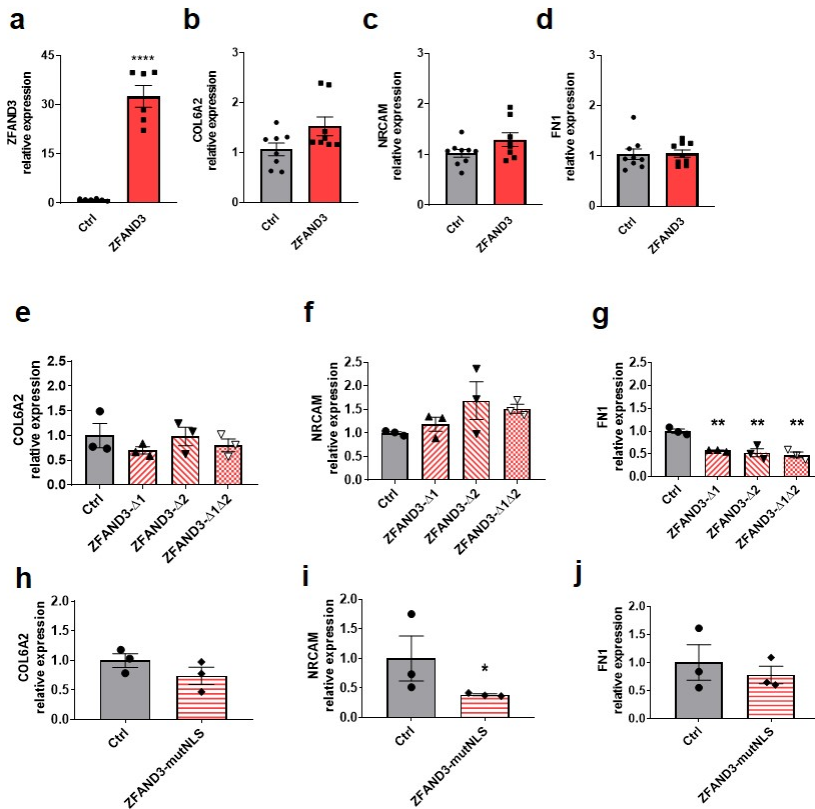
Supplementary Figure 7



Supplementary Figure 7: Analysis of RNA sequencing, BioID and Co-IP/MS data. a) RNA sequencing was performed on control HI cells and two knockdown clones (shZFAND3-1 and shZFAND3-2). Differentially expressed genes were analysed at FDR=0.05, $\log_2\text{FC} = -0.5$ (n=3 per condition). Venn diagram displaying downregulated genes upon ZFAND3 KD resulting in 58 common genes in both shZFAND3-1 and shZFAND3-2. b) Volcano plot of RNA sequencing data of shCtrl compared to shZFAND3-1 HI cells. c) BioID analysis was performed in control NI and ZFAND3-FLAG overexpressing NI cells (n=3). GO analysis of the BioID results reveals enrichment of specific GO terms classified by cellular compartment. d) Volcano plot of Co-IP/MS results showing 432 proteins significantly enriched in ZFAND3-FLAG expressing cells compared to cells expressing FLAG-Tag alone. Two-sample t test was performed with a Benjamini-Hodgberg based FDR < 0.01. GO analysis reveals enrichment of specific GO terms classified by cellular compartment (e) or biological process (f) For the GO analysis p-value and q-value cutoff was at 5%, n and minimum 3 proteins per category as threshold. g) Interaction between 22 common proteins found in ZFAND3-FLAG IP and BioID were

determined by network analysis using STRING database. Splicing-related proteins, proteasome related proteins and nuclear import proteins are highlighted. h) Co-IP/Western blot from NI GSCs overexpressing either FLAG-tag alone (lanes 1-3) or FLAG-tagged ZFAND3 (lanes 4-9) demonstrating physiologically relevant protein-protein interaction between ZFAND3 and PUF60. FLAG-antibody was applied for lanes 1-3 and 7-9, while control IgG antibody was applied to lanes 4-6 (n=3).

Supplementary Figure 8



Supplementary Figure 8: Target gene expression upon stable overexpression of ZFAND3 and mutant constructs. qPCRs showing relative expression of ZFAND3 (n=6) (a), COL6A2 (n=8) (b), NRCAM (n=9) (c) and FN1 (n=9) (d) in HI cells upon ZFAND3 overexpression. No increase in gene expression was observed upon overexpression of mutant constructs ZFAND3-Δ1, ZFAND3-Δ2, ZFAND3-Δ1Δ2, or ZFAND3-mutNLS (n=3). Results are displayed as average \pm SEM and results were analysed with an unpaired, two-sided t-test. * $p_{\text{value}} < 0.05$, ** $p_{\text{value}} < 0.01$, **** $p_{\text{value}} < 0.0001$.

Supplementary Figure 9

Figure 3b

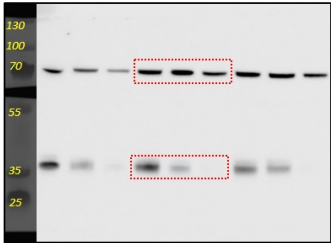


Figure 4b

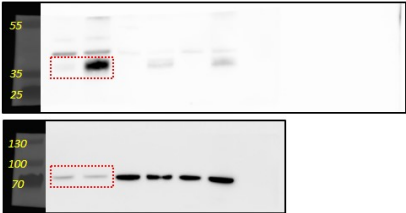


Figure 5c

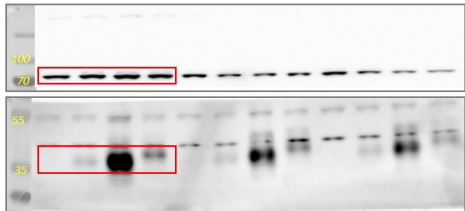


Figure 5i

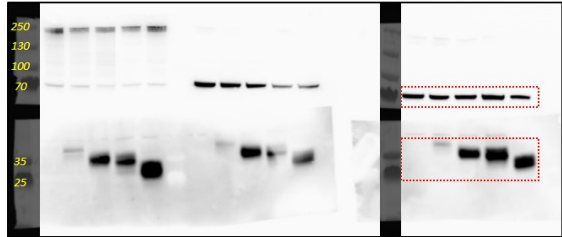


Figure S4b

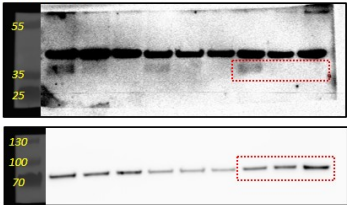


Figure S5c

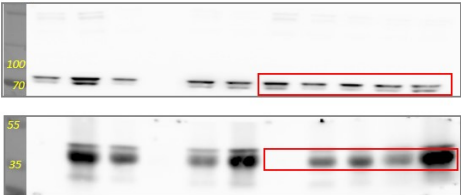
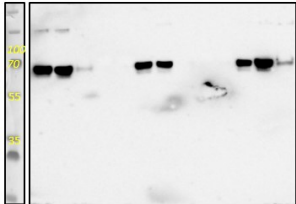


Figure S7h



Supplementary Figure 9: Original Western blot membranes corresponding to indicated figures.

Supplementary Tables

Supplementary Table 1: Primer sequences

<i>Gene</i>	<i>Forward primer</i>	<i>Reverse primer</i>
CDH1 (N-cadherin)	GGTGGAGGAGAAGAAGACC	GGCATCAGGCTCCACAGT
COL6A2	GACTCCACCGAGATCGACCA	CTTGTAGCACTCTCCGTAGGC
EF1 α	TTGTCGTCATTGGACACGTAG	TGCCACCGCATTATAGATCAG
EGFR	CCCACTCATGCTCTACAACCC	TGCACCTTCTTACACTTGCGG
FN1	AGGAGCACCACCCAGACATTACT	CCAGGCCGGGACTCAGTTAT
MMP2	CGTCTGTCCCAGGATGACATC	ATGTCAGGAGAGGCCCCATA
NRCAM	TCCAACCATCACCCAACAGTC	TGAGTCCCATTACGGGTCCAG
NRP1	ACGTGGAAGTCTTCGATGGAG	CACCATGTGTTTCGATGTCAGA
SNAI2	CGCCTCCAAAAGCCAAACT	ACAGTGATGGGGCTGTATGC
ZEB1	TTCACAATTACTCACCTGTCCA	TGCGTCACATGTCTTTGATCTC
ZFAND3	CCAGACGATGATTCCGCTCC	GCGTGGTTATCGAGGTATTGTT
ZFAND3 (2)	CGATAACCACGCCAACTCTT	GGACCGTTCCGTATTCTCAA
COL6A2 S1 ChIP	TGAGCAAGCCGGACACAGGACA	TGGGACTCGCCCCTTGGTA
COL6A2 S2/3 ChIP	CAGCCAGGTCGTCCGGGAAAT	AGGCTGGAGGAGGTGGAGAG
COL6A2 S7 ChIP	TCGGGAGCGGAGCCTCCTCGGGA	AGGCTGGAGGAGGTGGAGAG
COL6A S8/9/10 ChIP1	GCGACTTGGGGCCACCTCCC	GACCCGAACCGCTCGCAGAC
COL6A2 S8/9/10 ChIP2	CCTGTGGCTCCGCGTCTCTG	GTGCCGGGTCGTCTCGGGAG
NRCAM S1/2/3 ChIP	CTAAATCCCAGCCATCCTAGCC	CAACCTCCGTCAGCCTGCCA
NRCAM S4/5/6/7/8 ChIP1	AGCCCATTCGCTGCCGTC	CTCCCGCCCTCTCCGCTC
NRCAM S4/5/6/7/8 ChIP2	GTTGGCCAGGAGGGGAGGAG	ACCCTGGCGAAGCCGAGGC
FN1 S7 ChIP1	GACCCCTAAGCATGTTGAGAC	GAAGGGATTTTCCCGCAGGTT
FN1 S7 ChIP2	GACCCCTAAGCATGTTGAGAC	CACCTTCTGGAGGCGACAAC

Supplementary Table 2: shRNA sequences against ZFAND3

<i>Name</i>	<i>Target</i>	<i>Sequence</i>	<i>Company</i>	<i>Clone ID</i>	<i>Catalogue number</i>
shZFAND3-1	ZFAND3	TACAGAACACATAACCGCA	Dharmacon	V3LHS_363696	RHS4531_E G60685
shZFAND3-2	ZFAND3	TAGTGAACCTAAGAACAGCG		V3LHS_409051	

Supplementary Table 3: Antibodies

<i>Target</i>	<i>Company</i>	<i>Catalog number</i>	<i>Purpose and dilution</i>
HA	Sigma	H6908	WB 1:500 ; IF 1:100
mouse IgG1	Abcam	ab18447	Co-IP 7 μ g/mg beads

mouse IgG1 isotype control	CST	5415S	Co-IP 5µg/mg beads
FLAG M2	Sigma	F1804	Co-IP 5 µg/mg beads, WB 1:1000
Lamin B1	Abcam	ab16048	WB 1:1000
P53	Ventana Medical Systems, Roche	790-2912	clone: DO7, ready-to-use
Vimentin	Millipore	MAB3400	IHC 1:200
ZFAND3	Atlas Antibodies	HPA016755	WB: 1:250 - 1:500; IF culture: 1:100; IHC 1:50
ZFAND3	Atlas Antibodies	HPA016755	IHC: 1:600, IF: 1:1000 (paraffin sections)
GAPDH	Cell Signaling	5174S	WB 1:10000
COL VI	Abcam	ab182744	WB 1:000
Fibronectin 1	Abcam	ab2413	WB 1:500-1000
NRCAM	Cell Signaling	55284	WB 1:500
ZBED4	Bio-Connect	orb158740	WB: 1:2000 ChIP
PUF60/Pontin52	Atlas Antibodies	HPA059714	WB: 1:500
TIP49/RUVBL1	abcam	ab51500	WB: 1:100
TCOF1/Treacle	Atlas Antibodies	HPA038237	WB: 1:500
Iba1	Wako Pure Chemical Industries		IF: 1:3000
NeuN	Chemicon	clone: A60	IF: 1:500
Goat anti Mouse IgG HRP	Jackson Laboratory	115-035-003	WB 1:10000
Goat anti Rabbit HRP	Jackson Laboratory	111-035-003	WB 1:00000
Goat anti Rabbit IgG Alexa 555	Invitrogen	A21428	IF: 1:1000

Supplementary Table 4: Constructs

Name used in publication	Full Plasmid name	Purpose	Origin	Cell line
shScr	pGIPZ-sh non targeting control	Control, non targeting sh expressing GFP	Open Biosystems/GE Dharmacon	HI (NCH601), HI-2 (NCH465)
shZFAND3-1	pGIPZ-shZFAND3-1	ZFAND3 knockdown mature antisense: TACAGAACACATAACCGCA expressing GFP	Open Biosystems/GE Dharmacon (V3LHS_363696)	HI (NCH601), HI-2 (NCH465)
shZFAND3-2	pGIPZ-shZFAND3-2	ZFAND3 knowckdown mature antisense: TAGTGAACATAAGAACAGCG expressing GFP	Open Biosystems/GE Dharmacon (V3LHS_409051)	HI (NCH601), HI-2 (NCH465)
Ex-Ctrl	Ex-negcon. LV225	lentiviral plasmid; EF1promoter-IRES2-eGFP-IRES-puromycin	GeneCopoeia	NI (NCH644)
Ex-ZFAND3	Ex-ZFAND3-LV225	lentiviral plasmid; EF1promoter-ZFAND3-IRES2-eGFP-IRES-puromycin	GeneCopoeia	NI (NCH644)
NA	pCDH-EF1α-MCS-IRES-Neo	basic lentiviral plasmid for all this paper overexpression plasmids	System Bioscience (#CD533A-2)	NA
Ctrl-HA	pCDH-EF1-HA-IRES-neo	HA-tag only control plasmid	this paper	NI (NCH644)

ZFAND3-OE	pCDH-EF1-ZFAND3-HA-neo	ZFAND3 overexpression with C-terminal HA-tag	this paper	NI (NCH644)
ZFAND3 Δ1	pCDH-EF1-ZFAND3_DD1-HA-IRES-neo	ZFAND3 with deletion of Znfinger domain1, expression as HA-tagged protein	this paper	NI (NCH644)
ZFAND3 Δ2	pCDH-EF1-ZFAND3_DD2-HA-IRES-neo	ZFAND3 with deletion of Znfinger domain2, expression as HA-tagged protein	this paper	NI (NCH644)
ZFAND3 Δ1Δ2	pCDHEF1-ZFAND3_DD1D2-HA-IRES-neo	ZFAND3 with deletion of both Znfinger domains, expression as HA-tagged protein	this paper	NI (NCH644)
ZFAND3-OE-mutNLS	pCDH EF1-ZFAND3mutNLS-HA -IRES-neo	overexpression of ZFAND3 with mutated NLS and HA tag	this paper	NI (NCH644)
ZFAND3-OE-mutNLS-NLS	pCDH EF1-ZFAND3mutNLS-NLS-HA -IRES-neo	overexpression of ZFAND3 with mutated NLS fused to cMYC NLS (PAAKRVKLDG) and HA tag	this paper	NI (NCH644)
NA	pcDNA3.1 myc BioID	non lentiviral plasmid overexpressing myc-BirA(R118G)	gift from Kyle Roux (Addgene plasmid # 35700 ; http://n2t.net/addgene:35700 ; RRID:Addgene_35700)	NA
myc-BioID	pCDH-EF1-myc-BioID-IRES-neo	overexpression of BioID with N-terminal myc-tag	this paper (myc_BioID was amplified from Addgene plasmid #35700)	NI (NCH644)
myc-BioID-ZFAND3	pCDH EF1-myc-BioID-ZFAND3-IRES-neo	overexpression of myc_BioID-ZFAND3 fusion protein	this paper	NI (NCH644)
Ctrl-Flag	pCDH-EF1-3xflag-IRES-neo	Overexpression of 3x Flag tag	This paper	NI (NCH644)
ZFAND3-OE Flag	pCDH-EF1-ZFAND3-3xflag-IRES-neo	overexpression of ZFAND3 with a C-terminal 3xflag tag	this paper	NI (NCH644)
ZFAND3_M1	pCDH-EF1-ZFAND3_M1-3xflag-IRES-neo	overexpression of mutated ZFAND3 (C32A + C35A) with a C-terminal 3xflag tag	this paper	NI (NCH644)
ZFAND3_M2	pCDH-EF1-ZFAND3_M2-3xflag-IRES-neo	overexpression of mutated ZFAND3 (C176A +C181A)with a C-terminal 3xflag tag	this paper	NI (NCH644)
ZFAND3_M1M2	pCDH-EF1-ZFAND3_M1M2-3xflag-IRES-neo	overexpression of mutated ZFAND3 (C32A + C35A + C176A +C181A)with a C-terminal 3xflag tag	this paper	NI (NCH644)

Supplementary Table 5: Promotor sequences (for Reporter Assay)

COL6A2

CCTGACCCGGGGCCTCTCGCGGGAGGCCTGAGCAAGCCGGACACAGGACACGGGGTAGGGGAGGGGTGGGGGGGCTGATGGG
GGGAACCTCTGACCCCCAGGGCAGCTGCTACCAAGGGCGAGTCCAGGGCCCCCGTGGCCCTGCGTGCGGGGCGGGTCCC
CAACACCCAGGGCCCCGGAGGCGGACACAGCCCCAGCCAGGTCGTCCGGAAATGGGGCGGGGGCGACGGGGCGG
CCGGGCCCGGGACGCGAAGTCCGAGCAGCAGCGGGCAGGGGCTGGCGGGGAGCTCGGCC
CGGGTGCAGGGGGTCCCCACCTCTCCACCTCTCCAGCTCCCGCCCTCGAGGGTCC
CCGCTTCCCTCCATCCCCCTCCGTGCCCGGCCCTCTCCATCCGCGGGGCCG
AGCGCTTCTGGCGGGGGGGCGGTAGGCCGGCGGGGGGTATAAAGGGGGCGGCGC
CGGCCGCGGTCCCTCCCTGCTGTTACTGGCGCCCGCGCTCGGGCCGTGGGAGCGG
AGCCTCTCGGGACAGGTGAGCGCTCCCGACCCCGACCTGGAAGCCGCTCGGCC
GCGGGGGTGACCCGAGTCTGGGAAGGCGGGCGGGGCTCCGTCCCTCGGGTCCCC
GGGAAGGGGACTCCAGCCCCAGGACGGCGGGGGGCTGGCGGGTTCGGGGTCTCTCT
CGCGGGGCTGGGGCCGCGCTGCCCTGTGGTCCGCGTCTCTGGTCCGACCTCGGGC
GCGGACTTGGGGCCACTCCCCGCGCTCTCTGGGGGAGCCGGCCTGGGGGGGT
GGGGGGTCCCTGTCTGCGCCGAGCTCGGTGCTGGGACCCCGCTCCCGAGACGCC
GGCACCGACGCCCGCAGGCCCGCTCTGCGAGCGGTTGGGTCCGGTCCGGCCCCG
CGGGGAAGACGCCCGGTGGTGGACCTCCGGGGCGCAGGGCCTCTCCCGGGCCGG
ACGGAAGGGCGGGGGGGGGGAGGAGGGGCTTTCGGTGCCCGAGGGCGGGACTGGG
CGGGGAGGGGACGCGGGTGGCCCCGACGCCCATCGTGCGCCCTCCCGGCTGGAGCC

COL6A2mut

CCTGACCCGGGGCCTCTCGCGGGAGGCCTGAGCAAGCCGGACACAGGACACGGGGTAGGG
GAGGGGTTCGGGGGGTGTATGGGGGAACCTGACCCACAGGGCAGCTGCTACCAAGGG
GCGAGTCCAGGGCCCCGTGGCCCTGCGTGGGGGCGGGTCCCCAACACCCAGGGCC
CCGGAGGCGACACAGCCCCAGCCAGGTGCTCCGGAAATGGGGCGATGCGACGGGCGG
CCGGGCCCGGACGCGAAGTCCGAGCAGCAGCGGGCAGGGGCTGGCGGTGGAGCTCGGC
CGGGTGCAGGGGGTCCCCACCTCTCCACCTCTCCAGCTCCCGTCTCGAGGGTCC
CCGCTTCCCTCCATCCCCCTCCGTGCCCGGCCCTCTCCATCCGCGGGGCCG
AGCGCTTCTGGCGGGGGGGGGTCCAGGCCGGCGGGGGTATAAAGTGGCGGCGC
CGGCCGCGTCCCTCCCTGCTGTTACTCGCGCCCGCGCTCGGGCCGTGGGAGCGG
AGCCTCTCGGGACAGGTGAGCGCTCCCGACCCCGACCTGGAAGCCGCTCGGCC
GCGGGTGGTACCCGAGTCTGGGAAGGCGGGCGGGGCTCCGTCCCTCGGGTCCCC
GGGAAGGGGACTCCAGCCCCAGGACGGCGGGGGGCTCGGGGGTTCGGGGTCTCTCT
CGCGGGTGGGGCCGCGCTGCCCTGTGGTCCGCGTCTCTGGTCCGACCTCGGGC
GCGGACTTGGGGCCACTCCCCGCGGCTCTCTGGTGGGAGCGCCCTGTGCGGGGT
GTGGGGTCCCTGTCTGCGCCGAGCTCGGTGCTGGGACCCCGCTCCCGAGACGACCC
GGCACCGACGCCCGCAGGCCCGCTCTGCGAGCGGTTGGGTCCGGTCCGGCCCCG
CGGGGAAGACGCCCGGTGGTGGACCTCCGGGGCGCAGGGCCTCTCCCGGGCCGG
ACGGAAGCGCGGGGGGGTGGAGGAGGGGCTTTCGGTGCCCGAGCGGGGACTGGG
CGGGGAGGGGACGCGGGTGGCCCCGACGCCCATCGTGCGCCCTCCCGGCTGGAGCC

NRCAM

AAAACAAACCCCAAACCACTACCCAATCTCAACCACCCCAACTGATGAATTCGAA
GAAAGTGCTTTTTAAAAAGAAAAACTAGAAGACCACAGACTCCACAGAAAGCTAAA
CCCATGAGAGTGGCATTCAAAAACCTACCCATTTTCTGAAACATCTTTGTAGCTAAATCC
CAGCCATCTAGCCCCGAACACTCCCGCCTCCGTCCCCGACCCCAACCCCGCCGCC
ACACGCGCTCGCAGGCTGACGGAGGTTGGCGGTGGGGCGGCCGCTCAGGTGAGGGGCCAC
CCAGTCCCTCGAGGCGCGGGCTGGAGCCATTGCTGCGTCCGTCGAGCAGCAGGGA
GAGGGGTTGGCCAGGAGGGGAGGAGCGGAGGACCCCGAGGGAGTGCGGGGGAGGGG
GACGGGAGGACGCTAAGGAGAGCCGGGAGGGGCAAAGCACGCGCGGGGAGGGGAGCG
GAGAGGGCGGGAGCGGGGGGGCGCGCCGGCGGGGCCAGCCTCGCTTCCGAGGGT
CGCTGCGGACGCGCGCCGAGTCCGAGCCTCAGACGCGGGCGGGGGACGCGCGCAG

NRCAMmut

AAAACAAACCCCAAACCACTACCCAATCTCAACCACCCCAACTGATGAATTCGAA

GAAAGTGCTTTTTAAAAAAGAAAAAAGTCTAGAACACACAGACCTCCACAGAAAGCTAAA
CCCATGAGAGTGGCATTCAAAAACCTACCCATTTTCTGGAACATCTTTTGTAGCTAAATCC
CAGCCATCCTAGCCCCGGAACACTCCCGTCTCCGTCCTCCCGCACCCACACGCCCCGCGC
ACACGCGCTCGCAGGCTGACGGAGGTTGGCGGTGGGGCGGCCCTCAGGTGAGGGGCCAC
CCAGTCCCTCGAGGCGCCGCGGCTGGAGCCATTGCTGCCGTCGAGCAGCAGGGCAA
GAGGGGGTTGGCCAGGAGGGGAGGAGGCGGAGGACGCCCGAGGGAGTGCAGCGGAGGGC
GACGGGAGGACGCTAAGGAGAGCCGGGAGGGGCAAAAGCACGCGCGGGGAGGGCGGAGCG
GAGAGCGCGGGAGCGCGGTGGCGCGCCGCGCGGGGCCAGCCTCGCTTCGCCAGGGT
CGCTGGCGGACGCGCGCCGAGTCCGAGCCTCAGACGCGGGCGCGGGGACGGCGCAG

FN1

TCCCTTCCCCATCCCCTAAAAAGTTTGATGACCGCAAAGGAAACCGAAAAAAGTTGTC
TTGCCCACTCTGGCGGGCCATCAGCATCTCTTTTGTTCGCTGCGAACCCACAGTCCCC
CGTGACGTACCCGGAGCCCGGGCAATCGGCGCGGTCGGCTGCGGCGGCCGCGGGC
GGGCGGCGGGTGGGGTGGGGCGGGGCGGGGACAGCCCGCGGGTCTCTCTCCCCCGC
CCCCGGCCTCCAGAGGGGCGGGAGGGGACCGTCCCATAAAGCCCCGGTCCCCGGCGT
CGGACGCCGCGCCGGTGTGCTGCACAGGGGAGGAGGGAAACCCAGCGCGAGCGG
GAAGAGGGGACCTGCAGCCACAATTCTGCTCTGCTCCCTTCTGCTCCCTCCACC
CGTCCCTTCCCCACCTCTGCCCCACCTTCTGGAGGCGACAACCCCGGGAGGCAT
TAGAAGGGATTTTTCCCGCAGTTGCGAAGGGAAGCAAATTGGTGCAACTTGCTCCC
GGTGGCGGCTCTCTCCCCACCTCTCAACATGCTTAGGGGTCGCGGGCCCGGGTCT

FN1_no ATG (used in HEK)

TCCCTTCCCCATCCCCTAAAAAGTTTGATGACCGCAAAGGAAACCGAAAAAAGTTGTCCTTCCCCAGTCTGGCGGGCCATCAG
CATCTCTTTTGTTCGCTGCGAACCCACAGTCCCCGTGACGTACCCGGAGCCCGGGCCAATCGGCGCGCGGTGCGTGCAGCGG
CCGGCGGGCGGGCGGGTGGGGTGGGGCGGGGCGGGGACAGCCCGCGGGTCTCTCTCCCCCGCGCCCCGGGCTCCA
GAGGGGCGGGAGGGGACCGTCCATATAAGCCCCGGTCCCGCGCTCGGACGCCGCGCGGCTGTGCTGCACAGGGGAGG
AGAGGGAACCCAGGCGGAGCGGGAAGAGGGGACCTGCAGCCACAATTCTGCTCTGCTCATCCCTTCTGCTCCCTCCACC
GTCCCTTCCCCACCTCTGCCCCACCTTCTGGAGGCGACAACCCCGGGAGGCATTAGAAGGGATTTTTCCCGCAGTTGCG
AAGGGAAGCAAACCTGTTGGCAACTGCTCCCGTGCAGGCGTCTCTCCCCACCTCTCAAC

FN1mut_no ATG (used in HEK)

TCCCTTCCCCATCCCCTAAAAAGTTTGATGACCGCAAAGGAAACCGAAAAAAGTTGTCCTTCCCCAGTCTGGCGGGCCATCAG
CATCTCTTTTGTTCGCTGCGAACCCACAGTCCCCGTGACGTACCCGGAGCCCGGGCCAATCGGCGCGCGGTGCGTGCAGCGG
CCGGCGGGCGGGCGGACGGTGGGGTAGGCGGGGCCGGGACAGCCCGCGGGTCTCTCTCGCCCGCGCCCCGGGCTCCAG
AGGAGCGGGAGGGGACCGTCCCATAAAGCCCCGGTCCCCGGCTCGGACGCCGCGCGGGTGTGCTGCACAGGGGAGGA
GAGGGAACCCAGGCGGAGCGGGAAGAGGGGACCTGCAGCCACAATTCTGTTCTCTGATCCCTTCTGCTCCCTCCACCG
TCCCTTCCCCACCTCTGCCCCACCTTCTGGAGGCGACAACCCCGGGAGGCATTAGAAGGGATTTTTCCCGCAGTTGCGA
AAGGGAAGCAAACCTGTTGGCAACTGCTCCCGTGCAGGCGTCTCTCCCCACCTCTCAAC

Supplementary Table 9: Anonymized patient demographics

ID	Sexe	Age diagnosis
1	Male	83
2	Male	43
3	Male	80
4	Male	71
5	Male	65
6	Female	60
7	Male	82
8	Male	52
9	Female	38
10	Female	75
11	Male	80
12	Male	57
13	Male	57
14	Female	35
15	Male	75
16	Female	85
17	Female	72

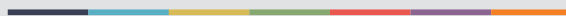
Supplementary References

1. Bowman, R.L., Wang, Q., Carro, A., Verhaak, R.G. & Squatrito, M. GlioVis data portal for visualization and analysis of brain tumor expression datasets. *Neuro Oncol* **19**, 139-141 (2017).
2. Tang, Z. *et al.* GEPIA: a web server for cancer and normal gene expression profiling and interactive analyses. *Nucleic Acids Res* **45**, W98-W102 (2017).

III



Graphic design: Communication Division, UIB / Print: Skjipes Kommunikasjon AS



uib.no

ISBN: 9788230842430 (print)
9788230855010 (PDF)